

OVERLAPPING LATTICE MODELING FOR CONCRETE FRACTURE
SIMULATIONS USING SEQUENTIALLY LINEAR ANALYSIS

A THESIS SUBMITTED TO
THE GRADUATE SCHOOL OF NATURAL AND APPLIED SCIENCES
OF
MIDDLE EAST TECHNICAL UNIVERSITY

BY

BEYAZIT BESTAMİ AYDIN

IN PARTIAL FULFILLMENT OF THE REQUIREMENTS
FOR
THE DEGREE OF MASTER OF SCIENCE
IN
CIVIL ENGINEERING

JANUARY 2017

Approval of the thesis:

**OVERLAPPING LATTICE MODELING FOR CONCRETE FRACTURE
SIMULATIONS USING SEQUENTIALLY LINEAR ANALYSIS**

submitted by **BEYAZIT BESTAMİ AYDIN** in partial fulfillment of the requirements for the degree of **Master of Science in Civil Engineering Department, Middle East Technical University** by,

Prof. Dr. Gülbin Dural Ünver
Dean, Graduate School of **Natural and Applied Sciences**

Prof. Dr. İsmail Özgür Yaman
Head of Department, **Civil Engineering**

Prof. Dr. Barış Binici
Supervisor, **Civil Engineering Dept., METU**

Prof. Dr. Kağan Tuncay
Co-Supervisor, **Civil Engineering Dept., METU**

Examining Committee Members:

Prof. Dr. Erdem Canbay
Civil Engineering Dept., METU

Prof. Dr. Barış Binici
Civil Engineering Dept., METU

Prof. Dr. Kağan Tuncay
Civil Engineering Dept., METU

Assoc. Prof. Dr. Yalın Arıcı
Civil Engineering Dept., METU

Assoc. Prof. Dr. Tolga Akış
Civil Engineering Dept., Atılım University

Date: Jan 18, 2017

I hereby declare that all information in this document has been obtained and presented in accordance with academic rules and ethical conduct. I also declare that, as required by these rules and conduct, I have fully cited and referenced all material and results that are not original to this work.

Name, Last name: Beyazıt Bestami Aydın

Signature :

ABSTRACT

OVERLAPPING LATTICE MODELING FOR CONCRETE FRACTURE SIMULATIONS USING SEQUENTIALLY LINEAR ANALYSIS

Aydın, Beyazıt Bestami

M.S., Department of Civil Engineering

Supervisor: Prof. Dr. Barış Binici

Co-advisor: Prof. Dr. Kağan Tuncay

January 2017, 81 pages

Estimation of the crack location and width in concrete structures is important due to the sustained damage in structures as a result of extreme loads and aging. The location and width of cracks are the most influential parameters for making decisions on the structure service life. Despite significant developments, the computational modelling of concrete fracture initiation and propagation are still challenging tasks.

Many different numerical approaches, most of them based on finite element analysis, have been used in the past employing the smeared or discrete cracking approaches. Such models lack the ability to capture local nature of cracking, the direction of crack propagation and require incorporating ad hoc approaches with extensive calibrations with tests. Recent studies in the last decade have focused on using particle based simulation methods (such as the discrete element method, the lattice-based methods, smoothed particle hydrodynamics, etc) to capture the local character of fracture phenomenon. Among these approaches, lattice modeling and particle based method of

peridynamics have been used as non-local fracture simulation tools. Peridynamics can be viewed as an overlapping lattice approach in which continuum is discretized using pin connected bar elements extending over a predefined horizon. The advantages of these tools are the relative ease of modeling and the simulation of crack propagation using a few key parameters with the ability to bridge various scales from micro to macro levels. In this work, an overlapping lattice approach is proposed, where the continuum is discretized using truss elements extending over a predefined horizon similar to the concept used in peridynamics with the sequentially linear analysis (SLA) technique which is a non-iterative direct solution technique for nonlinear problems. The key difference of our application from the literature is the use of a classical structural analysis with SLA for the simulations as opposed to a particle based approach and a novel calibration of the constitutive model parameters using tension test results. Simulation results for several reinforced concrete (RC) and unreinforced concrete tests focusing on the influence of the mesh size, horizon and the softening functions on the sensitivity of results demonstrate the ability of accurately predicting the direction of crack propagation and the crack widths with the proposed modeling approach with a rather simple and intuitive method.

Keywords: Concrete, fracture, peridynamic modeling, direct tension

ÖZ

SIRALI LİNEER ANALİZ İLE BETON ÇATLAMA SİMÜLASYONLARI İÇİN ÜST ÜSTE BİNDİRİLMİŞ KAFES MODELİ

Aydın, Beyazıt Bestami

Yüksek Lisans, İnşaat Mühendisliği Bölümü

Tez Yöneticisi: Prof. Dr. Barış Binici

Ortak Tez Yöneticisi: Prof. Dr. Kağan Tuncay

Ocak 2017, 81 sayfa

Beton yapılarda çatlak yerinin ve genişliğinin tahmin edilmesi, aşırı yüklerin ve yıpranmanın sonucu olarak yapılarda sürekli hasarın olması nedeniyle önemlidir. Çatlakların yeri ve genişliği, yapı ömrü hakkında karar vermek için en etkili parametrelerdir. Önemli gelişmelere rağmen, betonun kırılmaya başlamasının ve çatlağın yayılımının bilgisayar modellemesi hala zorlu görevlerdir.

Çoğu sonlu elemanlar analizine dayanan birçok farklı sayısal yaklaşım, geçmişte dağınık ve ayrık çatlama yaklaşımıyla kullanılmıştır. Bu tür modeller, çatlamanın yerel doğasını, çatlak yayılımının yönünü yakalamada eksiktir ve testlerle gerçekleştirilecek kapsamlı kalibrasyonlar ile geçici yaklaşımlar gerektirir. Son on yıldaki çalışmalar, kırık olgusunun yerel karakterini yakalamak için parçacık tabanlı simülasyon yöntemlerini (ayrık elemanlar yöntemi, kafes tabanlı yöntemler, düzleştirilmiş parçacık hidrodinamiği, vb.) kullanmaya odaklanmıştır. Bu yaklaşımlar arasında, yerel

olmayan kırılma simülasyon araçları olarak kafes modellemesi ve parçacık tabanlı peridinamik yöntem kullanılmıştır. Peridinamik, önceden tanımlanmış bir evrende uzanan pim bağlantılı çubuk elemanları kullanılarak sürekliliğin ayrıklaştırıldığı üst üste binmiş kafes yaklaşımı olarak görülebilir. Bu araçların avantajı, birkaç önemli parametre ile çatlak yayılımı simülasyonu ve modellemesinin nispeten kolay olması ve mikrodan makroya çeşitli ölçeklere köprü kurma yeteneğidir. Bu çalışmada, sıralı doğrusal analiz (SLA) tekniği ile peridinamikte kullanılan konseptte benzer şekilde önceden tanımlanmış bir evrende uzanan bağ elemanları kullanılarak, devamlılığın ayrıştırıldığı üst üste binmiş bir kafes yaklaşımı önerilmiştir. Uygulamamızın literatürdeki en önemli farkı, bir parçacık tabanlı yaklaşımın aksine simülasyonlar için SLA ile klasik bir yapısal analizin kullanılması ve gerilme testi sonuçlarını kullanarak kurucu model parametrelerinin yeniden kalibrasyonunun yapılmasıdır. Kafes büyüklüğü, evren ve yumuşama fonksiyonlarının sonuçların hassasiyeti üzerindeki etkisine odaklanan birkaç betonarme ve donatısız beton testi için simülasyon sonuçları, önerilen modelleme yaklaşımı ile oldukça basit ve sezgisel bir yaklaşım sunan çatlak yayılım yönlerini ve genişliklerini doğru olarak tahmin etme yeteneği göstermektedir.

Anahtar Kelimeler: Beton, Yırtılma, Peridinamik Model, Yalın Çekme

To My Family

ACKNOWLEDGMENT

I want to express my profound gratitude to my advisor Prof. Dr. Barış Binici and co-advisor Prof. Dr. Kağan Tuncay, whose knowledge, criticism, patience and support enabled me to develop the ideas behind this dissertation. From them, I have learned not only how to become a researcher but also how to have a strong character. I will always admire their attitude towards their students and carry the honor of working with them all my life.

My thanks go to my office mates Erhan Budak, Gizem Mestav Sarıca, Ali Gharibdoust and Ozan Demirel. I will always remember them with pleasure the inspiring discussions and activities we had.

My special thanks goes to my two-year office mate and my eternal friend Alper Aldemir. I think it was one of my luckiest times in my life when I had the chance to meet him. Because he proved me that good and unselfish guys still exist.

I would like to express my sincere gratitude to my beloved mother and father Hatice Aydın and Kadir Aydın for her eternal love, encouragement and trust.

The author wishes to thank all those people whose friendly assistance and wise guidance supported him throughout the duration of this research.

TABLE OF CONTENTS

ABSTRACT	V
ÖZ	VII
ACKNOWLEDGMENT	X
TABLE OF CONTENTS	XI
LIST OF TABLES	XIII
LIST OF FIGURES	XIV
LIST OF SYMBOLS / ABBREVIATIONS	XVII
CHAPTERS	
1 INTRODUCTION	1
1.1 GENERAL	1
1.2 LITERATURE REVIEW	3
1.3 OBJECTIVE AND SCOPE	25
2 OVERLAPPING LATTICE MODELING	27
2.1 GENERAL	27
2.2 OVERLAPPING LATTICE MODEL APPROACH (OLM)	27
2.3 SEQUENTIALLY LINEAR ANALYSIS AND THE OLM SIMULATOR.....	33
2.4 CALIBRATION OF THE CONSTITUTIVE MODEL PARAMETERS	35
2.4.1 <i>Gopalaratnam and Shah (1985) (GS)</i>	37
2.4.2 <i>Cornelissen et al (1986) (COR)</i>	40
2.4.3 <i>Numerical Experiments</i>	43
3 VALIDATION OF OLM	51
3.1 GENERAL	51
3.2 NOTCH BEAM TEST	51
3.3 SCALED DAM TEST	54
3.4 TENSION STIFFENING TEST	60
3.5 REINFORCED CONCRETE BEAM TEST	66
4 CONCLUSION	71

4.1 CONCLUSION.....	71
4.2 FUTURE WORK.....	72
REFERENCES.....	73
APPENDIX A	79
A. SEQUENTIALLY LINEAR ANALYSIS CODE.....	79
APPENDIX B.....	81
B. SEQUENTIALLY LINEAR ANALYSIS CODE WITH INITIAL LOADING.....	81

LIST OF TABLES

TABLES

Table 1. Multilinear Function Parameters and Properties of Specimens.....	48
---	----

LIST OF FIGURES

FIGURES

Figure 1.1. Concrete at Different Scales	2
Figure 1.2. Fracture Mechanics: (a); (b) Fracture Process Zone (F), linear zone (L), nonlinear zone (N); (c); (d) Fictitious Crack Model by Hillerborg (1976)	4
Figure 1.3. Truss Models in Early Ages.....	6
Figure 1.4. (a) Lattice Model and Deformation; (b) Shell Element and Equivalent Truss Lattice; (c) Three Loading Cases [Hrennikoff (1941)]	7
Figure 1.5. Fundamentals of CFT	8
Figure 1.6. (a) Stress trajectories for B and D-regions and (b) an example of elastic stress trajectories, elastic stresses and strut-and-tie-model [Schlaich et al 1987]	10
Figure 1.7. (a) Different Neighboring Circles and Their Truss Member; (b) Randomly Generated Specimen and Its Meshes; (c) Constitutive Law for Contact Region [Bazant et al 1990].....	11
Figure 1.8. (a) Basic Lattice of Square Pattern; (b) Constitutive Law for Regular Lattices [Jirasek and Bazant 1995].....	12
Figure 1.9. (a) Triangular Lattice Model [Schlangen and Van Mier 1992]; (b) The Model Projected on the Grain Skeleton; (c) Definition of Beams and (d) Crack Pattern at Crack Width of 80 μm	13
Figure 1.10. (a) Used Aggregate Distribution; (b) Corresponding Elements [Cusatis et al 2003a,b] and Results for (c) 100 mm Long and (d) 200 mm Long Specimen.....	15
Figure 1.11. (a) Interaction of Particles in Specific Distance (δ); (b) Brittle Behavior for Elements of Connecting Particles [Silling 2000]	17
Figure 1.12. Result of EMU for Concrete [Gerstle and Sau 2004].....	18
Figure 1.13. (a) First Order Micro Elastic Damage Model [Gerstle et al 2005; Gerstle et al 2007]; Interaction of Two Adjacent Particles in (b) Kinematics; (c) Kinetics Terminology [Gerstle et al 2007]	20
Figure 1.14. (a) Micropolar Constitutive Model; (b) Discretized Model of Uniaxial Tension/Compression Specimen and (c) Computed Uniaxial Stress-Strain Curve [Gerstle 2007b].....	21

Figure 1.15. (a) Softening Stress-Strain Diagram (dashed) and Saw-tooth Approximation (drawn) and (b) Result for Very Fine Mesh [Rots 2001]	23
Figure 1.16. Comparing SLA Models.....	24
Figure 2.1. Lattice Model for (a) $\delta = 1.5d$ and (b) $\delta = 3.01d$	28
Figure 2.2. Constitutive Model for Overlapping Lattice Models for Different Element Lengths.....	30
Figure 2.3. Element Constitutive Diagrams (a) Force-Strain for Different Grid Sizes; Corresponding (b) Stress-Strain Diagram and (c) Stress-Displacement Diagram.....	31
Figure 2.4. Brittle Behavior for Long Elements	32
Figure 2.5. Force-Strain Diagram of Elements for (a) Steel Elements; (b) Links Connecting Steel and Concrete Particles	33
Figure 2.6. Illustration of the SLA with Saw-Tooth Behavior	34
Figure 2.7. (a) Stress-Displacement Curve of Cornelissen et al (1986); (b) Stress-Crack Width Curve Compared with Experiments	36
Figure 2.8. Comparison Formulation and Experiments (a) Stress-Displacement for Gopalaratnam and Shah (1985); (b) Cornelissen et al (1986).....	37
Figure 2.9. Test Specimen [Gopalaratnam and Shah 1985].....	38
Figure 2.10. Force-Deformation Curves with (a) $\delta=1.5d$; (b) $\delta=3.01d$ [Gopalaratnam and Shah 1985].....	38
Figure 2.11. Damage Patterns with Different Initial Spacing with $\delta=1.5d$	40
Figure 2.12. Damage Patterns with Different Initial Spacing with $\delta=3.01d$	40
Figure 2.13. View of Test Specimen and Testing Equipment	41
Figure 2.14. Force Deformation Curves for (a) $\delta=1.5d$ and (b) $\delta=3.01d$ [Cornelissen et al 1986]	41
Figure 2.15. Damage Patterns with Different Initial Spacing with $\delta=1.5d$	42
Figure 2.16. Damage Patterns with Different Initial Spacing with $\delta=3.01d$	43
Figure 2.17. (a) Numerical Experiment Specimen; for Other Structural Problems, (b) Specimen 1 and (c) Specimen 2 (all units in mm)	44
Figure 2.18. Force Deformation Curves for (a) $\delta=1.5d$ and (b) $\delta=3.01d$ for Numerical Tests.	44
Figure 2.19. Damage Patterns for δ of (a) $1.5d$ and (b) $3.01d$	45

Figure 2.20. Stress-Change in Length Curves for Series of Direct Tension with $\delta=1.5d$	47
Figure 2.21. Stress-Change in Length Curves for Series of Direct Tension with $\delta=3.01d$	48
Figure 3.1. Experiment Geometry [Petersson 1981].....	52
Figure 3.2. Force Deflection Curve and Damage Patterns for $G_f=124$ N/m [Petersson 1981].....	53
Figure 3.3. Force Deflection Curve and Damage Patterns for $G_f=150$ N/m [Petersson 1981].....	54
Figure 3.4. Experiment Geometry [Aldemir et al 2015].....	55
Figure 3.5. Cracks in Experiments [Aldemir 2016].....	57
Figure 3.6. Load-Tip Displacement Response of OLM.....	58
Figure 3.7. Damage Patterns and Crack Lengths at Specific Points for G_f of 60,100,150 N/m for (a) $\delta=1.5d$ and (b) $\delta=3.01d$	59
Figure 3.8. Half of the Experiment Geometry	61
Figure 3.9. Different types of elements for both δ	61
Figure 3.10. Load Elongation Responses for $\delta=1.5d$ with Different Bond Strengths	62
Figure 3.11. Crack Patterns for $\delta=1.5d$ with Different Bond Strengths.....	63
Figure 3.12. Load Elongation Curves for $\delta=3.01d$ with Different Bond Strengths...	63
Figure 3.13. Crack Patterns for $\delta=3.01d$ with Different Bond Strengths.....	64
Figure 3.14. Load Elongation [Gijssbers and Hehemann 1977]. (Crack Pattern at Points Identified by Numbers are shown in Figure 3.15)	65
Figure 3.15. Damage Patterns at Specific Points (shown in Figure 3.14) and Crack Pattern by Rots (2008).....	65
Figure 3.16. Half of the Experiment Geometry (all units are in mm).....	66
Figure 3.17. Load Deflection Response for Different Bond Strengths	68
Figure 3.18. Crack Patterns for Different Bond Strengths.....	68
Figure 3.19. Load Deflection at Midspan Curve.....	69
Figure 3.20. Damage Patterns at Specific Points	69

LIST OF SYMBOLS / ABBREVIATIONS

ITZ	Interface Transition Zone
RC	Reinforced Concrete
CFT	Compression Field Theory
MCFT	Modified Compression Field Theory
RA-STM	Rotating Angle Softened Truss Model
FA-STM	Fixed Angle Softened Truss Model
STM	Strut and Tie Model
EMU	Molecular Dynamic Code developed by Silling (2000)
L_i	i^{th} Circle Length
L_j	j^{th} Circle Length
γ	Empiric Constant
r_i	Radius of i^{th} Circle
r_j	Radius of j^{th} Circle
L_m	Interparticle Contact Layer of Matrix Length
G_f^m	Fracture Energy of Contact Layer
ε_f	Fracture Strain
S_p	Peak Tensile Stress
e_p	Stretch at Peak Stress
e_f	Stretch at Complete Crack
PD	Peridynamic
δ	Horizon
\vec{f}	Pairwise Force Function
$\vec{L}(\vec{x})$	Force per Unit Reference Volume
\vec{u}	Displacement Field
t	Time
V	Particle Volume
\vec{x}	Location of Particle
\vec{b}	Prescribed Loading Force Density

ρ	Mass Density
\vec{L}	Resultant Force of a Particle
$W(x)$	Macro-elastic Energy Density
η	Relative Displacement Vectors
ϵ	Relative Position Vectors
ϑ	Weighted Average of the Extension of All the Springs Connecting x with All the Other Particle in the Body
e	Strain Energy Term
j	Scalar Valued Function
OLM	Overlapping Lattice Model
S_a, u^*	Critical Stretch Value
c_s	Spring Constant
G_o	Energy Released Rate
K	Bulk Modulus
c	Microelastic Constant
dV_i	Volume of i^{th} Particle
dV_j	Volume of j^{th} Particle
u_i	Displacement of i^{th} Particle
u_j	Displacement of j^{th} Particle
θ	Rotational Degree of Freedom
m	Moment Density
f	Force Density
SLA	Sequentially Linear Analysis
ϵ_u	Ultimate Strain
G_f	Fracture Energy
f_t	Tensile Strength
h	Crack Bandwidth
α	Reduction Factor
E	Modulus of Elasticity
d	Grid Distance
EA_t	Modulus of Elasticity*Cross Sectional Area of Truss
ϵ_x	Normal Strain in x direction
ϵ_y	Normal Strain in y direction

$Energy_{original}$	Total Elastic Energy Stored in the Original Geometry
w	Thickness
A	Volume per Unit Thickness Area into the Page
ν	Poisson's Ratio
$Energy_{OLM}$	Elastic Energy of a Truss Element
N	Element Force
L	Length of Element
ϵ_{cr}	Critical Strain
a_1, a_2, a_3	Multipliers of Strain
b_1, b_2	Multipliers of Force
F_{cr}	Critical Force
d'	Other Grid Sizes
f_{cr}	Critical Stress (i.e., Uniaxial Tensile Strength)
A_t	Pseudo Area
GS	Gopalaratnam and Shah (1985)
COR	Cornelissen et al (1986)
c_1, c_2	Normal Weight Concrete Constants
u_{ult}	Ultimate Crack Width
u	Average Crack Displacement within a Gauge Length
LVDT	Linear Variable Differential Transducer
NES	Numerical Experiment Specimen
S1	Specimen 1
S2	Specimen 2
$F_{threshold}$	Threshold Force Value
OBE	Operational Based Earthquake
MDE	Maximum Design Earthquake
MCE	Maximum Characteristic Earthquake
E_s	Modulus of Elasticity of Steel
f_{yield}	Yield Stress of Steel
ϵ_{yield}	Yield Strain of Steel
A_s	Steel Area
λ	Load Factor
λ_{min}	Minimum Load Factor

CHAPTER 1

INTRODUCTION

1.1 General

The concrete industry, which uses 12.6 billion tons (11.4 billion tonnes) of raw materials each year, is the largest user of natural resources in the world (Mehta 2002). Despite its widespread use, a detailed understanding of concrete mechanics is still not available. The modeling and the prediction of the performance of concrete structures are controversial due to its heterogeneous nature as a consequence of the highly complex microstructure. The determination of the crack initiation and propagation should provide information on structural weaknesses and retrofit regions. This makes it mandatory to understand the behavior of concrete in tension from an engineering point of view. Cracking of concrete in reinforced concrete structures is an evidence of increasing steel stresses owing to the bond between two materials. On the other hand, cracking in plain concrete structures may occur depending on the load pattern, aging or settlement. According to the locations of crack and patterns, assessment of existing structures should be conducted for a well-sustained built environment.

According to a 2013 Report Card for America's infrastructure from ASCE (2013), the infrastructure is in poor grade for USA so that the cost to repair/replace deterioration of infrastructure is estimated to be about 3.6 trillion dollars by 2020. Also, Michael Groschek, Transport Minister of North Rhine-Westphalia of Germany, mentioned that 80% of inspected 100 bridges are in desperate need to be repaired and maintained and it was estimated that some 4.2 billion euros must be invested (Der Spiegel website). Most of the damage in existing structures are somehow related to concrete cracking due to extreme repeated loads, environmental loads, corrosion or chemical attack. Hence, the prediction of damage, which means understanding and simulating the behavior of concrete in tension, is crucial for the next generation infrastructures.

Infrastructure problems will also accelerate for developing countries in the 21st century such as Turkey and China as the most of the structures such as bridges, railways etc. have started to be built by 1980s and 1990s. In this regard, finding the most suitable procedures for design and assessment plays a significant role for these structures in the short/long term.

Concrete is a complicated material due to the following reasons: 1- It is a heterogeneous material, 2- It does not follow mixture rules (Mehta 1993), 3- It exhibits significant variability. These properties make it extremely difficult to accurately track cracks. Micro cracks are dormant cracks and they usually cannot be observed in experiments. They may or may not be the cause of the main cracks and affect the load carrying capacity, durability and water tightness of concrete. The main reason for initiation of these cracks is the region surround the aggregate and cement paste (Figure 1.1). These interface regions, called as the interfacial transition zone (ITZ), are the weak zones due to higher porosity as a result of higher water/cement ratio. The available knowledge on concrete strength of ITZ is still insufficient making it extremely difficult to model concrete. Also, representation of concrete at different scales is shown in Figure 1.1.

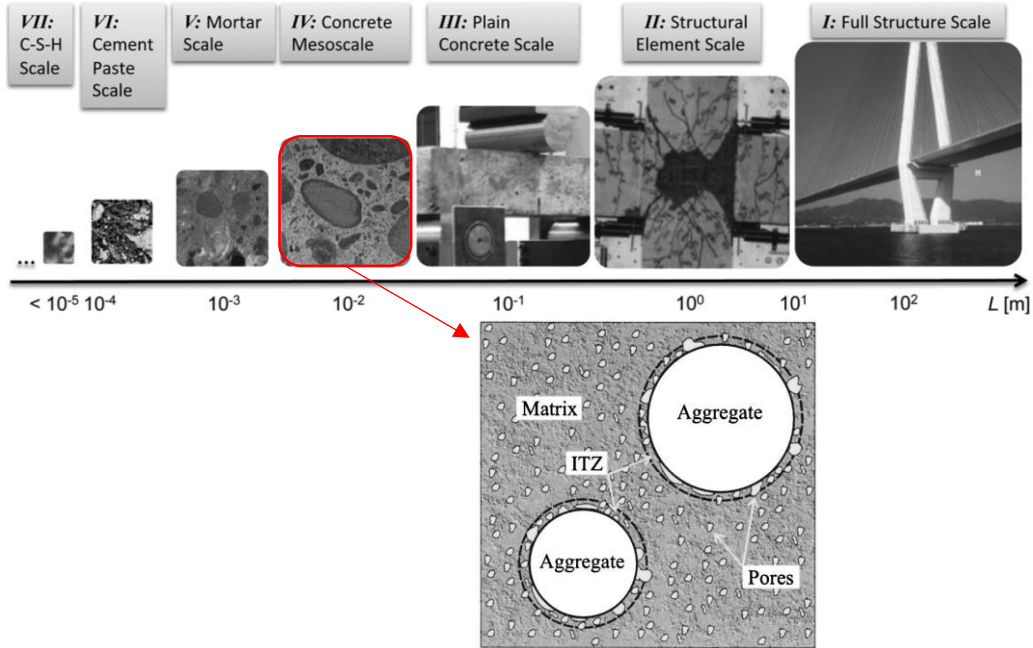


Figure 1.1. Concrete at Different Scales

1.2 Literature Review

Physical explanation of the tensile resistance of concrete is highly complicated. Foundation of (crack) fracture mechanics was developed by the pioneering work of Griffith (1920) by observing and describing the rupture of glass. Subsequently, Irwin (1958) explained the fracturing from the point of strain energy release rate and combined the idea with the Weibull's (1939) statistical approach for fracture strength. This fracture theory was incapable of describing the fracture of concrete because of the heterogeneous nature of concrete leading to a quasi-brittle response. Linear elastic fracture mechanics (Figure 1.2.a) assumes that stress suddenly drops to zero at the crack tip and this cannot be used for concrete materials (Figure 1.2.b) as concrete can still carry tensile load at the crack tip, a phenomenon introduced for the first time by Kesler et al (1971). This is mainly because of the softening phenomenon in concrete as a result of the distributed and localized cracking in order to describe the fracture of concrete, Hillerborg et al (1976) proposed a new theory named as the Fictitious Crack Model (Figure 1.2.c). He and his co-workers stated that after concrete reaches its tensile strength, stress transmitted in the cracked region can still carry tension, however with a decreasing amount in the crack surface (Figure 1.2.d). The area under the stress-crack width at Figure 1.2.d was stated as the energy absorbed for the unit area of crack. Bazant and Oh (1983) later proposed their fracture process zone approach that led to the inclusion of the stress-displacement models to describe tensile behavior with using fracture energy and characteristic length concept in numerical simulations. This approach was adopted to reduce mesh dependency of computational results.

Starting from 1960s, concrete finite element simulations were conducted in two mainstream directions. The first approach was done by adjusting the material stiffness matrix (i.e., smeared crack concept) introduced by Rashid (1968). Then this approach was modified to incorporate size effects following the Hillerborg model by Rots (1988). A two-dimensional nonlinear finite element model was used by Vecchio (1989) for monotonic simulations and by Palermo and Vecchio (2003) for cycling loading scenarios. There are essentially two methods for smeared crack models, i.e., the rotating (Rots 1988, Vecchio and Collins 1986) and fixed crack models (Willam et al 1987, deBorst and Nauta 1985) to estimate the crack initiation and propagation directions. Names refer to the concept on the orientation of the crack. For the fixed

smearred crack model, the orientation of the crack remains fixed in the direction of the first crack during all steps. On the other hand, gradual re-orientation of the crack is permitted for the rotational crack model. The main drawback of the continuum based finite element modeling whether using fixed or rotating crack models, is the inability to represent the actual separation due to cracking and operating with average strains across a gauge length rather than the reporting actual crack openings.

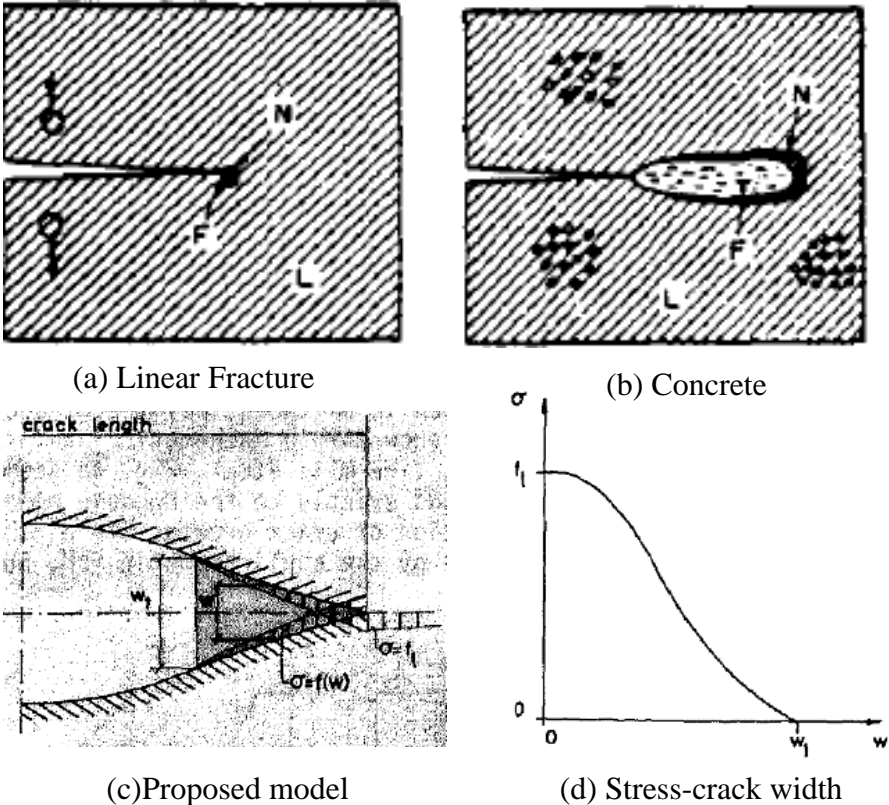


Figure 1.2. Fracture Mechanics: (a); (b) Fracture Process Zone (F), linear zone (L), nonlinear zone (N); (c); (d) Fictitious Crack Model by Hillerborg (1976)

Discrete crack models were developed to overcome the situation about the physical representation of cracking. The main idea was to discretize the element edges with special discontinuity elements at possible crack locations in the structure. Ngo and Scordelis (1967), who implemented such interface elements for the first time, placed links within the concrete for single reinforced concrete beams by using linear elastic analysis with predefined crack patterns. Later, Ingraffea and Saouma (1985) mentioned the deficiencies of this primitive discrete approach criticizing the difficulty of having to know the crack locations a priori. They developed a computer program

with a discrete crack approach and remeshing capabilities after each crack. Moreover, to enhance the discrete crack approach, Blaauwendraad (1985) proposed a technique where cracks can go into finite elements to eliminate difficulties about changing the topology of meshes. The performance of the interface elements was investigated for the cyclic behavior of concrete by Oliveira and Lourenço (2004). According to them, interface elements are essential to capture nonlinear behavior for micro-modeling of masonry structures. Koutromanos and Shing (2012) extended this approach for concrete and masonry structures under cyclic loads by using the discrete crack approach with a plasticity based constitutive model for the interfaces. Despite the apparent advantages of modeling the cracks via discrete elements explicitly, the issues of identifying crack locations a priori, remeshing, pre- and post-processing, and the necessity of defining different constitutive models for the cracks and continuum parts are the key disadvantages of discrete crack models.

Prior to the development of the finite element-based approaches, many researchers attempted to explain the force flow and load carrying capacity mechanisms in structural members. The most basic way could be thought as defining a structure by using truss networks. The pioneer of truss models, Ritter (1899), proposed the model for shear design for reinforced concrete beams. He noticed that the occurrence of cracks due to the diagonal tensile stresses, compression diagonals inclined at 45 degree as shown in Figure 1.3.a describe the load carrying mechanism through parallel chords. In parallel to this idea, Mörsch (1909) proposed his famous truss analogy for the shear transfer in reinforced concrete beams (Figure 1.3.b). Later, Mörsch (1920,1922) introduced that the angle can be different than 45 degree and employed his idea for torsion resistance of reinforced concrete beams. About the same time, Wagner (1929) presented the tension field theory to explain the behavior of thin metal webs in carrying shear in excess of their initial buckling loads. Although developed for steel plate structures, the key idea was similar to that of Mörsch (1922).

In light of the truss analogy as mentioned above, an alternative approach to discretize the continuum system was proposed by Hrennikoff (1941) by using a simple lattice truss network model (Figure 1.4.a) in the time that finite element method was not available. He calibrated the parameters for the truss elements so that the continuum has approximately similar elastic properties compared to a plane stress. This is

demonstrated in Figure 1.4.b where a shell element representing the elastic continuum and the equivalent lattice under generalized plane stress is shown. For determining the geometrical properties of the lattice members, three loading cases (pure tension in the x and y directions and pure shear) must be considered (Figure 1.4.c). Upon applying the equivalent nodal forces on the lattice network, two set of equations can be found; First Set:

$$A_1 = lw \frac{c^2 - v}{4v(1+v)c} \tag{1.1}$$

$$A_2 = lw \frac{2 - c^2 + 3v}{4(1+v)} \tag{1.2}$$

Second Set:

$$A_1 = lw \frac{2c^2 - 1 + 3vc^2}{4(1+v)c} \tag{1.3}$$

$$A_2 = lw \frac{1 - vc^2}{4v(1+v)} \tag{1.4}$$

Where $l=l_1$, $c=l_2/l_1$, w is the thickness and v is the Poisson's ratio. It can be shown that the lattice network is unique only for a Poisson's ratio of 1/3. Also, he mentioned that the results from structural analysis of the unit size were quite close to the exact solution in terms of stresses and deformations. If unit sizes were smaller, more reasonable results were taken. It was the first attempt to create a gridwork approach for continuum.

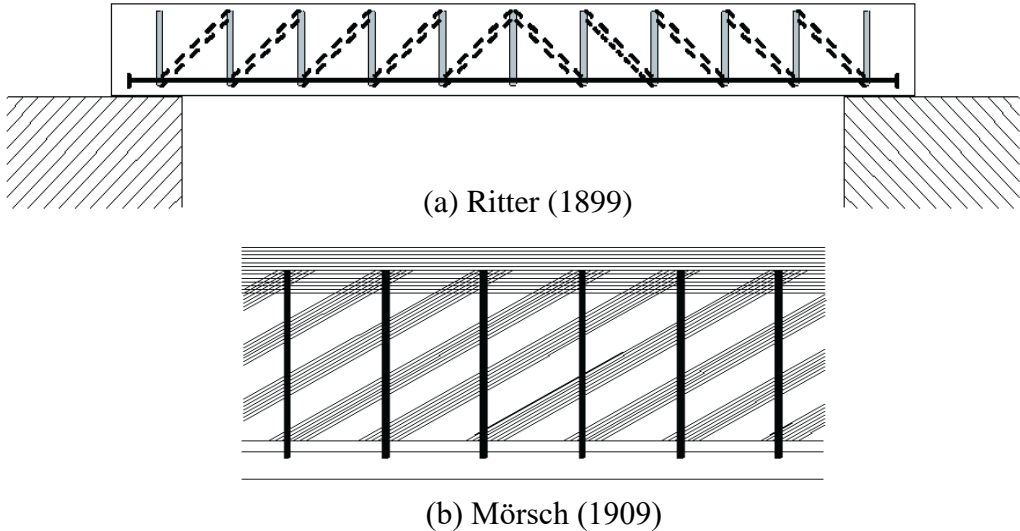


Figure 1.3. Truss Models in Early Ages

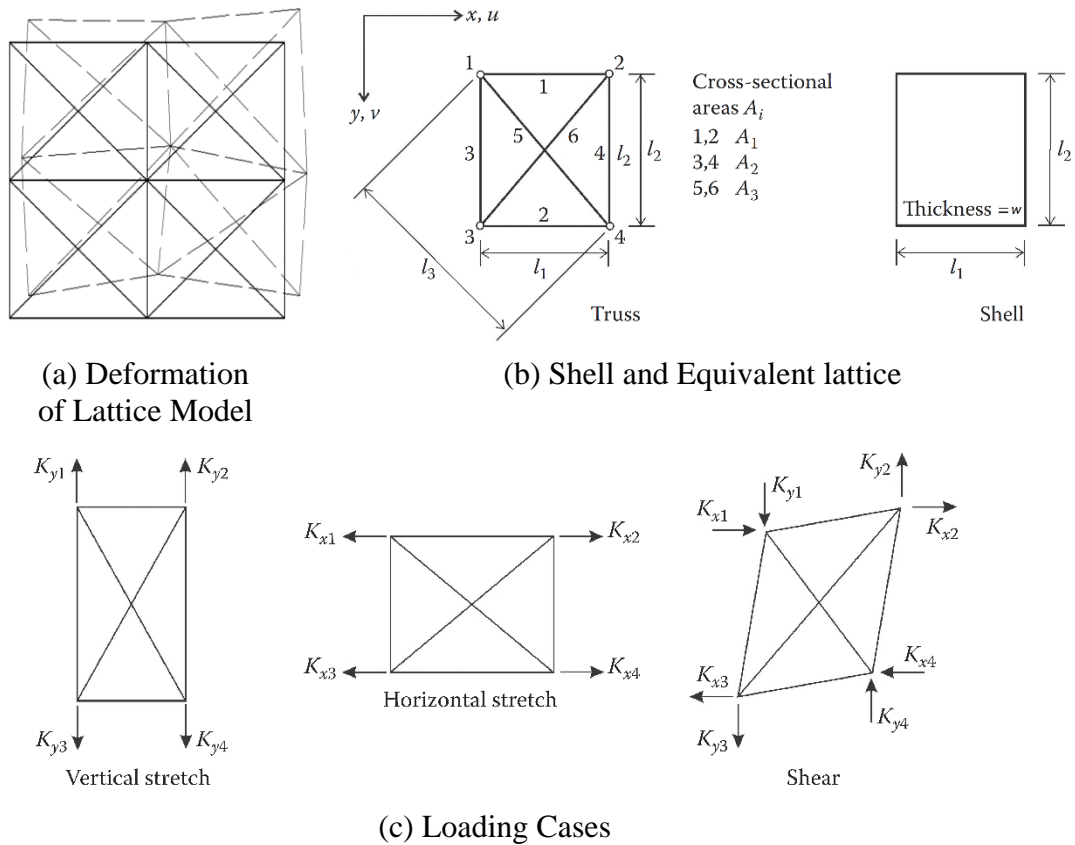


Figure 1.4. (a) Lattice Model and Deformation; (b) Shell Element and Equivalent Truss Lattice; (c) Three Loading Cases [Hrennikoff (1941)]

These remarkable early works inspired the later developments for analysis and design using trusses for RC structural members. For example, Mitchel and Collins (1974) established a new method called the Compression Field Theory (CFT). In this theory, using compatibility of the angle of the diagonal compression regions mentioned as Wagner (1929), use of equilibrium and constitutive equations for the trusses enabled to define the full range load deflection behavior of reinforced concrete. The basics of Compression Field Theory is shown in Figure 1.5. It can be observed that it was envisioned as a fully rotating smeared crack model. Principle strain direction was taken as same with principle stress direction by compromising from actual compatibility. Stress-strain model was employed in the principle stress direction as an orthotropic model. Then Vecchio and Collins (1986) validated this idea by conducting a number of experiments and finalized the Modified Compression Field Theory (MCFT) for both in shear and torsion. Around the same time, Hsu et al (1987) proposed his softened truss model. They performed a vast number of tests to understand the constitutive laws for the compression struts. Softened compression stress-strain relations and tensile

behavior of concrete and steel embedded in concrete were defined. The softened-truss model was developed with a systematic and unified manner and the response of membrane elements were simulated by using both as rotating angle softened truss model (RA-STM) (Hsu 1988) and fixed angle softened truss model (FA-STM) (Pang and Hsu 1996). In this way, the behavior of cracked concrete in shear was better described without violating compatibility.

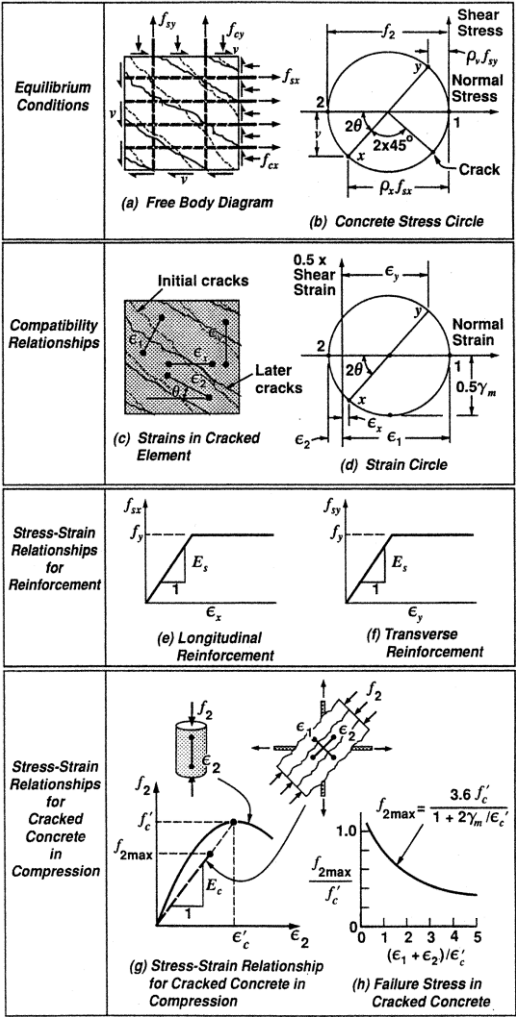
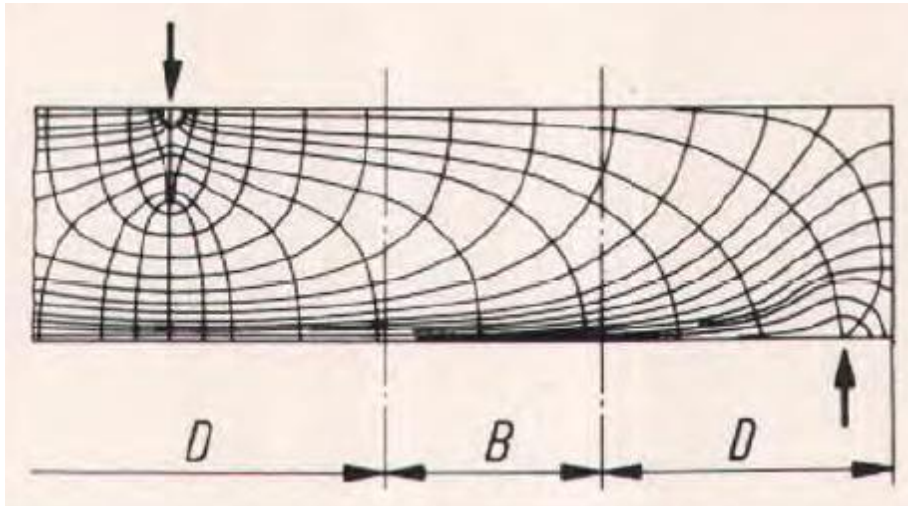


Figure 1.5. Fundamentals of CFT

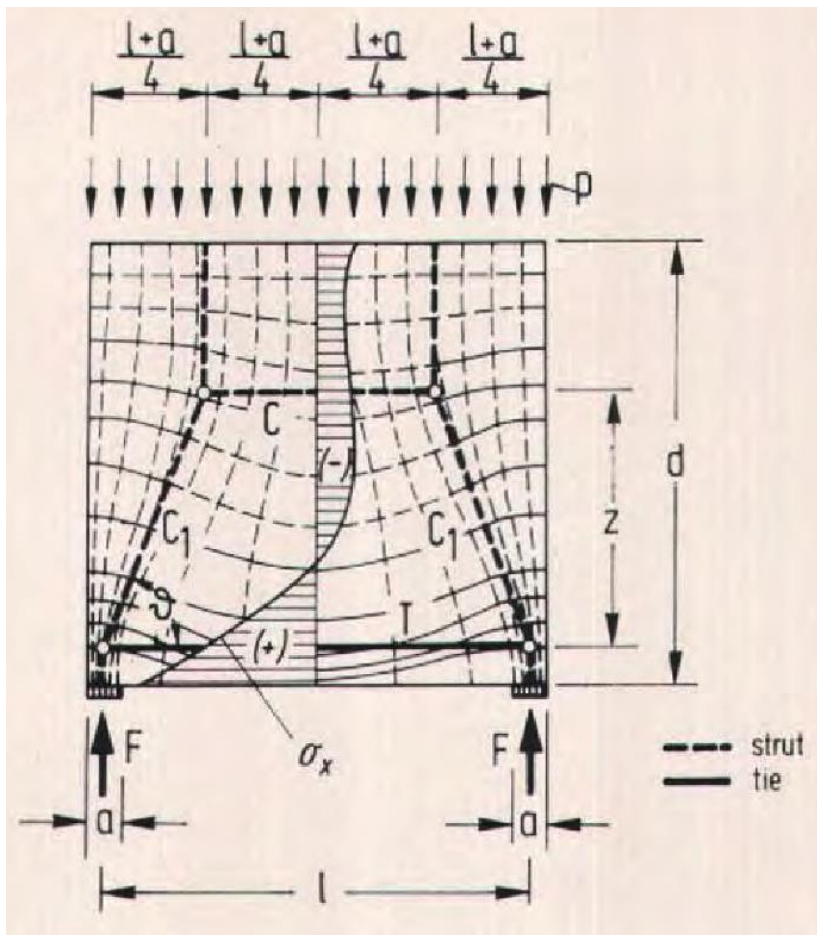
As mentioned above, explaining the force flow in design is quite important as it provides the engineers an intuitive approach. If the flow can be described by using simple components that can carry compression and tension, a handy design tool could be revised. A very intelligent approach along this line came from Schlaich et al (1987), who established a detailed design procedure named as the Strut and Tie Model (STM).

They employed the well-known truss model such that it can be used for every part (B and D-region) of the structure. The model was simple to understand because the main goal was to distribute the load applied the structure by using compression and tension members and nodes connecting them. The procedures were based on the separating the sections whether they have Bernoulli hypothesis of linear strain distribution (B-regions) or nonlinear strain distribution (D-regions). Definition of these regions were based on stress trajectories in the structure (Figure 1.6.a). An example of STM after determined stress trajectories is given in Figure 1.6.b.

These developments encouraged further seeking of such truss based models to simulate the concrete fracture. Simple lattice network that was composed of central force Hookean springs was conducted by Meakin et al (1989). The two dimensional triangular lattice model was inspired from the crack propagation model of Louis and Guinea (1987). According to them, the bond breaking probability was proportional with the strain of bond. A particle model with random generation of the system for aggregate or fiber composites was developed by Bazant et al (1990). Particles were connected with trusses and the softening stress-strain relationship was implemented at contact layers of the matrix based on the fracture energy approach. Problems due to material inhomogeneities were encountered during the simulations. For the fracture modeling, the softening of the particles were studied in detail. Substantially, their model was similar to Burt and Dougill (1977)'s random truss model. The trusses were constructed with nodes with randomly generated circular particles as can be shown in Figure 1.7.a-b. The lengths were determined by the two interaction circles as $L_i = \gamma r_i$ and $L_j = \gamma r_j$ where γ taken as 0.9 empirically and the two dimensional cross sectional areas of the truss were taken as $2 \min(r_i, r_j)$. The softening behavior was defined in the region of the matrix within a circle with the length of L_m . The employed triangular stress strain relationship is given Figure 1.7.c. For the relationship, the fracture energy concept was used with G_f^m . The main idea was to make the area under the triangular stress-displacement curve constant for every length because energy dissipation must be same with regard to fracture energy concept. This was done by calibrating the strain value (ϵ_f) of the complete crack.



(a) Stress Trajectories



(b) An example of STM

Figure 1.6. (a) Stress trajectories for B and D-regions and (b) an example of elastic stress trajectories, elastic stresses and strut-and-tie-model [Schlaich et al 1987]

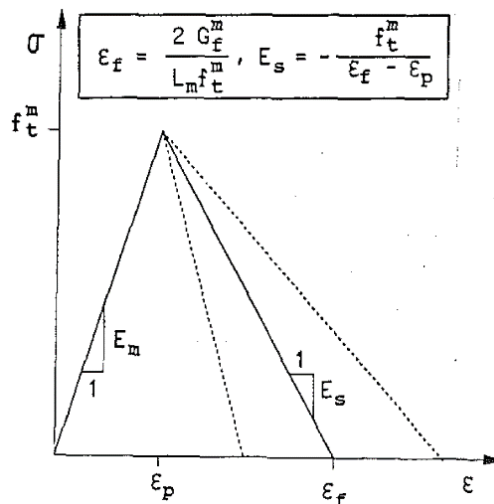
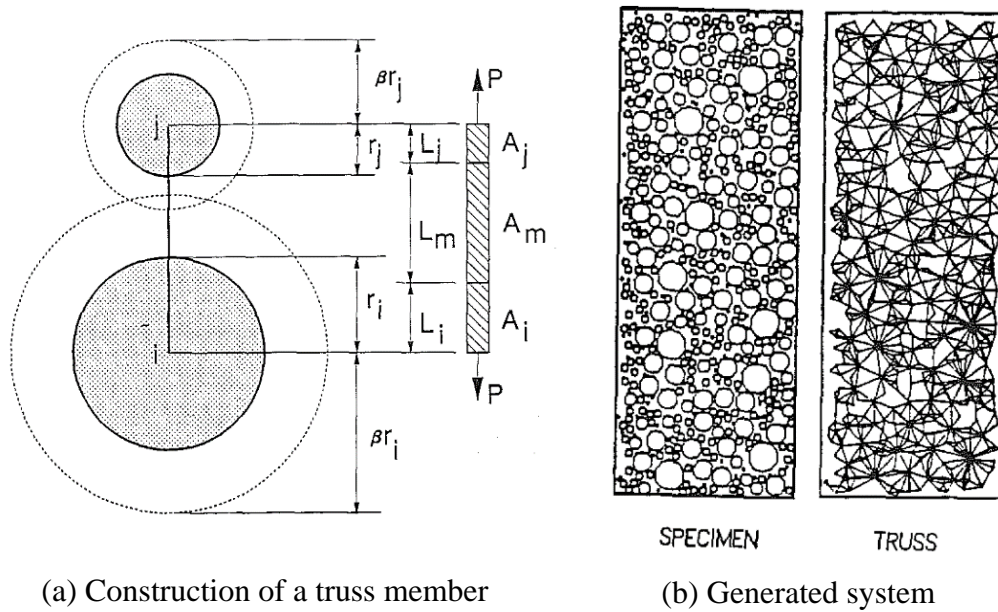


Figure 1.7. (a) Different Neighboring Circles and Their Truss Member; (b) Randomly Generated Specimen and Its Meshes; (c) Constitutive Law for Contact Region [Bazant et al 1990]

Jirasek and Bazant (1995) developed a particle model for quasibrittle fracture of solids with zones of distributed cracking and applied this model for ice with brittle and highly heterogeneous nature. The model incorporated the heterogeneity of sea ice which can be thought to be analogous to heterogeneity observed in concrete. They developed the model at the micro level by using a micro truss network. Due to the lack of data on the distribution of ice heterogeneity, the particle sizes were same for the model and a simple lattice geometry was used (Figure 1.8.a). In the micro level, a constitutive law

for ice particles were used to simulate the interaction between the ice floe and rigid particles. A three parameter force displacement model was defined for the elements as shown in Figure 1.8.b. where tensile threshold S_p , element stretching at peak stress e_p and element stretching at forming complete crack e_f were needed. Strength and fracture properties of the four principle and two diagonal elements were adjusted to provide optimum approximation of isotropy. The idea was to hold the maximum force per unit length fixed in each direction of cracking. It was needed to overcome the directional bias of crack propagation in the model. Explicit integration for the solution of the equation of motion was used. It was concluded that using a regular lattice network gave directional prejudice through the line that had lattice elements. Providing different strength values of the elements could not solve this type of problem regarding cracking whereas randomly generated particles gave reasonable agreement in terms of the isotropic fracturing.

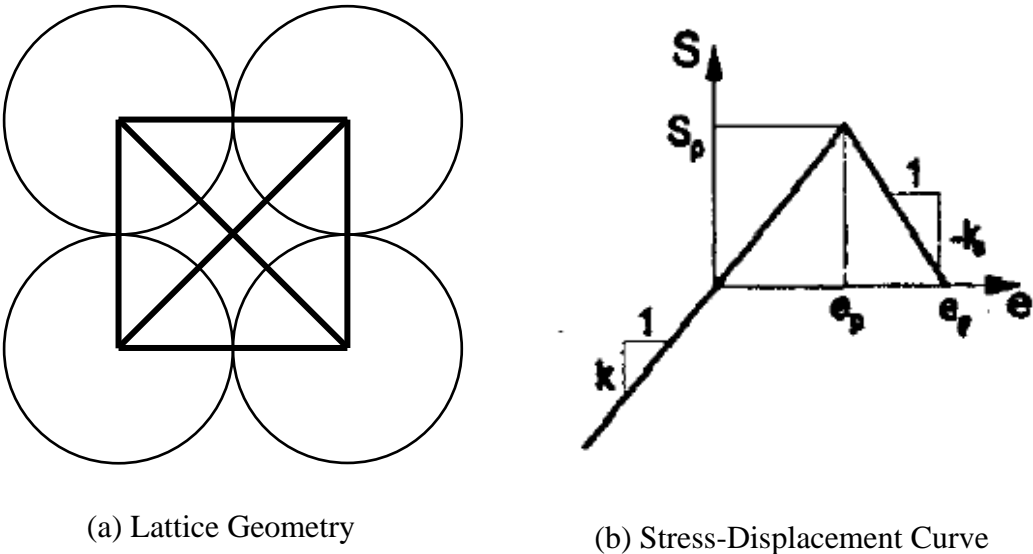


Figure 1.8. (a) Basic Lattice of Square Pattern; (b) Constitutive Law for Regular Lattices [Jirasek and Bazant 1995]

A regular lattice network modeling approach was studied by Schlangen and Van Mier (1992). Direct tension experiments with single edge notches based on the work of Herrmann (1988) was used for validation. The model constituted a triangular lattice model (Figure 1.9.a) with brittle breaking beams. The analysis process was conducted by removing beam elements from the mesh when it reached its maximum tensile strength computed based on beam theory. The heterogeneity of concrete was defined

by providing a distribution for the bar strength and stiffness. Another alternative considered was to generate numerical grain distribution either manually or using statistical tools so that strength and stiffness of the beams would be assigned (Figure 1.9.b). The beams were assigned three different properties representing aggregate particles, binding matrix and the interface between the matrix and the aggregate (Figure 1.9.c). The simulation result are presented in Figure 1.9.d demonstrating the crack propagation around aggregates.

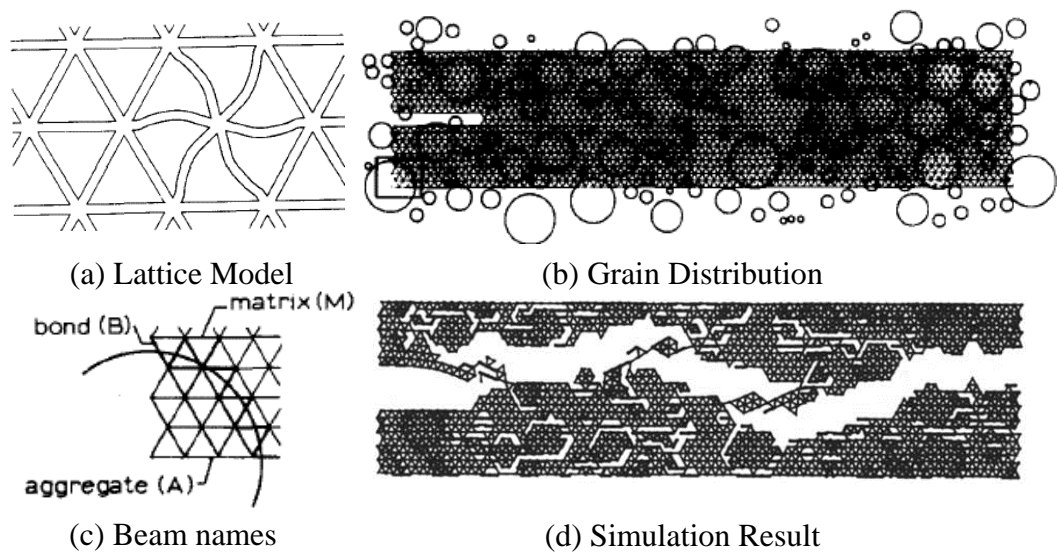


Figure 1.9. (a)Triangular Lattice Model [Schlangen and Van Mier 1992]; (b) The Model Projected on the Grain Skeleton; (c) Definon of Beams and (d) Crack Pattern at Crack Width of 80 μm

Schlangen and Garboczi (1996) proposed a 2D lattice model by using beam elements to simulate shear test conducted by Nooru-Mohammed (1993). The beam elastic properties were determined based on the calculation of the elastic energy stored within a unit cell of the lattice. The effect of orientation of the lattice geometry was also investigated. Influence of the element types (i.e., spring elements, spring and shear elements and beam elements with regular triangular networks) was studied and use of beam elements due to necessity of the elements with three degree of freedom in complex crack patterns. A random lattice model was also studied to simulate heterogeneity. Regular lattice network caused different crack patterns but the random mesh enabled the objectivity at the crack propagation. The main reason of the inability

of the demonstration of the actual crack pattern was the high directional constraint of regular lattice networks occurring naturally.

All of the lattice networks explained above employed beam or trusses for the lattice models. Cusatis et al (2003) argued that models calibrated according to only mode I fracturing (i.e., tensile cracking) were incapable of predicting other modes of fracture. A three dimensional lattice was used for their simulations by defining the response separately in tensile and compression. The elements were connected between adjacent aggregates which were distributed randomly. The model was different than the previous models as the particles were connected with both axial and shear springs. Cusatis et al (2003) argued that bending of beam like lattice networks (as in Schlangen and Van Mier 1992) could not reflect the real physics at the micro structures. ITZ region affects the properties of concrete at the macroscale. Thus; in mesoscale, discretization of this region was not implemented because it caused a high increase in the number of unknowns and expensive computations. The interaction of ITZ and mortar interaction was considered by using two elements coupled in series providing an indirect simulation. Behavior of ITZ and of mortar (or cement paste) was considered with common constitutive law of the element that connect particles. The experiment conducted by van Vliet and van Mier (1995) was used to calibrate the parameters of the model (Figure 1.10.a-b.) Results with these calibrated parameters of this model are shown in Figure 1.10.c-d. Two bounds of the experiments and numerical simulations were about the frictional stresses at the end of the specimens. According to this stress value, both peak stress and post peak load deflection response were influenced. Results from the numerical solution were in good agreement with the experiments.

A lattice model approach was implemented by Van Mier (2013) recently at the mesoscale. He modeled concrete explicitly by modeling aggregates, cement paste and ITZ separately with different material constants. Hence, the lattice network was described as a multi-scale approach for concrete simulations. This approach was successful for simulations of experiments but it was computationally expensive.

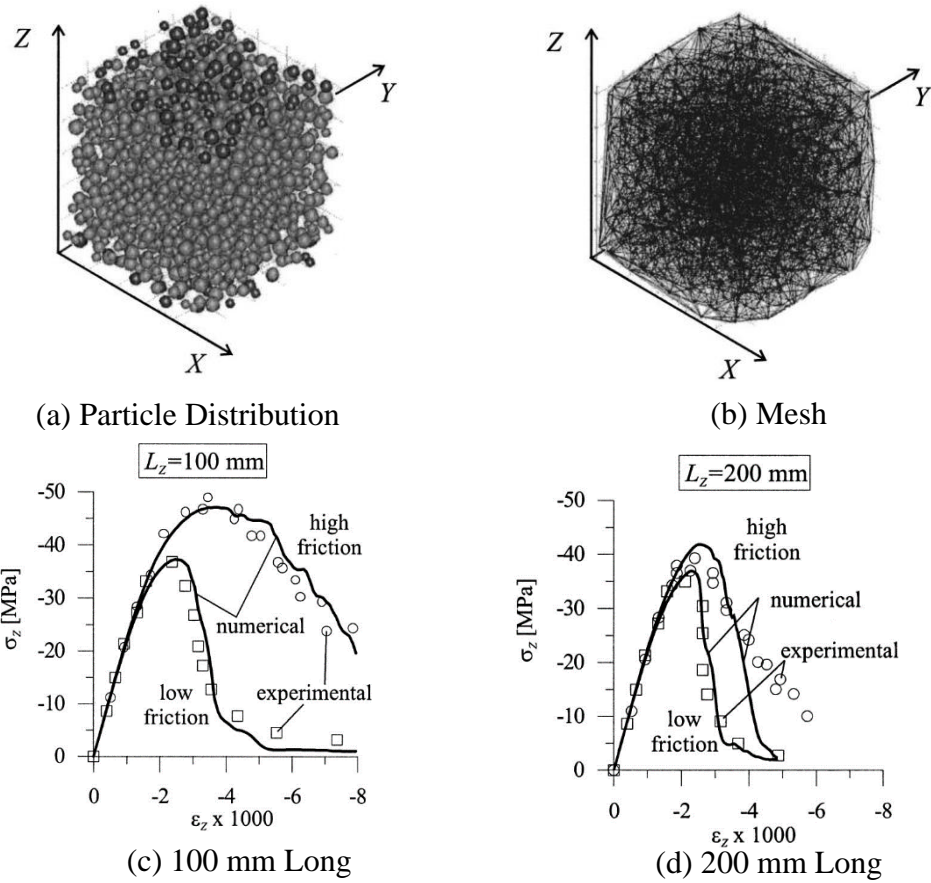


Figure 1.10. (a) Used Aggregate Distribution; (b) Corresponding Elements [Cusatis et al 2003a,b] and Results for (c) 100 mm Long and (d) 200 mm Long Specimen

Nonlocal and continuum aspects of numerical models have been investigated by many researchers. Silling (2000) mentioned that the main problem in solid mechanics was the discontinuity resulting from cracking. Classical approaches used partial derivatives arising from relative displacement and forces. The main advantage of his proposed model so called bond-based peridynamics (PD) was the integration rather than differentiation to determine the forces for a material particle by using the Newton's second law of motion applied for every infinitesimally small particle at a specific region. Accordingly, by using the relative displacement of two adjacent particles, a pairwise force function was proposed. The idea of the particle interactions was that a particle can interact with other particles within a specific distance creating the model nonlocality. This distance was called as the "material horizon (δ)" (Figure 1.11.a). Horizon was the most important parameter determining the nonlocality of the system, meaning that higher fine horizon corresponds to more nonlocal interactions. The original formulation for PD is shown in Eq. 1.5;

$$\vec{L}(\vec{x},t)=\int_{\mathbb{R}} \vec{f}(\vec{u}(\vec{x}_j,t)-\vec{u}(\vec{x}_i,t), \vec{x}_j-\vec{x}_i)dV_j \quad \forall \vec{x} \in \mathbb{R}, t \geq 0. \quad (1.5)$$

More concisely,

$$\vec{L}(\vec{x})=\int_{\mathbb{R}} \vec{f}(\vec{u}_j-\vec{u}_i, \vec{x}_j-\vec{x}_i)dV_j \quad \text{on } \mathbb{R} \quad (1.6)$$

Where \vec{f} is the pairwise force function arising from each pair of particle interaction, $\vec{L}(\vec{x})$ is the force per unit reference volume due to interaction with other particles, \vec{u} is the displacement field, t is time, V is particle volume and \vec{x} is the location of the particle. The PD equation of motion was used as Eq. 1.7;

$$\rho \vec{u}=\vec{L}+\vec{b} \quad \text{on } \mathbb{R}, \quad t \geq 0. \quad (1.7)$$

Where \vec{b} is some prescribed loading force density, ρ is the mass density, \vec{L} is the resultant force of a particle within δ .

There were restrictions on the Poisson's ratio due to the fundamental mathematical background of preliminary PD model Silling (2000). In the bond-based PD model, the Poisson's ratio was limited to 1/3 and 1/4 for the two- and three-dimensional problems, respectively. Restrictions on the Poisson's ratio for homogeneous deformations of linear isotropic materials could be eliminated with some adjustments. It would require fundamental changes of $\vec{L}(\vec{x})$. The main alteration was the modification of the macro-elastic energy density as given in Eq. 1.8;

$$\overline{W}(\mathbf{x})=W(\mathbf{x})+e(\vartheta(\mathbf{x})) \quad (1.8)$$

where

$$\vartheta(\mathbf{x})=\int j(|\mathcal{E}|)|\mathcal{E}+\eta| dV' \quad \text{on } \mathbb{R} \quad (1.9)$$

η is the relative displacement vectors, \mathcal{E} is the relative position vectors, the value of ϑ is a weighted average of the extension of all the springs connecting x with all the other particles in the body, e is the function of a volume dependent strain energy term and j is scalar valued function. Poisson's ratio was restricted if only for the bond between two particles interactions was thought. However; adjustment of the original PD models was done by changing the idea of the calculation of the strain energy density from the interaction of just two particles to include local volume change (Macek and Silling 2007). In other words, bond properties depend on stretch of all neighboring particles to overcome the restriction of Poisson ratio.

As the internal length approached zero for a problem with no damage, the method converged to results obtained with classical continuum mechanics. PD was capable of representing linear theory of elasticity if the response function was used with the vanishing length scale (Silling et al 2003). PD could be thought as springs or trusses connected between particles in the material horizon according to Silling (2000) (Figure 1.11.b). For brittle materials that exhibited no tension softening, after a bond broke, points at the ends of the bond were disconnected from each other. Damage was incorporated in the pairwise force function by allowing bonds to break when elongation was exceed. Wave propagation in solid mechanic was also studied by using PD. A PD formulation was developed to understand behavior of an infinite bar subjected to a self-equilibrated load distribution by Silling et al (2003). According to the study, the model had two main advantages: i-Discontinuities were included without any special treatment or as a priori, ii- Thanks to material horizon concept, forces could be transferred within a long range of particles.

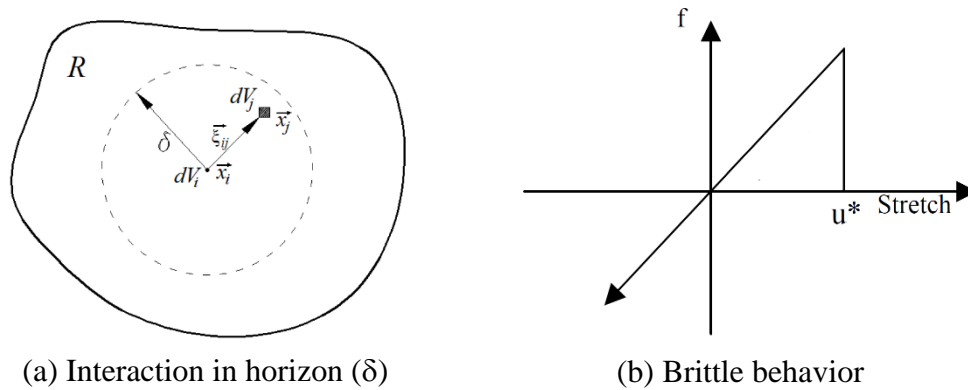
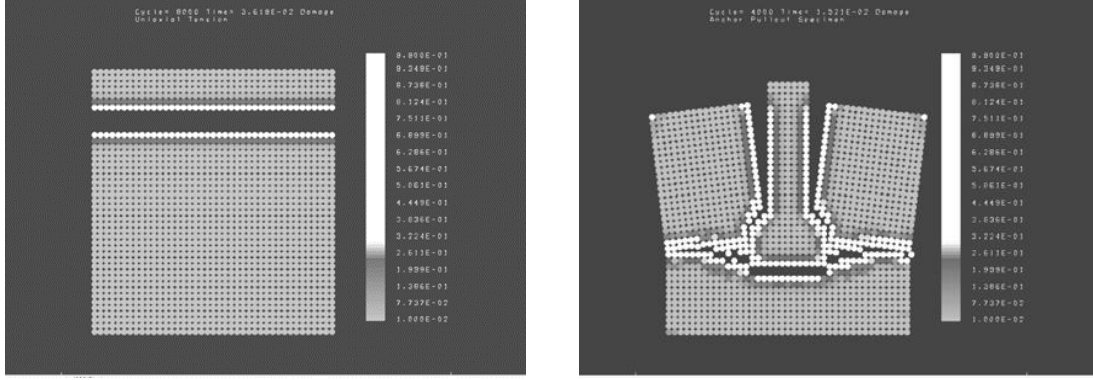


Figure 1.11. (a) Interaction of Particles in Specific Distance (δ); (b) Brittle Behavior for Elements of Connecting Particles [Silling 2000]

The PD of Silling works on multiple scale of modeling and did not need any stress-strain concepts. Gerstle and Sau (2004) used this model to simulate concrete for the first time. Simulations of plain and reinforced concrete was proposed by using the EMU (Silling 2000) a molecular dynamics code. A micro elastic PD model was used for concrete which connected particles as shown in Figure 1.11.b. The modeling of a specimen in uniaxial tension and an anchor pullout problem were conducted and the tensile fracture was simulated (Figure 1.12.).



(a) Uniaxial Tension

(b) Anchor pullout

Figure 1.12. Result of EMU for Concrete [Gerstle and Sau 2004]

Constitutive models in PD was discussed by many other researchers in 2000s. For example, Silling and Bobaru (2005) proposed a constitutive model for the tearing and stretching of rubbery sheets to simulate membranes. PD was capable of simulating bond softening/breakage and the resulting load redistribution was calculated with the solution of the equation of motion. This enabled the method to simulate autonomous multi-crack initiation, interaction, and propagation, and the consequential anisotropy. When the bonds were represented with lines, the bond-based PD can be viewed as an overlapping lattice model (OLM) as defined in the title of this work. Silling and Askari (2005) attempted to find critical stretch value, s_0 (shown in Figure 1.9.b. as u^*). First, the required energy released rate, G_0 , to break all the bonds per unit fracture area was found by Eq. 1.10;

$$G_0 = \frac{\pi^2 c_s s_0^2 \delta^5}{10} \quad (1.10)$$

$$c_s = \frac{18K}{\pi \delta^4} \quad (1.11)$$

where c_s is the spring constant, K is the bulk modulus. Solving these two equations for the critical stretch value, Eq. 1.12 is obtained;

$$s_0 = \sqrt{\frac{5G_0}{9K\delta}} \quad (1.12)$$

Moreover, the horizon could be thought as the interaction between the atoms or molecules in nanoscale. However, for PD in macroscale, horizon was recommended as three times the grid spacing. A horizon longer than the recommended value is shown to create excessive wave dispersion while requiring very expensive computations (Silling and Askari 2005). Gerstle et al (2005) employed PD for plain and reinforced

concrete elements subjected to different loadings. A zeroth-order micro elastic damage (i.e., brittle response) was used. For materials that exhibited tension softening, the bond force could be a nonlinear function of elongation. They also determined breaking stretch, s_0 (shown in Figure 1.9.b. as u^*), with objectively by using fracture energy concept for their brittle constitutive model with the Eq. 1.13;

$$S_0 = \frac{2}{\delta^2} \sqrt{\frac{G_f}{ct}} \quad \text{for 2D} \quad (1.13)$$

where δ is the material horizon, c is a micro elastic constant.

In order to overcome the limitation on the Poisson's ratio (i.e., 1/3 in 2D, 1/4 in 3D), a number of approaches were developed. Silling et al (2007) enhanced the PD model with the idea of a state concept which was called later as "State-Based Peridynamic Model". The model was a generalization of the bond based PD augmented by the deformation and force states by using the principle of virtual work. In state-based PD, the response of material points was dependent on the deformation of a region. Collective behavior of all the points was used to determine the material response.

The bond based PD model was generalized for concrete and other quasibrittle structures by Gerstle et al (2007). The model was called as "micro-polar peridynamic model". The main idea was to implement extra moment density with a pairwise force density. They changed the "micro-truss" model to a "micro-beam" one with both axial and bending stiffness. In Figure 1.13.b, i and j represent adjacent particles and dV_i and dV_j are volumes of the particles. Classical approach already had u_i and u_j which are displacements of the particles whereas in the micro-polar model, rotational degree of freedom (θ_i, θ_j) was added. Obviously, the moment densities (m) and the force densities (f) were combined (Figure 1.13.c). The first order micro elastic damage model (Figure 1.13.a) was implemented as a constitutive model by Gerstle et al (2007). In order to decrease the computational cost, the model was implemented in a finite element framework by using implicit solution algorithm for parallel processing. Then the micro-polar PD model was enhanced by Gerstle and coworkers (Gerstle et al 2007a, Gerstle et al 2007b, Gerstle et al 2009). Different constitutive models for the bonds which connect two close particles within the horizon were conducted to represent the fracture mechanics of concrete. An example of using micropolar constitutive model for concrete proposed by Gerstle et al (2007b) are shown in Figure

1.14.a. This model was used for uniaxial specimen. Discretized model of this specimen is shown in Figure 1.14.b. The response from simulation and damages are shown in Figure 1.14.c with the color coding presented in constitutive model curve. Blue curve represents the results of the micropolar peridynamic simulation; red curve represents a typical laboratory response.

Researchers have chosen different models for PD. For example, after proposed micropolar PD model, Mitchell (2011) developed a state-based model as a nonlocal ordinary perfect plasticity model. Also, in 2013, Beckmann et al used bond based PD model by using trusses to model of the system under thermal load. The PD model with increasing horizon ensured the increase of directions reducing the grid-dependency of results commonly observed in lattice models. The model could be used for flow problems using general state based PD formulations as well. (Katiyar et al 2014).

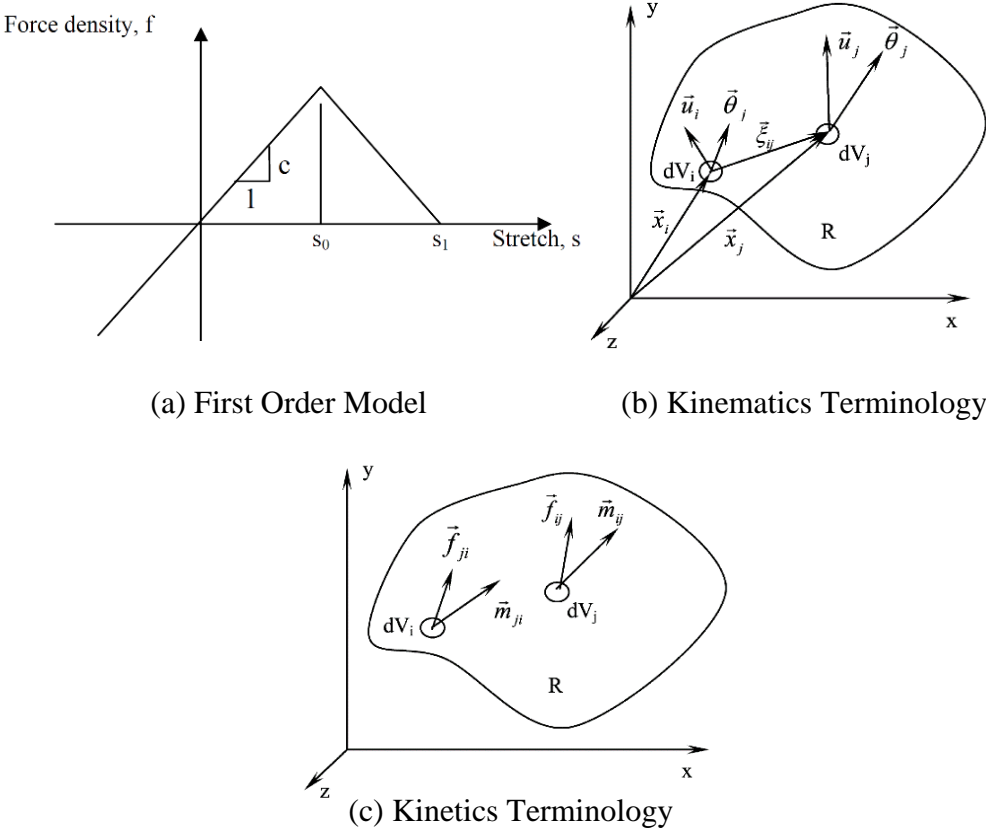
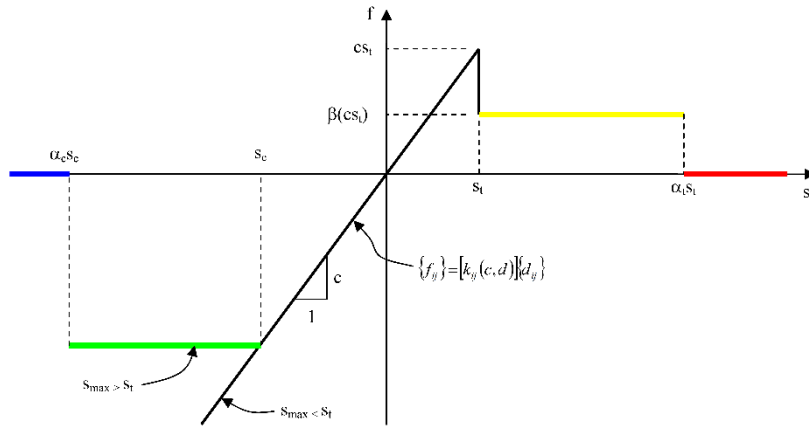
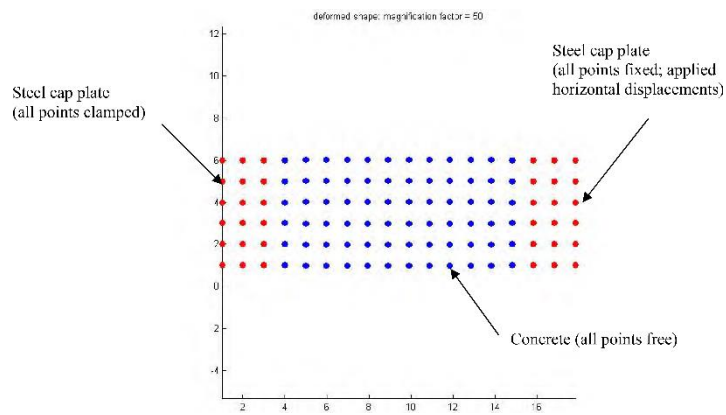


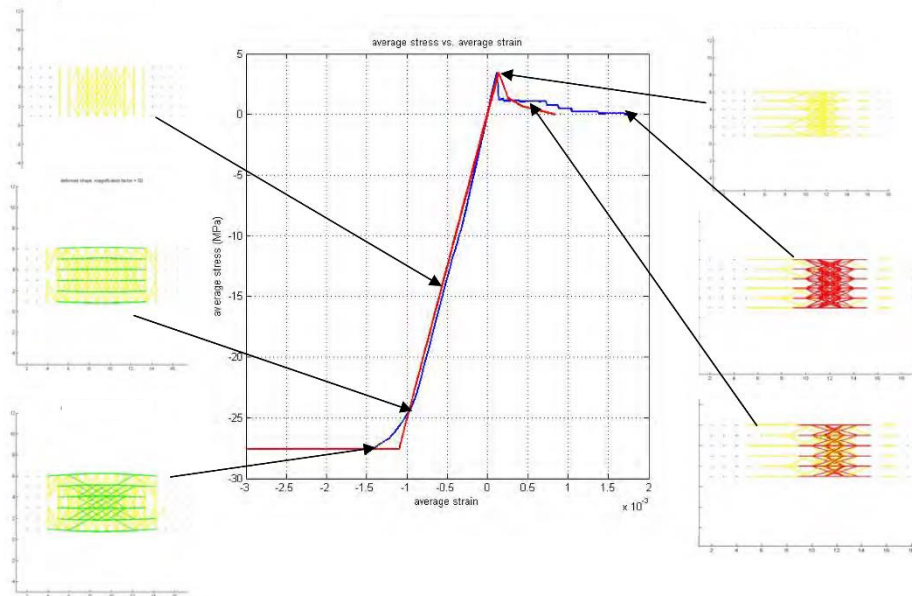
Figure 1.13. (a) First Order Micro Elastic Damage Model [Gerstle et al 2005; Gerstle et al 2007]; Interaction of Two Adjacent Particles in (b) Kinematics; (c) Kinetics Terminology [Gerstle et al 2007]



(a) Micropolar Constitutive Model



(b) Uniaxial Specimen



(c) Computed Stress-Strain Curve

Figure 1.14. (a) Micropolar Constitutive Model; (b) Discretized Model of Uniaxial Tension/Compression Specimen and (c) Computed Uniaxial Stress-Strain Curve [Gerstle 2007b]

In order to solve the nonlinear response for crack propagation simulations, methods such as Newton-Raphson, arc length methods etc are commonly employed. Such algorithms are prone to convergence problems due to severe softening and snap-back response that can be observed in the simulation of quasi-brittle materials. In order to overcome these limitations, the load deformation response of the system modeled with an overlapping lattice approach in this study was solved by using the Sequentially Linear Analysis (SLA) as proposed by Rots (2001). It is a solution method for nonlinear problems and offers a simple to a nonlinear problem as there is no convergence problems due to the softening or snapback phenomena. This provides an important advantage over other solution strategies.

A similar approach based on an element removal algorithm was successfully used by Schlangen and van Mier (1992) as explained before. Rots (2001) used SLA approach to solve structural mechanic problems within a finite element framework for the first time. Instead of removing elements, a softening function was used with a fracture mechanics framework by Rots (2001) (Figure 1.15.). The main procedure can be outlined as follows;

- External force is applied to the system as a unit load
- Linear elastic analysis is performed
- Critical element which has the highest value of current stress divided by its current strength is found
- Load factor, λ , that is the ratio of the strength and stress level is the scale value by which unit load elastic solutions are multiplied
- The stiffness and strength of critical element is reduced according to its constitutive model
- The procedure is repeated in a damage controlled manner

This procedure represented a saw-tooth curve. In SLA, the analysis sequence was controlled by the damage imposed on the most critically stressed element as opposed to direct force or displacement control. Series of linear elastic solution were always implemented rather than working with negative incremental slopes. This type of solution method always converges.

Fracture energy which was taken as the area under the stress displacement curve was used to determine the ultimate strain, ϵ_u in Eq. 1.14;

$$\epsilon_u = \frac{2*G_f}{f_t*h} \quad (1.14)$$

where G_f is the fracture energy, f_t is the tensile strength and h is the crack band width. Modulus of elasticity of the critical element was reduced with arbitrary reduction factor, α . Afterwards, new strength was found by using this new Young's modulus and constitutive diagram. A saw-tooth curve was proposed for an initial Young's modulus E of 38000 N/mm^2 , initial tensile strength f_t of 3 N/mm^2 , fracture energy G_f of 0.06 N/mm , crack band width h of 5 mm and a reduction factor α of $1/2$ with 10 steps by Rots (2001) as shown in Figure 1.15.a. ϵ_u was found as 0.008 by using Eq. 1.14. The result of an analysis of a notched beam conducted with a very fine mesh is also shown in Figure 1.15.b.

DeJong et al (2008) further extended this method for non-proportional loads within a finite element framework. SLA is easy to program as it only requires elastic analysis with no iterations and is capable of obtaining the response even with a snapback behavior. The analysis results are usually jagged as given in Figure 1.15.b due to the sequential elastic nature of the analysis and the solution obtained is accepted as the envelope of the response curve.

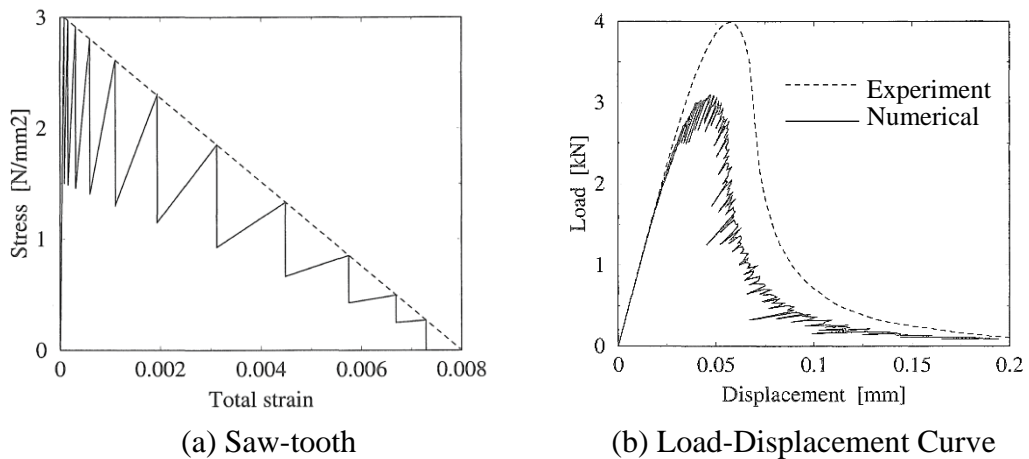


Figure 1.15. (a) Softening Stress-Strain Diagram (dashed) and Saw-tooth Approximation (drawn) and (b) Result for Very Fine Mesh [Rots 2001]

There are some alternative robust SLA models proposed by Rots (2008) to solve other structural problems in the literature. Revised and first implemented models were compared. The main reason for the requirement to construct revised model was to employ the actual fracture energy in the stress strain response. In the previous approach, the energy dissipation observed in constitutive model was taken from the area under saw tooth curve and it was different than the actual fracture energy depending on the chosen reduction factor for the modulus of elasticity. Thus, the new model was conducted to overcome this misrepresentation. A constitutive model was constructed according to the given fracture energy with Eq. 1.14. The graphical representation on the previous and the updated models are shown in Figure 1.16. In the revised version, the energy dissipation could be matched to the actual fracture area defined by the model if the tensile strength of the curve was taken as slightly more than the actual one.

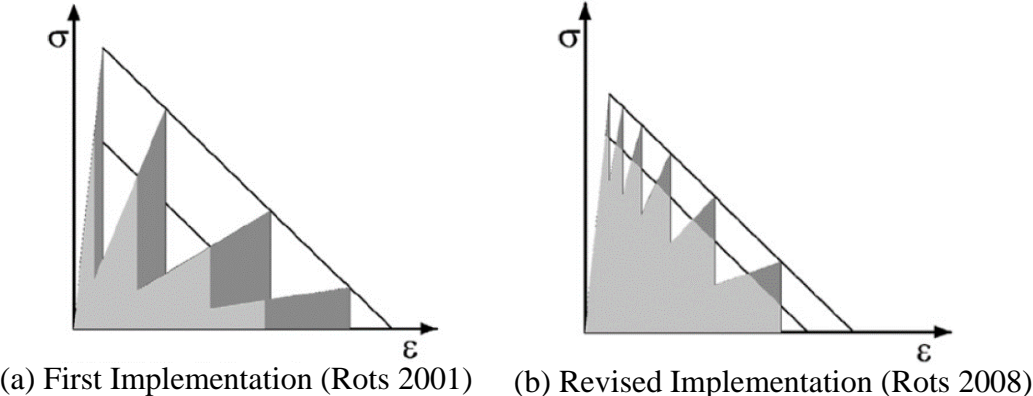


Figure 1.16. Comparing SLA Models

These studies demonstrate that the fracture energy concept for concrete and its simulation techniques are recently shifting from the finite elements to particle and lattice based methods. The main concern for this direction is to obtain a good prediction of the actual crack patterns and response of the structures. Classical structural analysis technique has not been implemented into the lattice framework including the horizon concept of the PD by any researchers. Combining these two concepts leads to a decrease in the computational efforts to solve full structural problems. In addition, we could not find published research on calibration of the

softening response observed in average length of the concrete for microscale in the literature until this time.

1.3 Objective and Scope

This study provides a new computational approach named as the overlapping lattice model to simulate the autonomous fracture initiation and propagation in concrete media. It follows the truss network analogy to model the concrete and borrows the idea of using different horizon distances in connecting nodes from peridynamics. The study is conducted at the mesoscale (i.e., few millimeters of mesh resolution), however the concrete continuum is treated as a single phase medium to preserve engineering practicality. In contrast to the approaches presented in the literature, a new calibration approach is presented while retaining the grid size objectivity. The sequentially linear analysis (SLA) technique is employed for all simulations. The success of the proposed approach and its potential in simulating structural problems is discussed. The objectives of the study are:

- To propose an overlapping lattice model along with the appropriate constitutive models and their calibrations
- To validate the overlapping lattice model for crack propagation and response in unreinforced concrete
- To validate the overlapping lattice model for the prediction of the response of reinforced concrete.

The details of the overlapping lattice model are explained in Chapter 2. In this chapter, the calibrations of element constitutive model are also presented. In Chapter 3, the validation of the Overlapping Lattice Model for several structural experiments in literature for both the plain and reinforced concrete cases is presented. Finally, in chapter 4, some conclusions and future works are drawn.

CHAPTER 2

OVERLAPPING LATTICE MODELING

2.1 General

In this chapter, the overlapping lattice model (OLM) is explained. Afterwards, the constitutive model is presented along with the Sequentially Linear Analysis (SLA) used for the nonlinear solutions. Calibration of softening parameters for constitutive models is conducted by simulating uniaxial tension tests along with numerical experiments.

2.2 Overlapping Lattice Model Approach (OLM)

In the proposed OLM, each node interacts with points within a predetermined distance called horizon (δ) to account for the nonlocal effects. For the two-dimensional problems defined with uniformly distributed particles separated by a grid spacing, d , in x , y directions, a particle located away from its neighboring elements is connected to 8 and 28 nodes for δ of $1.5d$ and $3.01d$, respectively (Figure 2.1.a-b). To consider the optimum horizon, δ was commonly taken slightly more than three times d in the previous studies (Silling and Askari 2005). With such a horizon, the number of elements connected to a node within the δ can better represent the formation of cracks at various directions despite the use of a structured grid. The horizon ($3.01d$) is chosen slightly larger than $3d$ in order to take all the nodes including those at a distance of $3d$. Using a horizon size longer than $3.01d$ may lead to take very large computational times due to exponential increase in the number of elements. For example, the simulation time of the direct tension test discussed in Section 2.4.1 for a grid size of 3 mm, 10202 total number of elements and $1.5d$ horizon is 168 seconds. The computation time increases to 1800 seconds upon increasing the model to $3.01d$ horizon with 34702 elements. On the other hand, computational time increases to 25922 seconds when the grid size is reduced from 3 mm to 1 mm for a $1.5d$ horizon. Simulations were conducted with Intel Core i7-4720 HQ processor and 16 GB ram. A classical structural analysis approach to treat the interaction forces between nodes was used for

simulations as opposed to the explicit integration commonly used in the particle based approach. This approach was confirmed to be valid by Macek and Silling (2007).

The slope of the linearly elastic segment EA_t (modulus of elasticity times cross sectional area of truss elements) can be obtained from simple energy principles. First, a deformation field introduced to estimate the elastic properties of elements in OLM (for example $\epsilon_x = \text{constant}$, $\epsilon_y = 0$). ϵ_x is taken as an arbitrary constant by giving deformation in the x direction i.e., multiplying every node only x location (i.e., $1 + \epsilon_x$). Then, the total elastic energy, $\text{Energy}_{\text{original}}$, stored in the original geometry is computed using the modulus of elasticity as shown in Eq. 2.1 for the plane stress problems. Appropriate modifications should be made for plane strain problems.

$$\text{Energy}_{\text{original}} = \frac{E \cdot \epsilon_x^2 \cdot w \cdot A}{2 \cdot (1 - \nu^2)} \quad (2.1)$$

Above E is the modulus of elasticity, ϵ_x is strain in the x direction, w is the thickness of the system, A is the volume per unit thickness area into the page (i.e., multiplying w and A give the volume of the system), ν is the Poisson's ratio taken as 1/3 for 2D, 1/4 for 3D.

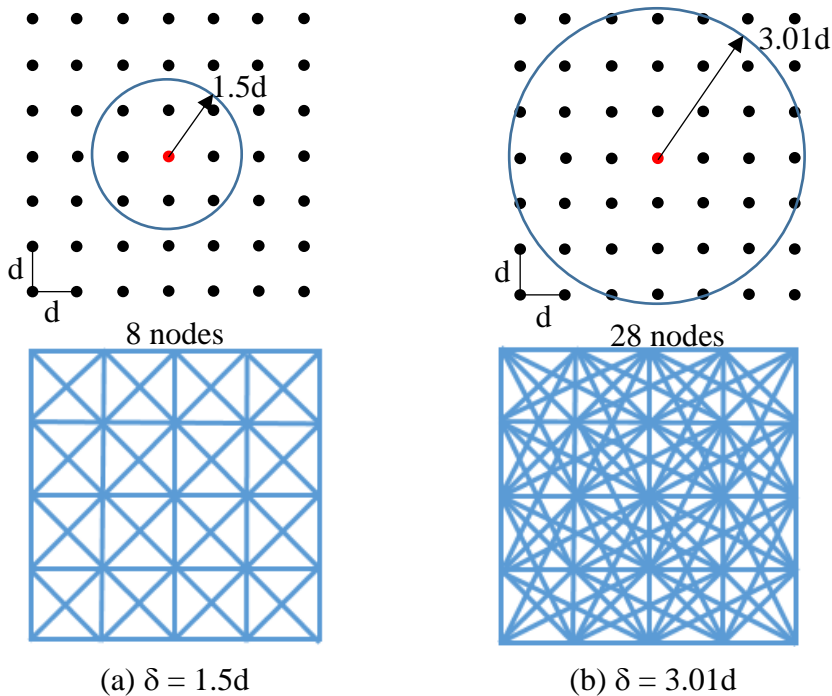


Figure 2.1. Lattice Model for (a) $\delta = 1.5d$ and (b) $\delta = 3.01d$

The deformation field from the OLM obtained by summing all the energy from lattice elements gives the total elastic energy, $Energy_{OLM}$. While computing $Energy_{OLM}$, EA_t was taken as 1. The elastic energy of a truss element is calculated by Eq. 2.2 due to the induced deformation field;

$$Energy_{OLM} = \frac{N^2 L}{2} \quad (2.2)$$

where N is element force and L is length of the element. The stored energy was proportional to the total elastic energy computed as the sum of all individual truss elements multiplied by EA_t . Therefore, EA_t can be computed as the ratio of original energy in the elastic system subjected to the deformation field by the energy of the lattice network with $EA_t=1$ as given in Eq. 2.3;

$$EA_t = \frac{Energy_{original}}{\sum Energy_{OLM}} \quad (2.3)$$

The same procedure is repeated for the deformation field in the y direction by using ε_y instead of ε_x in Eq. 2.1. Total elastic energy was computed by Eq. 2.2. EA_t value was then found by using Eq. 2.3. It is concluded that $Energy_{original}$ and $Energy_{OLM}$ values are close to each other for both directions as anticipated due to isotropy of the system.

Stiffnesses of all trusses in OLM were taken constant as EA_t , which can also be viewed as the slope of the force-strain diagram. It should be noted that EA_t computed above is the product of modulus of elasticity of concrete and A_t , which is a pseudo area that enforces the system to dissipate elastic energy similar to the energy in the elastic continuum. The modulus of elasticity for tension and compression are taken the same due to the assumed isotropy of the system.

The proposed OLM employs a multilinear softening force deformation response for truss elements. As concrete exhibits tension softening, beyond a critical strain (or cracking strain, ε_{cr}), the element can transfer further tension described with the softening function as shown in Figure 2.2. Nonlinear tension softening function is assumed to be in the form of a stepwise linear softening. The force-strain diagram is used for the structural analysis (instead of a stress displacement response), as EA_t is already available from the previous energy calibration. As can be seen in Figure 2.2, there are five material model parameters which are multipliers of critical force (b_1 and b_2) and strain (a_1 , a_2 and a_3), F_{cr} , and ε_{cr} . The material model parameters for the tension

behavior of the truss elements are calibrated by using the approach presented below. Concrete in compression is assumed to be elastic as the focus of this research is the failure due to cracking or steel yielding. Compression performance of OLM is not studied within the scope of this thesis. It should be mentioned that compression failure in concrete is also related with cracking in different directions. However; detailed studies focusing on compressive failure simulations are needed in order to generalize the proposed OLM.

In order to minimize the mesh size dependency, a fracture energy regularization is proposed. The parameters of the softening functions are determined for the element with the smallest length (i.e., orthogonal elements in Figure 2.1) to avoid brittle behavior of the longer elements as explained later in detail. For other elements, strain values in the softening part are decreased in proportion to the ratio of lengths (i.e., d/L). The fracture energy is the energy required to open a unit area of crack surface and it is taken as a material property independent from the size of the structure. This energy is the area under the stress-displacement response of the concrete. According to CEB-FIB Model Code 1990, fracture energy is related to maximum aggregate size and compressive strength of concrete. So, for truss elements with lengths other than the minimum length of an element (d), a_1 , a_2 and a_3 values are multiplied by d/L so that the area under the force-displacement response for each truss member is approximately the same as illustrated in Figure 2.2.

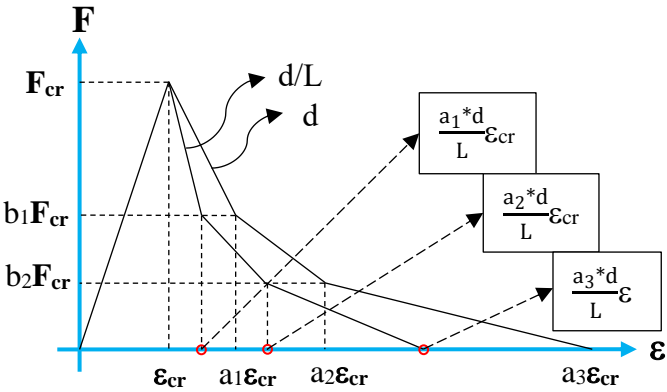


Figure 2.2. Constitutive Model for Overlapping Lattice Models for Different Element Lengths

The length scaling procedure described above is also applied for different grid sizes, (d' shown in Figure 2.3), different than the grid size d to ensure the incorporation of

size effect. The fracture energy concept is applied similarly for a different grid size by ensuring same stress-displacement curve for all member sizes. It should be noted that for a grid size different than d , F_{cr} value can be different (Figure 2.3.a) because of a different EA_t value computed from energy balance. ϵ_{cr} is taken a material property and is computed from f_{cr}/E . However, A_t may change depending on the grid size which can result in a different force-displacement response as shown in Figure 2.3.a. F_{cr} value can be computed as $f_{cr} * A_t$. To conclude, for all members regardless of their grid size or mesh size, critical stress and strain values, fracture energy and stress-displacement curves are same in the proposed OLM.

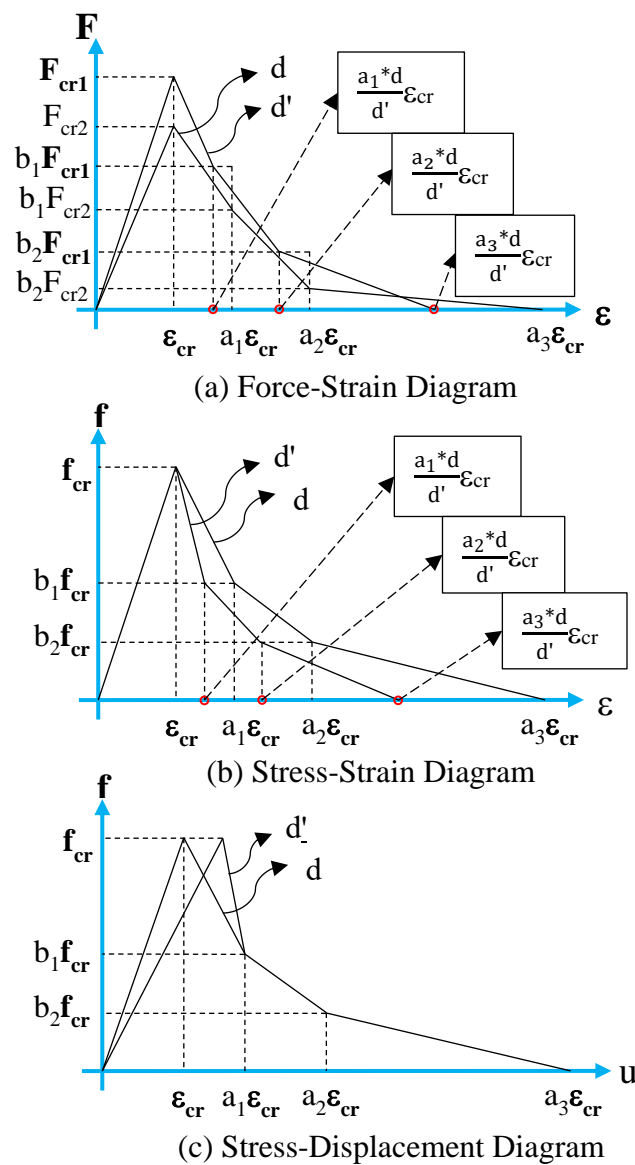


Figure 2.3. Element Constitutive Diagrams (a) Force-Strain for Different Grid Sizes; Corresponding (b) Stress-Strain Diagram and (c) Stress-Displacement Diagram

The proposed approach outlined above is a mesoscale approach (i.e., elements in the order of few millimeters). This requires modeling of the force displacement response of the concrete ingredients to relate the meso- and macro-scale response instead of taking ITZ, cement paste and aggregates separately. However, an engineering approach, where the truss elements have similar force-deformation response curves, a homogenized continuum was assumed in this study. In this way, the number of parameters was kept to a minimum while providing a global match of the force-deformation response along with the crack propagation pattern.

When long elements exist in the OLM, then there is a potential of snap-back behavior for force-strain response. For this case, brittle behavior was assumed i.e., sharp drop is employed for that element as seen in Figure 2.4. For reinforced concrete simulations, steel elements are assumed to have elastic perfectly plastic load-strain response (Figure 2.5.a.). Elements connecting steel and concrete nodes must also be calibrated. For steel-concrete connecting elements, studies indicate that all connecting elements could be assumed to carry at least 70% of the tensile critical force of concrete (f_{cr}) ensure perfect bond. Accordingly, an elastic perfectly plastic load-strain response is assigned to elements connecting to steel and concrete nodes (Figure 2.5.b). This requirement is found to be necessary to stop pullout of steel from concrete. In addition, strain hardening was not considered for steel elements as the conducted simulations for RC structures in this study do not experience strain values beyond the onset of strain hardening.

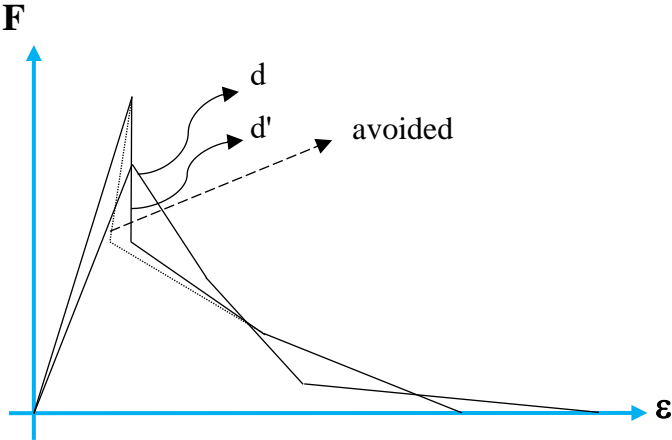


Figure 2.4. Brittle Behavior for Long Elements

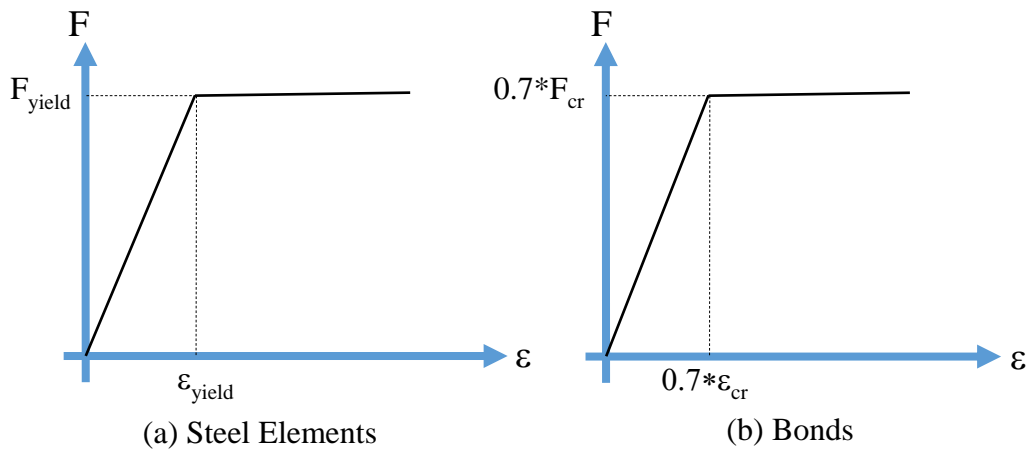


Figure 2.5. Force-Strain Diagram of Elements for (a) Steel Elements; (b) Links Connecting Steel and Concrete Particles

2.3 Sequentially Linear Analysis and The OLM Simulator

SLA is chosen as the solution algorithm in this study. SLA has the following advantages;

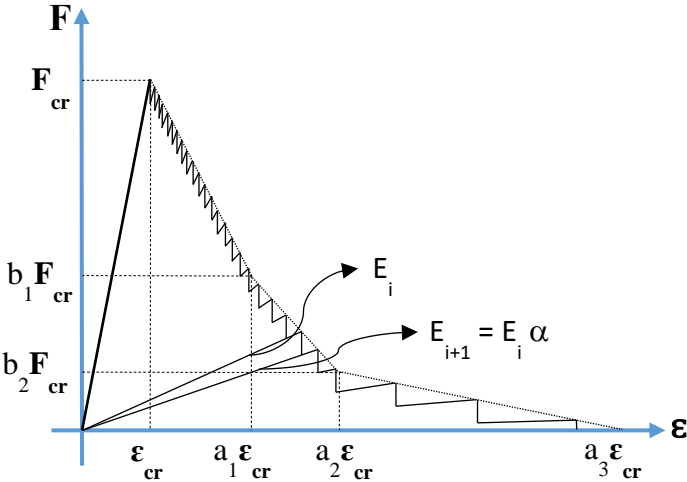
- i- SLA ensures that results are obtained even for snapback type response
- ii- SLA is easy to implement and run
- iii- SLA is quite suitable for the calibration of constitutive model with steep softening function

In this thesis, the 2001 version of SLA was used (Rots 2001). The main object is not to enhance the state of the art of SLA, but rather use it as a simulation tool. Illustration of the saw-tooth curve for the constitutive law can be seen in Figure 2.6 for concrete and steel elements. The reduction factor of modulus of elasticity, α , is taken as 0.995 in all the simulations. This step reduction is much smaller than the number used by Rots (2001). The reason of selecting such a small α is for accuracy with a reasonable computation time. After EA_t reaches to $EA_r \cdot 10^{-3}$, α is taken as 0.8. In this way, EA_t is reduced faster for completely failed elements to increase the efficiency of the computational method.. In reinforced concrete simulations, the reduction of EA_t for steel is taken as 0.9.

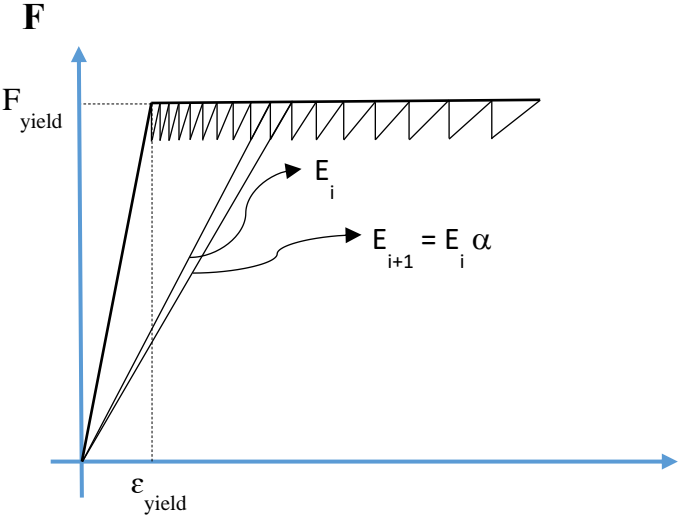
A computer program was developed to automatically create the OLM with a predetermined element size and δ , to conduct SLA steps with a preconditioned

conjugate gradient iterative solver for the solution of the algebraic set of equations. The code was slightly different compared to the earlier SLA implementations. For example, force ratios to determine load factor were used instead of using stress ratios as discussed in Rots (2001). Algorithm of the code is given in Appendix A.

The provided essential input needed for the overlapping lattice simulations are E , tensile strength (f_{cr}) and the fracture energy (G_f) obtain from traditional material tests. In addition, the multilinear softening function parameters (a_1, a_2, a_3 and b_1, b_2) of the truss elements are also required for the calibration of the constitutive model (Figure 2.6.a).



(a) Concrete Elements



(b) Steel Elements

Figure 2.6. Illustration of the SLA with Saw-Tooth Behavior

2.4 Calibration of The Constitutive Model Parameters

The preliminary simulations revealed that the softening function of truss elements, when selected from the available softening models in the literature, cannot provide accurate tensile response predictions mainly due to the local nature of the OLM. It is well known that all available softening models were derived from average displacement measurements from tension tests and cannot reflect the meso-scale response of concrete in tension. An example to explain the local nature of the OLM can be given from stretching the OLM model in the Figure 2.1.a. When the overlapping trusses are stretched in one direction, series of two diagonal and one orthogonal members are in tension. Combining the responses of these members give the total response of the specimen. Thus, assigning total response of the specimen in a gauge length as a member response can be a misrepresentation. Therefore, the fracture energy concept for explaining the stress displacement response of concrete in tension cannot be related with the individual lattice members directly. Furthermore, the softening parameters cannot be directly taken from a typical tension test due to the absence of reliable test data with densely located local displacement measurements similar to the overlapping lattice grid. Therefore, tensile stress-average displacement (within a specific gauge length) curves can be employed to calibrate the multilinear softening function parameters. For different grid sizes, the length scale can then use to adjust the input stress-strain function similar to the approach used in the mesh regularization in finite element simulations (Bažant and Oh 1983). Afterwards, structural member simulations are performed by using the input material properties and calibrated softening function parameters.

The first set of calibrations were performed by using the tension test results of Gopalaratnam and Shah (1985) (GS), and Cornelissen et al (1986) (COR). In order to consider a larger notch for the model, a numerical test simulation was conducted. GS and COR simulation results were compared with their experiment results. Thus, for numerical experiments due to the lack of experimental data, the stress-displacement model of Cornelissen et al (1986) (Figure 2.7.a) given in Eq. 2.4. was employed as the “representative” test result for the softening part and the calibration of the input parameters conducted based on those results.

$$\frac{f(u)}{f_{cr}} = \begin{cases} \left(1 + \left(c_1 \frac{u}{u_{ult}}\right)^3\right) \exp\left(-c_2 \frac{u}{u_{ult}}\right) - \frac{u}{u_{ult}} (1 + c_1^3) \exp(-c_2), & 0 < u < u_{ult} \\ 0, & u_{ult} < u < \infty \end{cases} \quad (2.4)$$

where

$$u_{ult} = 5.136 * \frac{G_f}{f_{cr}} \quad (2.5)$$

f_{cr} is the uniaxial tensile strength, and c_1 and c_2 values are the constants. u_{ult} is the ultimate crack width, G_f is the fracture energy and u is the average crack displacement within the gauge length. Cornelissen et al (1986) conducted these experiments using both lightweight and normal weight concretes. In this study, normal weight concrete considered so c_1 and c_2 constants were taken as 3 and 6.93, respectively. The accuracy of this equation is shown in Figure 2.7.b by comparing it with test results. Elastic part was added to Figure 2.7.a in order to obtain full stress-displacement plot. G_f and tensile strength, f_{cr} , parameters are the necessary parameters to construct the stress displacement plot. Finally, the measurement length and the net cross section area of specimen (i.e., notch region) are needed to obtain results for a given gauge length. GS and COR experimental results and predictions from Eq. 2.4 and 2.5 are compared in Figure 2.8.a-b. The results are in very good agreement stating that this formulation can be used as “representative” test results.

Three uniaxial direct tension tests were simulated by using OLM to calibrate the multilinear softening function parameters. Two of them are from experiments (GS and COR) and the other from numerical experiments. The simulations were conducted for different δ (1.5d and 3.01d) and grid sizes.

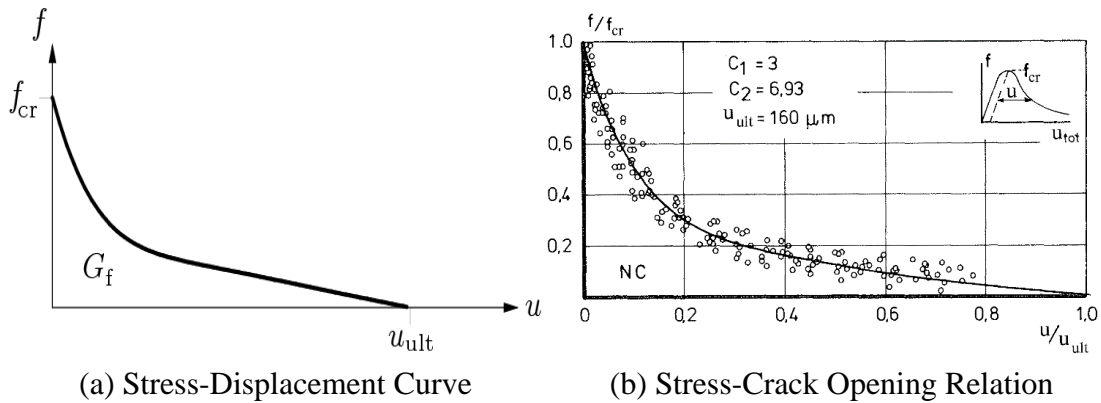


Figure 2.7. (a) Stress-Displacement Curve of Cornelissen et al (1986); (b) Stress-Crack Width Curve Compared with Experiments

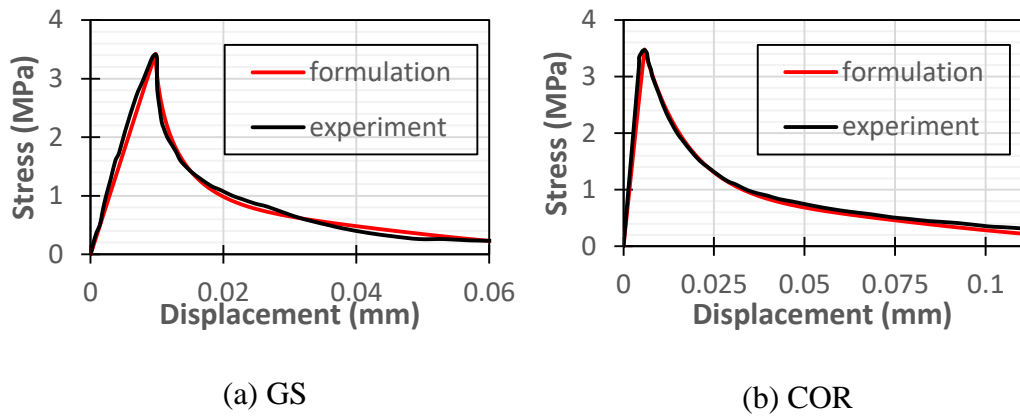


Figure 2.8. Comparison Formulation and Experiments (a) Stress-Displacement for Gopalaratnam and Shah (1985); (b) Cornelissen et al (1986)

2.4.1 Gopalaratnam and Shah (1985) (GS)

A specimen was tested to observe softening response of plain concrete in direct tension by GS (1985). The rectangular prism specimen had dimensions of 76 mm x 19 mm x 305 mm. The test specimen is shown in Figure 2.9. Notches at both side had heights of 13 mm and width of 3 mm. E , f_{cr} , and G_f values are taken as 29.1 GPa, 3.41 MPa, 0.054 kN/m from test results. The measurement gauge length of the experiment was reported as 83 mm. In the comparisons of simulation results, the closest points to the measurement length used in the experiment were used. The displacement differences between these two points were calculated to determine the change in length. For uniaxial tension test simulations, average changes in the lengths of the left end, right end, and midpoint were recorded.

The test specimen was modeled with a grid spacing, d , of 1 mm. Afterwards, the optimum parameters for a_1 , a_2 , a_3 , b_1 , and b_2 that minimized the difference between the reported and computed fracture energies were determined with a tolerance of 10% (difference between the areas under stress-displacement responses of experiment and simulations). Simulations were also conducted for grid spacing of 3 mm, 5 mm and 15 mm in δ of 1.5 d . In addition, 1 mm and 3 mm grid spacings were used with for δ of 3.01 d in the simulations. Whenever an OLM analysis was performed with an initial spacing other than 1 mm for GS, a_1 , a_2 and a_3 values were computed with the ratio of the length scales (a_1 , a_2 and a_3 decreased proportional with increasing element length)

as explained in Section 2.2. Therefore, the smallest grid size for a given δ always dictated the selection of a_1 , a_2 and a_3 . Simulations showed that the best match was obtained when b_1 and b_2 values were kept constant as explained later.

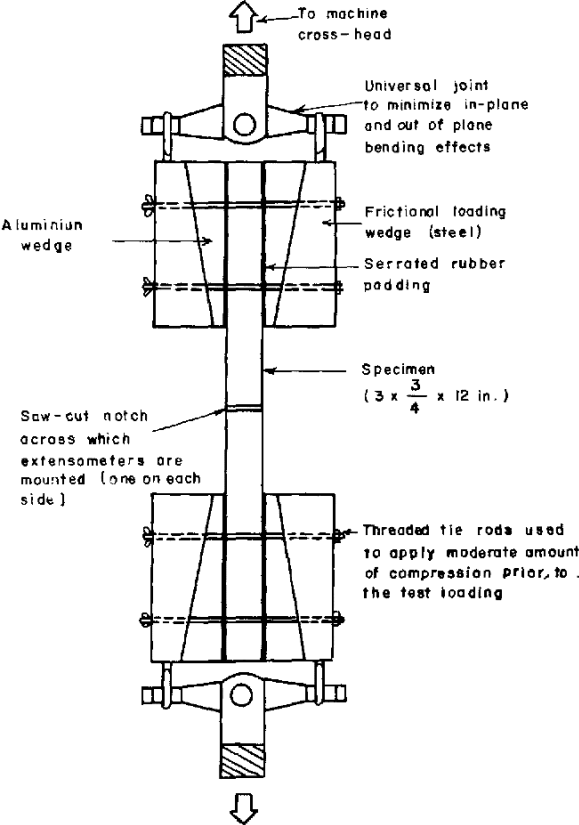


Figure 2.9. Test Specimen [Gopalaratnam and Shah 1985]

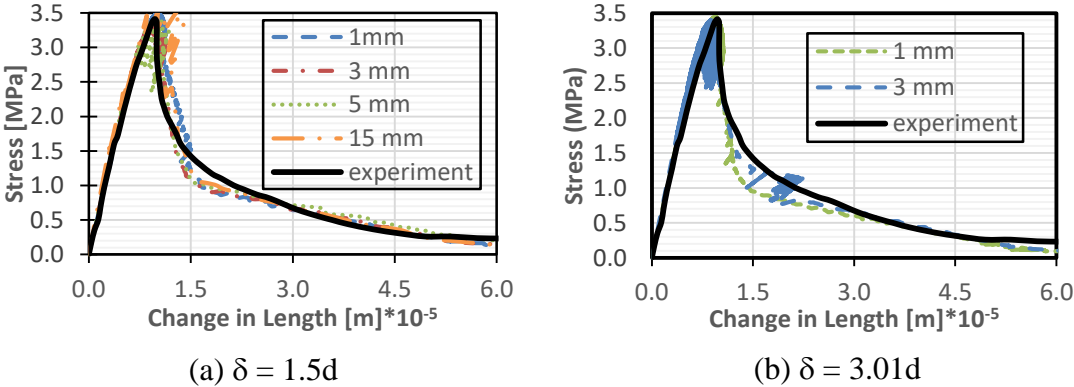


Figure 2.10. Force-Deformation Curves with (a) $\delta=1.5d$; (b) $\delta=3.01d$ [Gopalaratnam and Shah 1985]

The comparisons of the experimental and analysis results for stress-deformation responses are presented in Figure 2.10 for $\delta=1.5d$, $\delta=3.01d$. The damage patterns at the end of simulations (i.e., changes in length are at 5.5×10^{-5} mm) are shown in Figure 2.11 for $\delta=1.5d$. In all uniaxial tension damage patterns, color legend denotes the strain value of elements ranging from 0.00012 to 0.02. Amplification factor for the deformation field presented for the notch region is 20 for illustration purposes. Only notch region of the specimens is shown. Furthermore; for coarse grids whose length exceeded the notch height, the elements that were in the notch region were weakened by multiplying ε_{cr} value with an appropriate small number for $\delta=1.5d$ (i.e., 4.6×10^{-9} and 3.5×10^{-5} were used for d of 5 mm and 15 mm, respectively for GS, 9.5×10^{-5} was used for d of 20 mm for COR) to account for the notch geometry.

Multilinear function parameters optimized with tension test results are shown in Table 1. The analysis results upon increasing the δ is shown in Figure 2.12 for $\delta=3.01d$. It should be noted that the use of a longer δ required the change of only a_1 among all parameters as shown in Table 1 in order to match accurately the tension test results. The results for the δ of 3.01d results have different crack patterns compared to 1.5d cases as the cracks tended to extend beyond the notch region. This was due to the increasing nonlocal effects, which tended to diffuse the crack beyond the notch region. The key reason for this situation is the presence of long diagonal elements connected from the notch region to the region outside the notch. This is believed to spread the cracking and misrepresentation of the nonlocal damage interactions.

A close agreement between the test and simulation results were observed even with significantly large grid spacings. It is interesting to note that the mesh regularization by scaling the softening function seemed to provide objective results while slight differences in the response estimations stemmed from the inability of placing the notch accurately when the mesh sizes are larger than the notch depth.

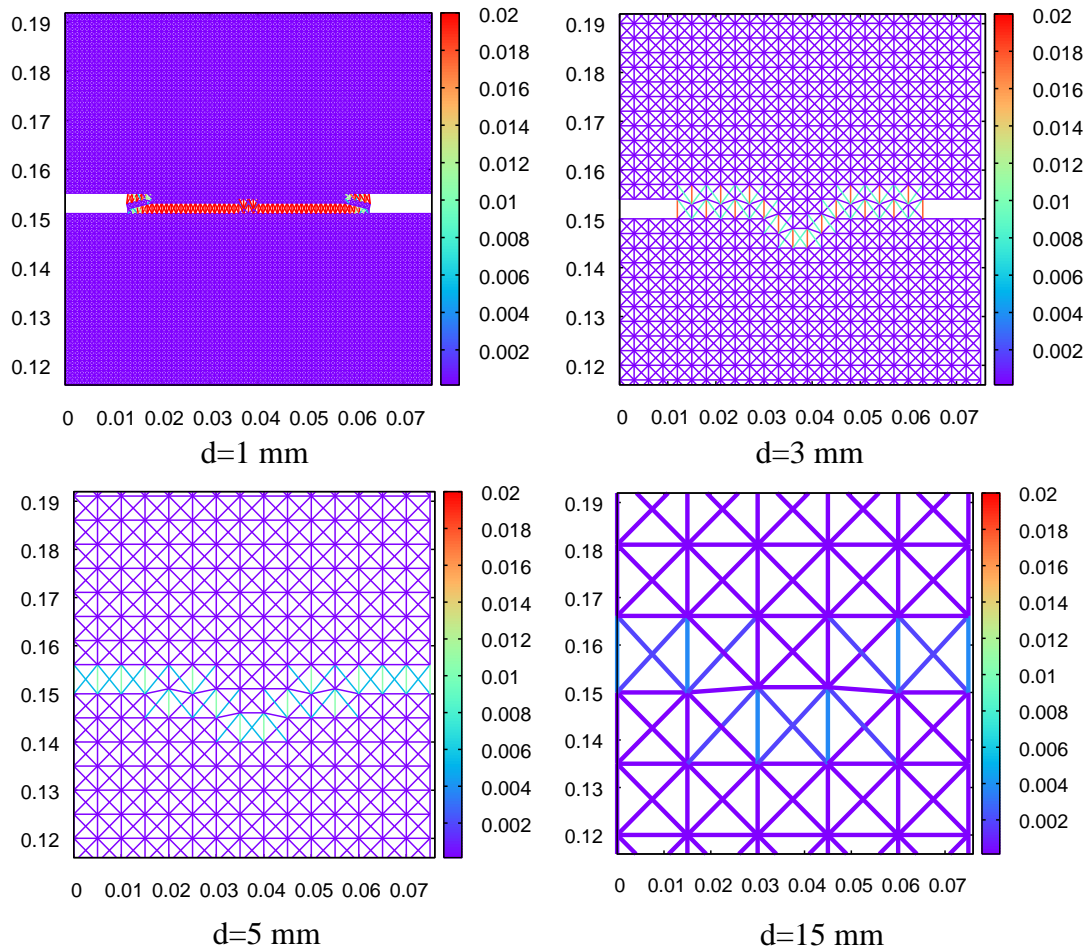


Figure 2.11. Damage Patterns with Different Initial Spacing with $\delta=1.5d$

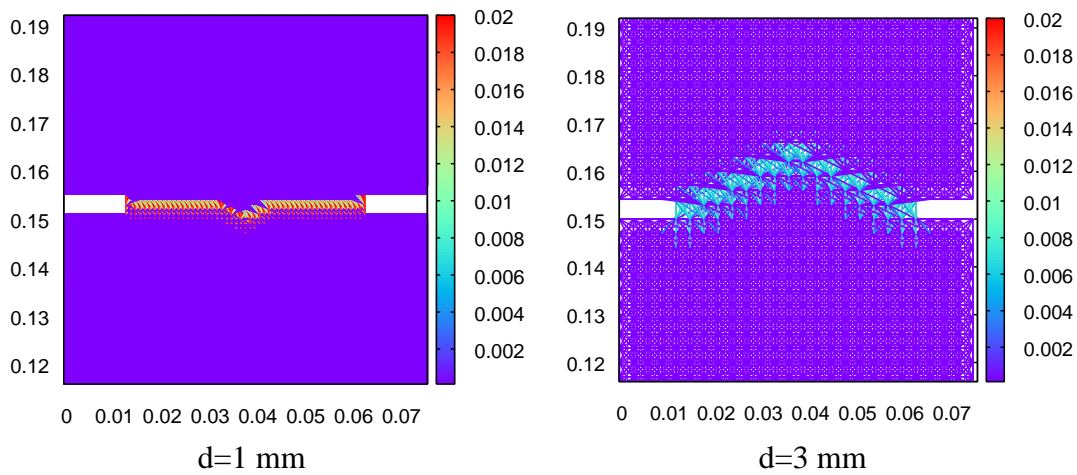


Figure 2.12. Damage Patterns with Different Initial Spacing with $\delta=3.01d$

2.4.2 Cornelissen et al (1986) (COR)

COR conducted uniaxial tension tests to understand fracturing of concrete subjected to tension. The specimen dimensions were 250 mm x 60 mm x 50 mm (Figure 2.13).

Saw-cut notches at both sides had heights and widths of 5 mm, which reduced the net cross section to 50 mm x 50 mm. E , f_{cr} , and G_f values were taken as 21.0 GPa, 3.47 MPa, 0.1 kN/m from test results. LVDTs that were used to measure the displacements within a gauge length of 35 mm.

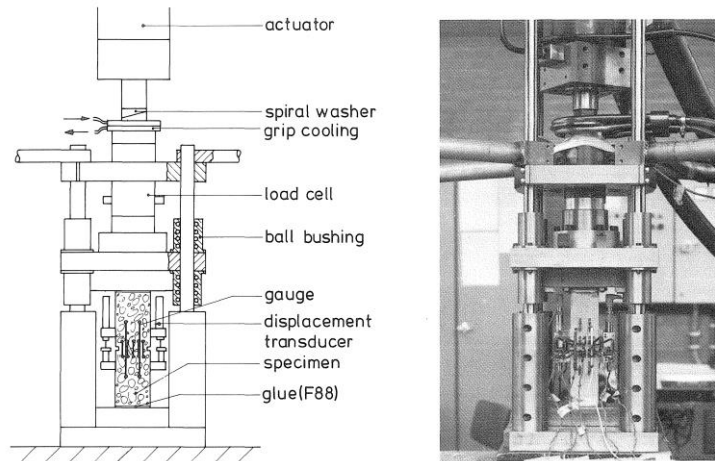


Figure 2.13. View of Test Specimen and Testing Equipment

This experiment was modeled first with a grid spacing of 2.5 mm. Then the length scaling was reflected on the force strain curve for other grid sizes and element lengths. Calibrated parameters a_1 , a_2 , a_3 for different specimens and horizons are presented in Table 1 for a grid spacing (d) of 2.5 mm. Simulations were conducted for d values of 2.5 mm, 5 mm and 25 mm for δ of 1.5 d , and 2.5 mm and 5 mm for δ of 3.01. The comparisons of the experimental and analysis results for stress-deformation responses are presented in Figure 2.14 for both $\delta=1.5d$, $\delta=3.01d$.

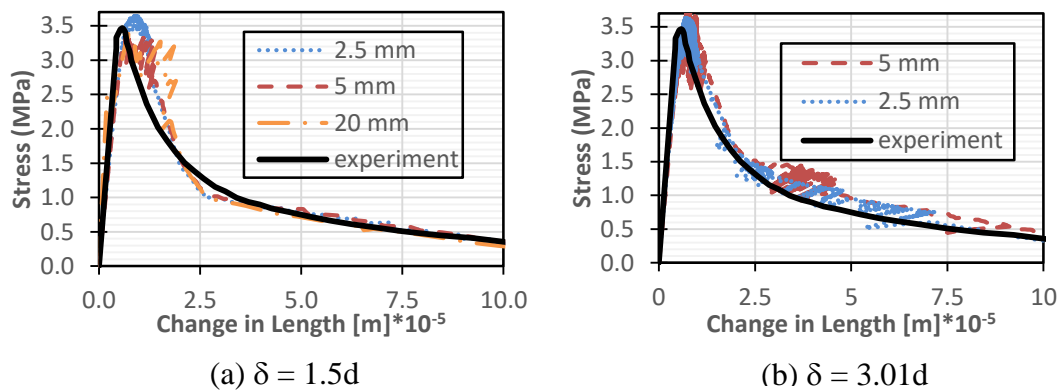


Figure 2.14. Force Deformation Curves for (a) $\delta=1.5d$ and (b) $\delta=3.01d$ [Cornelissen et al 1986]

The results of simulations are in good agreement with the test results in terms of force deformation response. Also, mesh regularization which is the size effect corrections using fracture energy for different grid sizes gave objective results for this simulation (i.e., mesh independent). The damage patterns at the end of simulations (i.e., changes in length are at 9.5×10^{-5} mm) are shown in Figure 2.15 for $\delta=1.5d$. The damage patterns after simulations with increasing the δ for 2.5 mm and 5 mm grid spacing are shown in Figure 2.16 for $\delta=3.01d$. Again, the only problem was the spread of the cracks beyond the notch. The reason was thought to be the long diagonal elements connected from the notch region to the region outside the notch causing a misrepresentation of the nonlocal damage interactions as explained before. In order to objectively observe the effect of δ on the tension test results, a numerical experiment was conducted on a specimen with a relatively large notch in the next section.

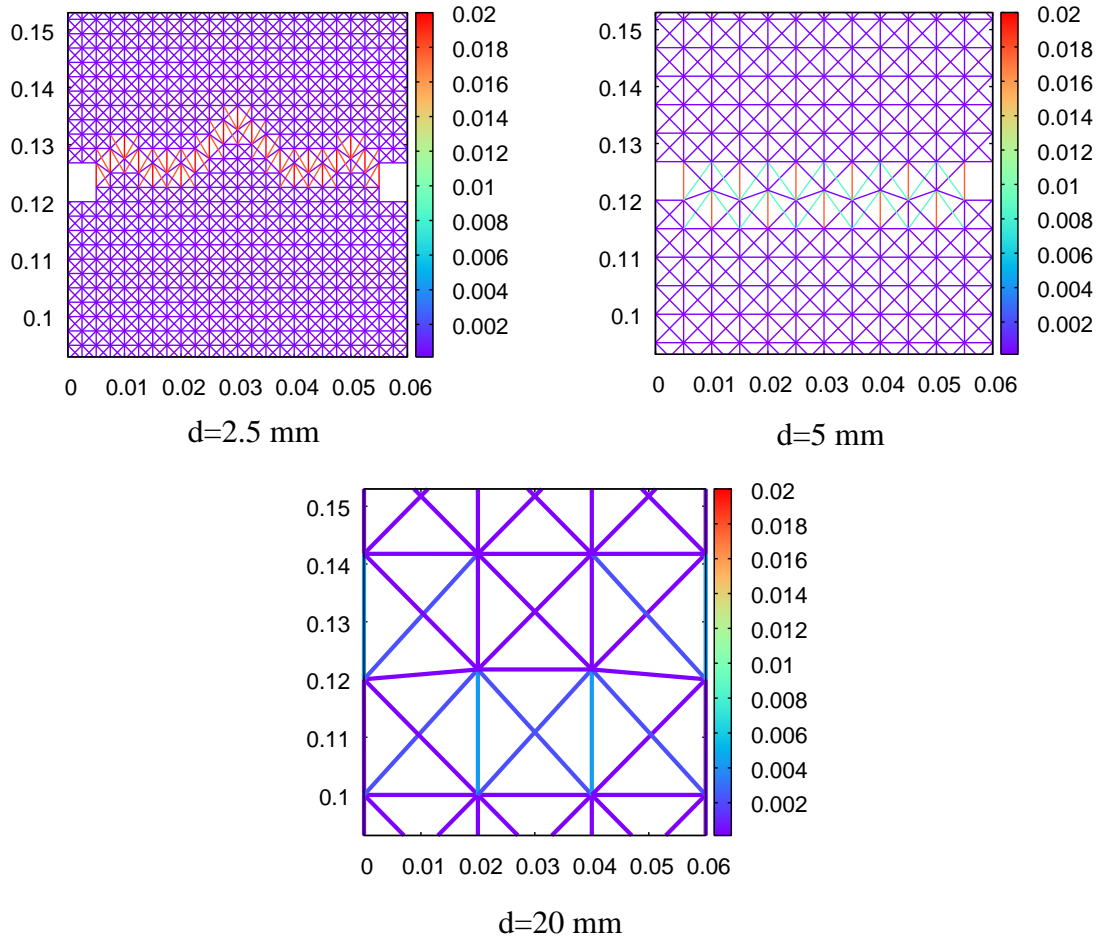


Figure 2.15. Damage Patterns with Different Initial Spacing with $\delta=1.5d$

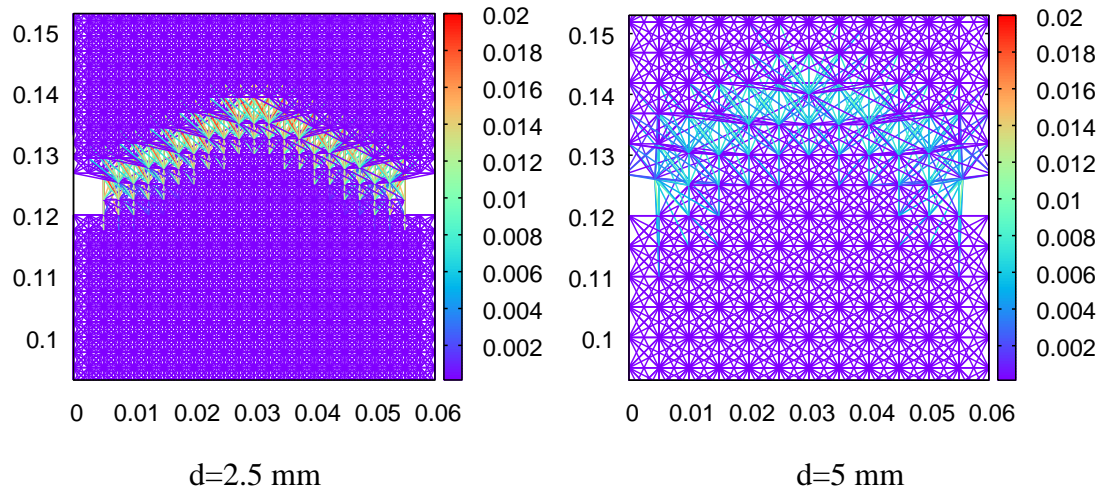


Figure 2.16. Damage Patterns with Different Initial Spacing with $\delta=3.01d$

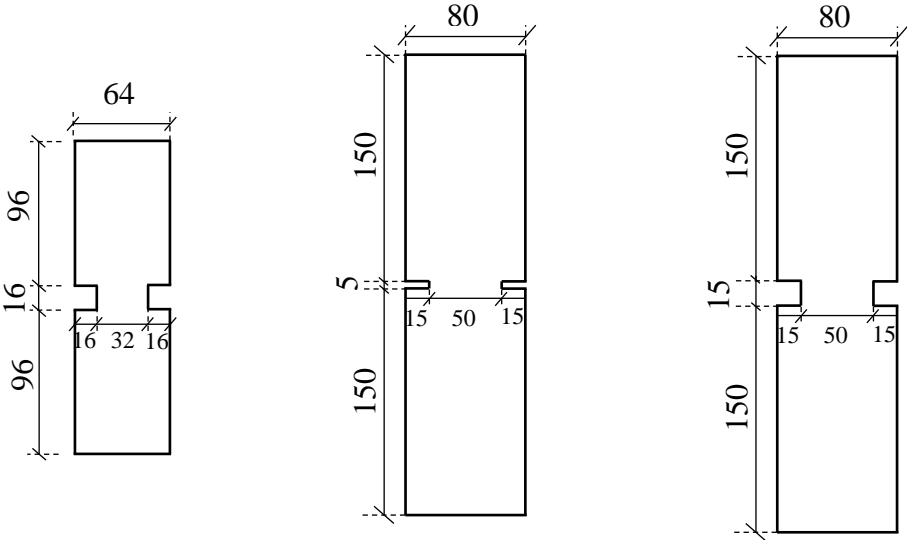
2.4.3 Numerical Experiments

A relatively large notched numerical specimen was prepared properly to observe the δ effect objectively. This specimen was prepared with a height of 208 mm, width of 64 mm and thickness of 32 mm. The notch height and width were taken as 16 mm which made the specimen net area 32x32 mm. With this larger notch, it was ensured to have a sufficiently dense mesh within the notch region with a reasonable element size. The prepared specimen (NES) can be shown in Figure 2.17.a. E , f_{cr} , and G_f , and gauge length values were taken as 27.0 GPa, 3.1 MPa, 0.07 kN/m, and 48 mm for NES, respectively. The stress displacement model given Eq. 2.4 and 2.5 was used as the “representative” result which were assumed as an experimental result. Simulations were done for d of 2 and 4 mm for $\delta=1.5d$ and $\delta=3.01d$. The stress-deformation results were represented in Figure 2.18 for both δ .

The damage patterns are presented in Figure 2.19 for both δ . Only notch region of the specimen is shown. The cracks are shown for change in length value at $7 \cdot 10^{-5}$ mm. Color legend denotes the strain value of elements ranging from 0.00012 to 0.02. Amplification factor for the deformation field presented for the notch region is 20 for illustration purposes.

Two new numerical specimens named as S1 and S2 were created as shown in Figure 2.17.b-c. The notch sizes on these two specimens were selected as even multiples of the selected grid size of 5 mm which was later used in structural element simulations.

In this way, a uniform grid could be used for calibrations in the absence of tension tests. In addition, a 5 mm grid size for S1 and S2 were selected such that the diagonal elements remain within the notch region. Simulations from S1 and S2 are used as benchmark results of tension tests needed for structural simulations described in Chapter 3.



(a) Numerical Experiment Specimen (NES) (b) Specimen 1 (S1) (c) Specimen 2 (S2)

Figure 2.17. (a) Numerical Experiment Specimen; for Other Structural Problems, (b) Specimen 1 and (c) Specimen 2 (all units in mm)

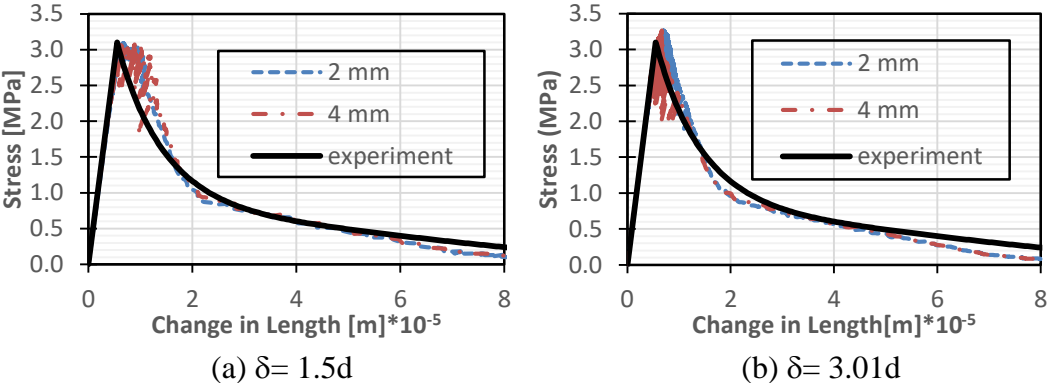


Figure 2.18. Force Deformation Curves for (a) $\delta=1.5d$ and (b) $\delta=3.01d$ for Numerical Tests.

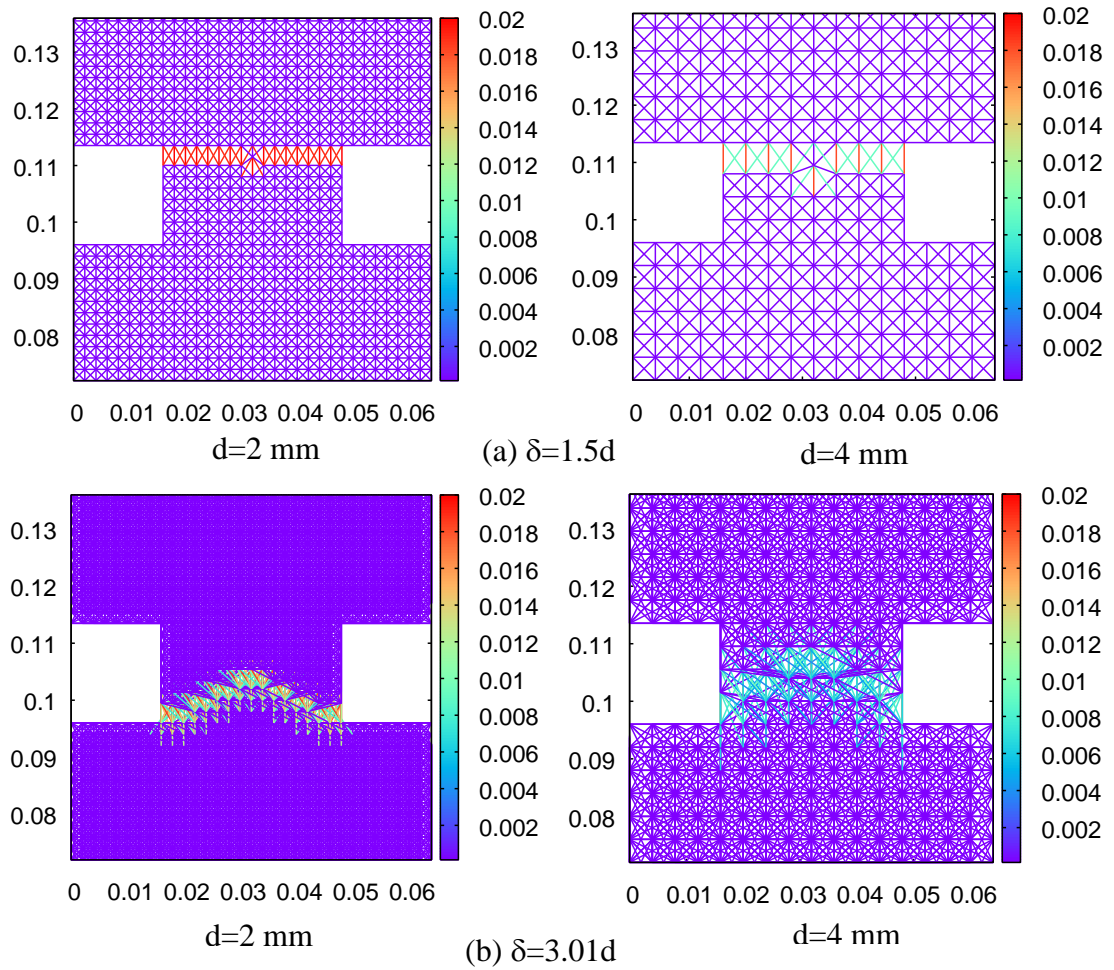


Figure 2.19. Damage Patterns for δ of (a) $1.5d$ and (b) $3.01d$

Heights and widths of the notches were 5 mm and 15 mm for specimen 1, 15 mm and 15 mm for specimen 2 respectively. S1 was used with $\delta=1.5d$ while S2 was used with $\delta=3.01d$ simulations. Both specimens had 80 mm width but their thickness were taken similar as the thickness used for the validation problems. Heights of S1 and S2 were taken as 305 mm and 315 mm respectively (Figure 2.17.b-c). For both S1 and S2, the strain gauge value was taken as 45 mm. In order to ensure mesh objectivity, S1 was simulated with $\delta=1.5d$ and S2 was simulated with $\delta=3.01d$.

The material model for the problems simulated in the next chapter were found by first simulating a tension test with the models S1 or S2. All multilinear function parameters were determined for both $\delta=1.5d$ and $\delta=3.01d$. Parameters of the notched beam (Pettersson 1981) were determined for G_f of 124 N/m and 150 N/m. Parameters for the dam test (Aldemir et al 2016) were conducted for G_f of 60 N/m, 100 N/m and 150

N/m. Finally, parameters of the tension stiffening test (Gijbbers and Hehemann 1977) were computed (Table 1). With using S1 and S2 and material properties provided from experiments, series of direct tension tests were implemented. Results from simulations are represented in Figure 2.20 for $\delta=1.5d$ and Figure 2.21 for $3.01d$. Errors of the area under the curves are also presented in the same figures. In the response curves of numerical experiments, Eq. 2.4 calculation results are represented as ‘experiment’.

The optimum parameters of OLM for a grid size of 2 mm for NES and 5 mm for S1 and S2 are shown in Table 1. It must be noted that initial stiffness of global response of the systems is always in agreement with the “representative” solution for all simulations so it can be concluded that the energy balance approach is quite satisfactory for the linear elastic regime.

In summary, optimum a_1 , a_2 and a_3 were determined for the smallest grid size in $\delta=1.5d$. For $\delta=3.01d$, only a_1 value was investigated for the best match with correct stress-deformation curve and other grid size parameters was taken as the parameters from $\delta=1.5d$ as can be seen in Table 1. Interestingly, the values of b_1 and b_2 were found as 0.6 and 0.2, respectively, regardless of the fracture energy, δ or mesh size. Collecting responses of all elements within the damage zone provide the global response of the specimen to tension force as described in Section 2.4. Simulations show that rather than the values of a_1 , a_2 and a_3 , slopes play an important role in the response. As seen in Figure 2.2, there are three slopes in the softening part of constitutive model in OLM. The first descending slope in softening part influences both the capacity and the softening slope of the global response. The second and third slopes are of secondary importance and they affect the global response for high strains. All parameters that give these curves are represented in Table 1 with the smallest grid size.

These numerical experiments revealed three important conclusions: i- the increase of the δ seem to provide a better match of the softening part resulting in a better representation of the coalescence of cracks. ii- The mesh regularization upon scaling the input softening function for different mesh sizes seem to be successful for larger horizons similar to the lattice results as long as sufficiently small mesh size are used

to account for the geometry of the notch. iii- Thanks to the larger notch length, the crack was contained within the notch region for the numerical experiments. These results provided confidence on the ability of estimating cracks for concrete in tension tests while accurately modeling the average stress-displacement response with the overlapping lattice approach.

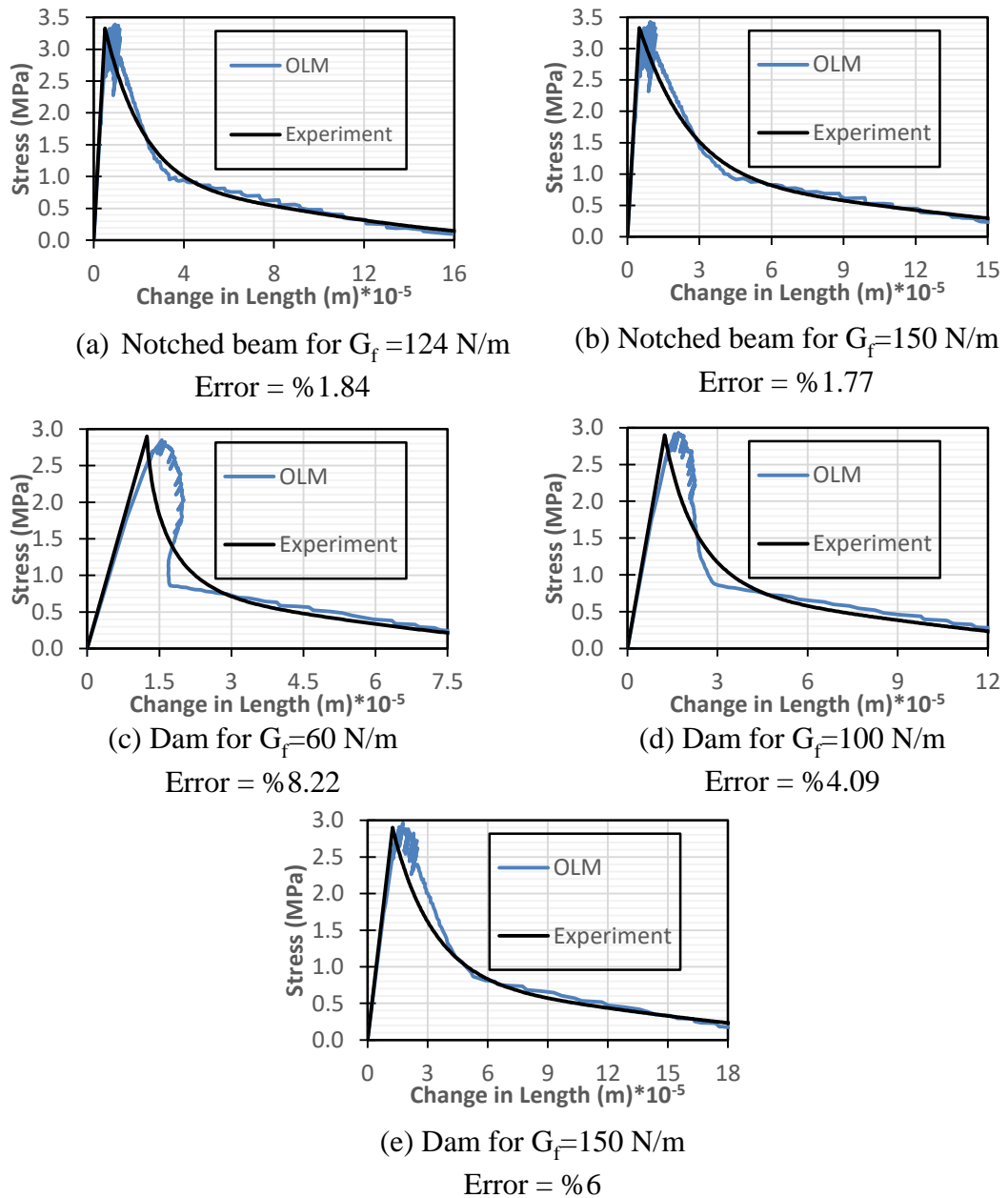
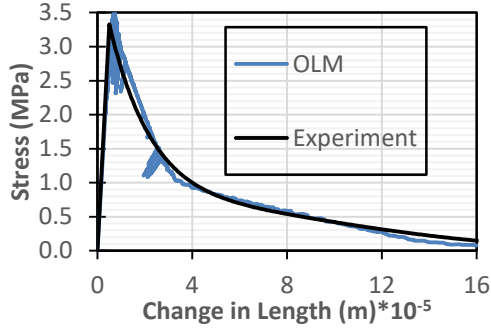
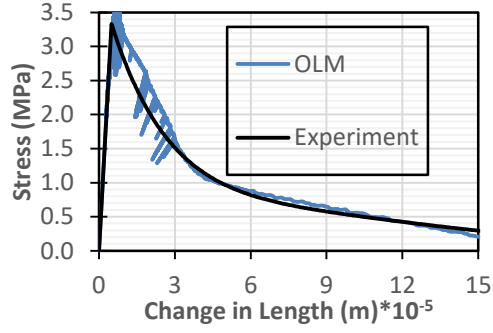


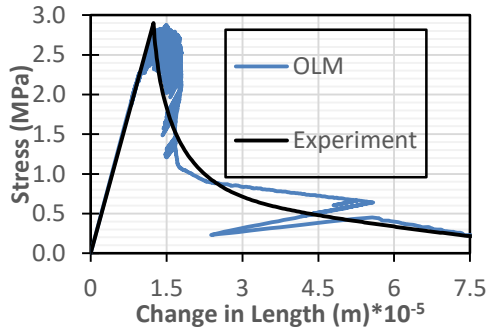
Figure 2.20. Stress-Change in Length Curves for Series of Direct Tension with $\delta=1.5d$



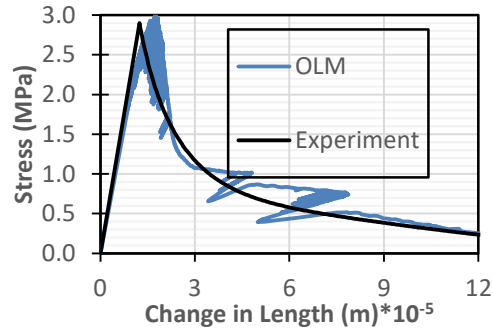
(a) Notched beam for $G_f=124$ N/m
Error = %0.76



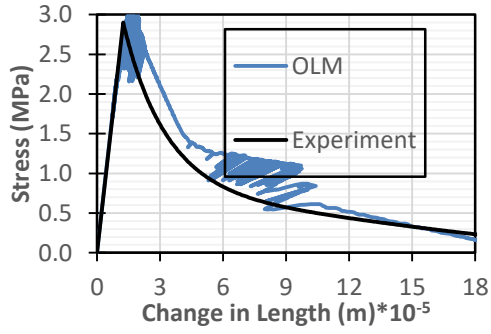
(b) Notched beam for $G_f=150$ N/m
Error = %4.76



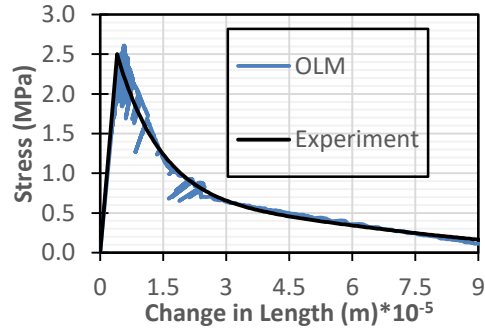
(c) Dam for $G_f=60$ N/m
Error = %11.22



(d) Dam for $G_f=100$ N/m
Error = %7.41



(e) Dam for $G_f=150$ N/m
Error = %23.01



(e) Tension Stiffening
Error = %1

Figure 2.21. Stress-Change in Length Curves for Series of Direct Tension with $\delta=3.01d$

Table 1. Multilinear Function Parameters and Properties of Specimens

	$\delta=1.5d$			$\delta=3.01d$			Smallest Grid Size	Properties			
	a_1	a_2	a_3	a_1	a_2	a_3	d^*	E^*	f_{cr}^*	G_f^*	w^*
<i>GS</i>	6.6	75	450	12	75	450	1	29.1	3.41	54	19
<i>COR</i>	3.6	40	280	5.0	40	280	2.5	21.0	3.47	100	50
<i>Numerical</i>	3.2	60	300	6.2	60	300	2	27.0	3.10	70	32

Table 1. (continued)

Notched Beam G_f=124	1.5	40	240	3.1	40	240	5	30.0	3.33	124, 150	50
Notched Beam G_f=150	1.5	50	280	3.1	50	280					
Dam G_f=60	3	6	60	4	6	60		10.5	2.90	60, 100, 150	200
Dam G_f=100	2.5	12	100	3.5	12	100					
Dam G_f=150	2	25	130	3.1	25	130					
Tension Stiffening G_f=60	-	-	-	3.1	30	200		28.0	2.50	60	68

*: Dimensions for E , f_{cr} , G_f , w and d are GPa, MPa, N/m, mm and mm respectively

CHAPTER 3

VALIDATION OF OLM

3.1 General

In this chapter, OLM is employed for the nonlinear static analysis of unreinforced and reinforced concrete problems. First, three point bending test for a notched beam is modelled with OLM. Then, a gravity dam test is simulated. Tension stiffening and four point bending beam tests were studied to explore the performance of OLM to predict reinforced concrete behavior. Detailed parametric studies are conducted. Effect of δ is investigated in the studied examples. In the structural simulations, effect of fracture energy on the global response is studied at the member level. The response and crack pattern of all conducted validations of OLM examples are presented and discussed in detail.

3.2 Notch Beam Test

Three point bending experiment was performed by Petersson (1981) to determine the fracture energy of beams. This beam test was simulated in order to assess the performance of the overlapping lattice approach for a bending induced crack propagation problem. The geometry of the specimen can be seen in Figure 3.1. The notch height was half the width of the beam i.e., 100 mm. Notch geometry information was not provided in the conducted experiment report. So, a 5 mm notch width was assumed. E , f_{cr} , and G_f values were taken from the test results as 30.0 GPa, 3.33 MPa, 0.124 kN/m, respectively. The thickness of the beam was 50 mm as can be seen in Table 1. First, the parameters required for the lattice elements were determined such that the numerical direct tension test results (for S1 and S2) of stress-average displacement matched with the response function in Eq. 2.4. The calibrated model parameters are prevented in Table 1.

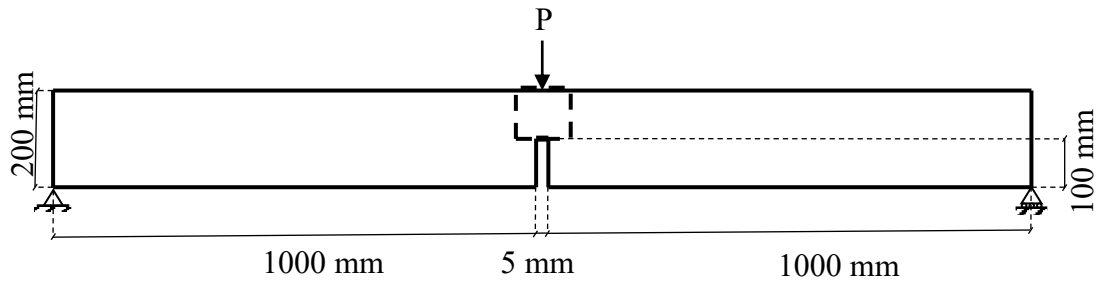
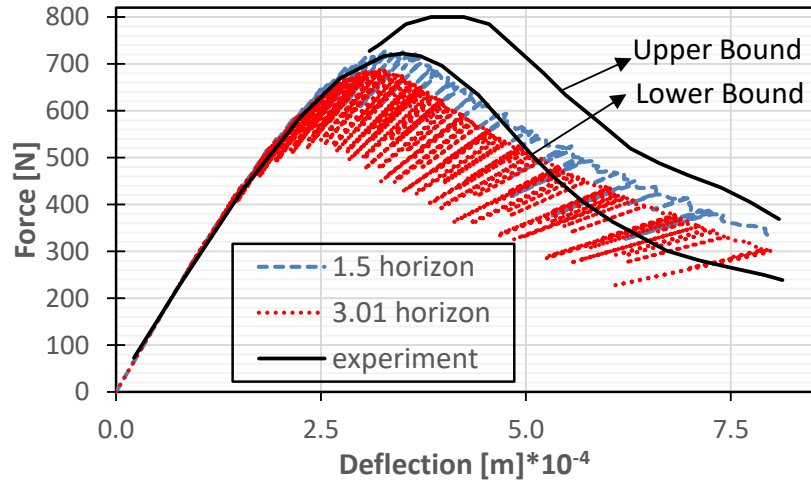


Figure 3.1. Experiment Geometry [Petersson 1981]

As can be seen Figure 3.1, a point load was applied at middle of the specimen, where two ends of the beam were restrained against to translations. The transverse deflection was monitored under the loading point at the middle of specimen in the experiment. The load was applied as a distributed load over 5 mm spanning to two elements as the actual loading plate width was not reported.

The OLM was constructed for the beam test by using the parameters (modified according to length scale) obtained from the uniaxial tension test for a grid size of 5 mm. The load deflection curve results and obtained crack patterns are shown in Figure 3.2 where the two black lines represent the experimental values obtained by Petersson (1981), the blue line ($\delta=1.5d$), and the red line ($\delta=3.01d$) represent the computational predictions. The damage pattern of the selected around the notch is shown as a square region in Figure 3.1.b for $\delta=1.5d$ and Figure 3.2.c for $\delta=3.01d$. The color contours in the damage figures show the strain values in the elements (i.e., ϵ_{cr} ranging from 0.00012 to 0.02). Amplification factor for the deformation field presented for the notch region was taken as 10 for illustration purposes. All crack patterns were reported for the end of the simulations.

In the performed tests, six beams were tested. The fracture energy of these beams exhibited some variations. The mean fracture energy value of these beams was reported as 124 N/m. Considering the uncertainty in the experimental data, computational results seem to be in reasonable agreement with the bounds of the experimental results. The increasing δ caused a slight underestimation of the capacity computed to $\delta=1.5d$.



(a) Force-Deflection Curve

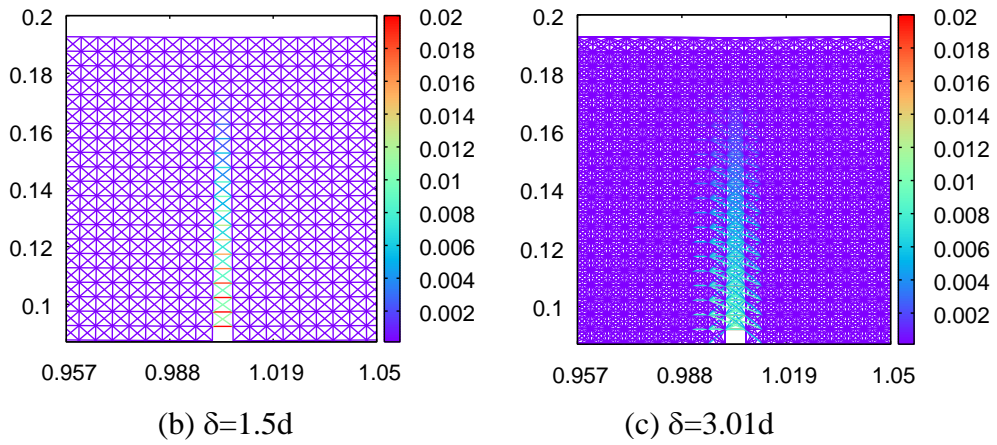
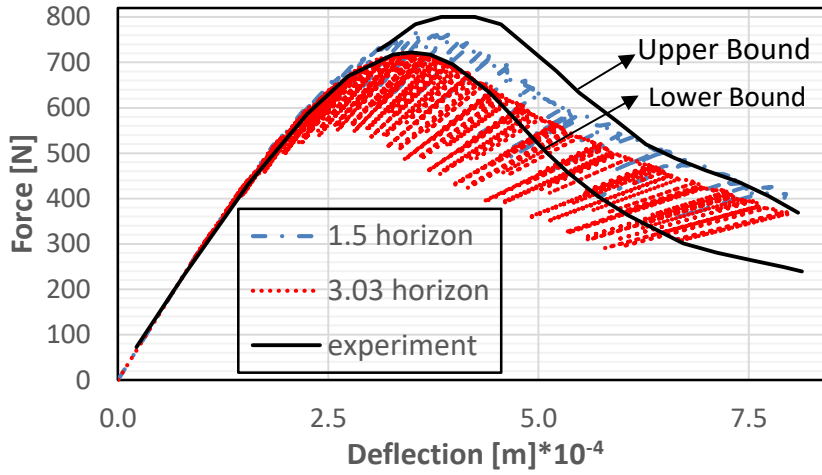


Figure 3.2. Force Deflection Curve and Damage Patterns for $G_f=124$ N/m [Pettersson 1981]

In order to observe the influence of the fracture energy on simulation results, OLM simulations were repeated by keeping all the parameters same while assuming a fracture energy of 0.15 kN/m. In the experiment, the highest and lowest fracture energies value of the tested six beams were reported as 0.137, 0.115 kN/m, respectively. Direct tension test for this fracture energy was re-conducted and calibrated parameters are shown Table 1. The force deflection curve and corresponding damage pattern for both $\delta=1.5d$ and $3.01d$ are shown in Figure 3.3.

It can be observed that increased fracture energy resulted in an enhanced capacity and better estimation of the load deformation response. As such, uncertainty in the fracture energy, which is usually uncovered by conducting a number of tests, can affect the computational estimations by using the OLM.



(a) Force-Deflection Curve

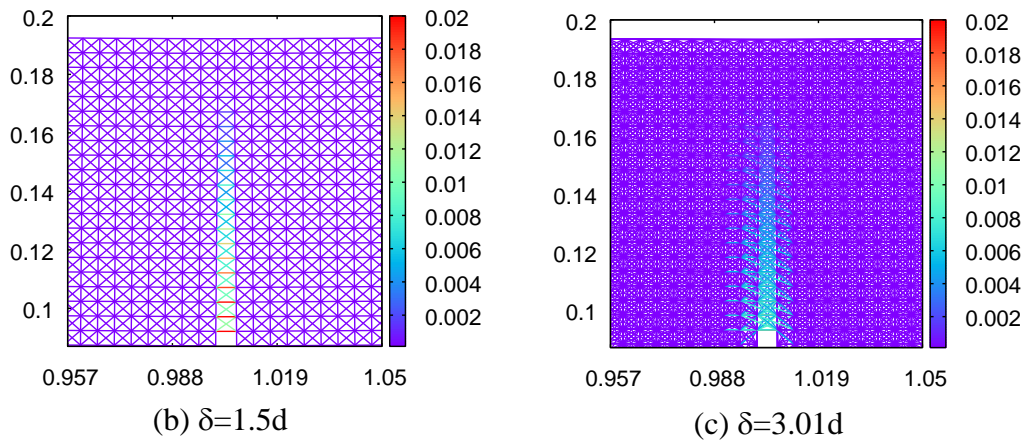


Figure 3.3. Force Deflection Curve and Damage Patterns for $G_f=150$ N/m [Pettersson 1981]

The crack pattern was in agreement with expected crack propagation starting from the top of the notch opened in the upward direction. The crack did not spread outside the notch region for $\delta=1.5d$. It was a zipper type crack. In the simulations conducted for both G_f values, increasing the δ resulted in a slight capacity reduction compared to the capacity obtained for $\delta=1.5d$. The damage patterns in simulations (i.e., the crack width and length) were observed to be in a better agreement with the experimental results for larger δ .

3.3 Scaled Dam Test

Aldemir et al (2015) conducted a pseudo dynamic and static conventional concrete dam experiment on a 1/75 scaled model of the 120 m high Melen Dam. Three different

scaled ground motions were applied to the dam by using the pseudo-dynamic testing technique. Then, the pushover experiment was also conducted. The original setup enabled the use of only the bottom half of the dam section and the inertial and hydrodynamic load effects were simulated using a lateral hydraulic actuator. The geometry and loading of the model is presented in Figure 3.4. The vertical dead load was applied to mimic the gravitational actions on the prototype dam.

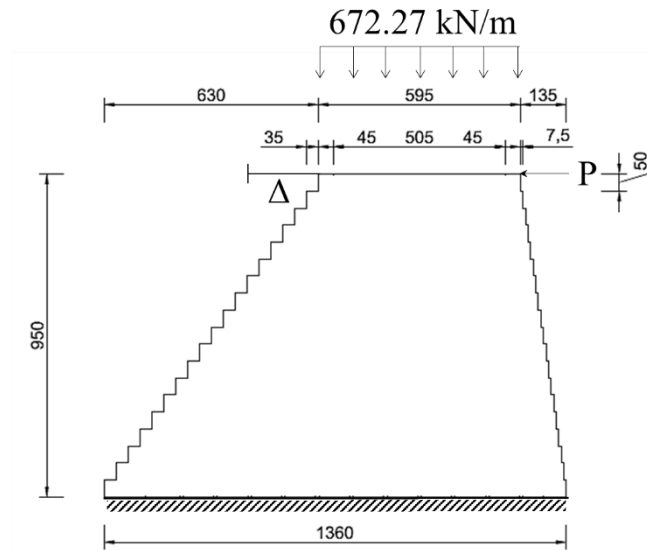


Figure 3.4. Experiment Geometry [Aldemir et al 2015]

The OLM was constructed by using a 25 mm grid size to observe the performance estimation for a continuum unreinforced concrete structure. A similar procedure as discussed above for the notched beam simulation was conducted initially to estimate model parameters by using a numerical uniaxial tension test since a laboratory uniaxial tension test was not available. The calibrated parameters for the softening function are given in Table 1 for the d of 5 mm. For the OLM of the dam appropriate length scaling was performed due to the smaller element length in the tension test simulation.

As no information regarding the fracture energy value of the specimen was available G_f values of 60 N/m, 100 N/m and 150 N/m were used in the simulations to investigate response predictions over a wide range of G_f . E , f_{cr} , and w values were taken as 10.5 GPa, 2.9 MPa and 200 mm, respectively, as reported in the test (Table 1) for these simulations. In addition, the elements within the top 300 mm, equipped with a specially designed threaded steel plate in the test to enable safe load transfer on the specimen,

were assumed to remain elastic. For this reason, F_{cr} as $F_{threshold}$ and stiffness of the top 300 mm of the lattice elements in this region were taken as 100 times of critical force, F_{cr} , and 10 times of EA_t .

First, the vertical load was applied (400 kN) and this loading was assumed as the initial stress condition. Afterwards, the specimen was loaded from the upstream direction gradually (Figure 3.4) in a damage controlled manner with SLA. A slight modification was conducted to incorporate initial stresses as explained in the original computer code in Appendix B. In the experiment, first, the hydrostatic loading was applied. The following earthquake loading patterns were operational based earthquake (OBE), maximum design earthquake (MDE) and maximum characteristic earthquake (MCE). After these loads, the pushover loading was applied. The crack patterns forming on the test specimen are shown in Figure 3.5.

LVDTs was placed at the top of the specimen. Similarly, displacement of the middle node was observed as the tip displacement in the simulations. For all G_f values and δ of 1.5d and 3.01d, the SLA results were compared with the experimental results found by combining the consecutive PsD and pushover test results as shown in Figure 3.6.

Envelopes of the response results of simulation are shown in the base shear and tip displacement curves for good representation. It can be observed that the initial stiffness estimation of the specimen was perfect whereas the estimation of lateral load capacity was about 20% lower than the test capacity. The deformation of the specimen was predicted in a reasonable manner with some drop of load carrying capacity around 1.5 mm. In addition, the results for $\delta=1.5d$ and $\delta=3.01d$ in terms of force deflection response of the specimen were quite similar. However, a smoother response curve was obtained when the larger δ is used (i.e., suddenly drop at the point tip displacement is about 1.7). The marked three points on the load tip displacement curve were used to compare damage patterns in this tip displacement value. It is interesting to note that variation of fracture energy seemed to affect the response in a limited manner. Using a 20% larger fracture energy value gave again a capacity enhancement of 1%.



(a) Hydrostatic Loading



(b) OBE



(c) MDE

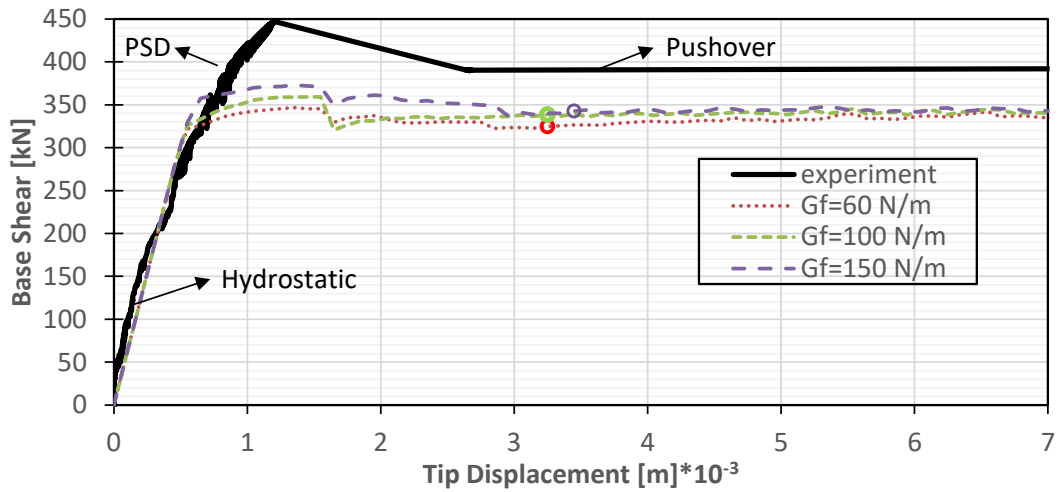


(d) MCE

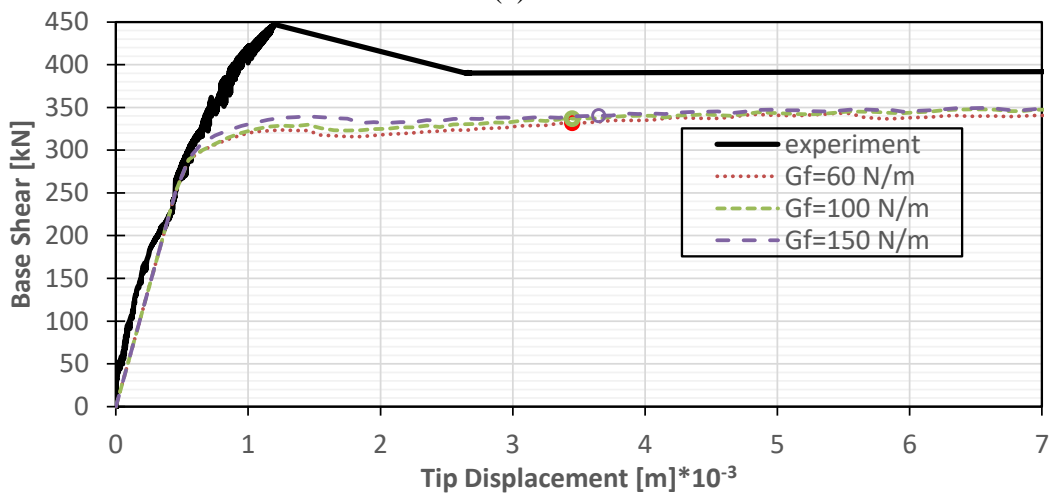


(e) Pushover Experiment

Figure 3.5. Cracks in Experiments [Aldemir 2016]



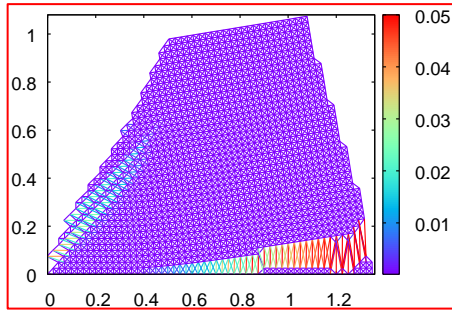
(a) $\delta=1.5d$



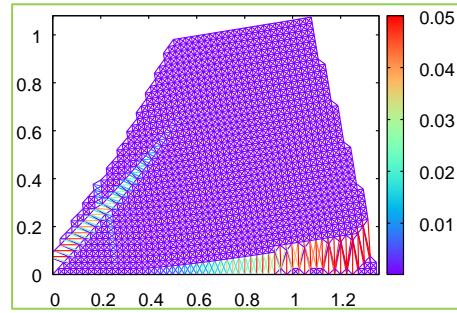
(b) $\delta=3.01d$

Figure 3.6. Load-Tip Displacement Response of OLM

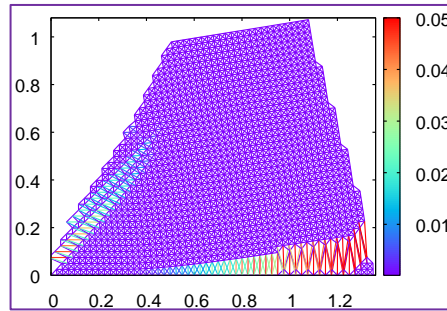
The crack patterns and lengths are shown in the Figure 3.7 around 3.5 mm tip displacement as the points at Figure 3.6 for both $\delta=1.5d$ and $\delta=3.01d$ and for different fracture energy value as mentioned. The color contours show the strain value in the element ranging from 0.00012 to 0.05. Amplification factor was taken as 45 to observed deflected shape well. As can be seen in the experiment geometry, x axis range is from 0 to 1.36 m which is the bottom width of the specimen while y axis range is from 0 to 1.08 m.



$G_f = 60 \text{ N/m}$ and $L=0.91 \text{ m}$

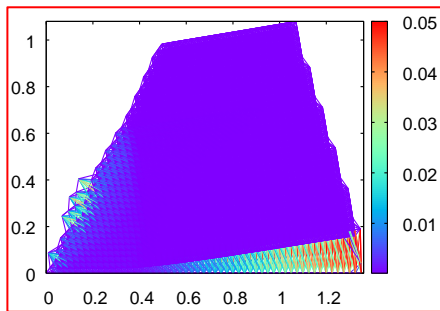


$G_f = 100 \text{ N/m}$ and $L=0.93 \text{ m}$

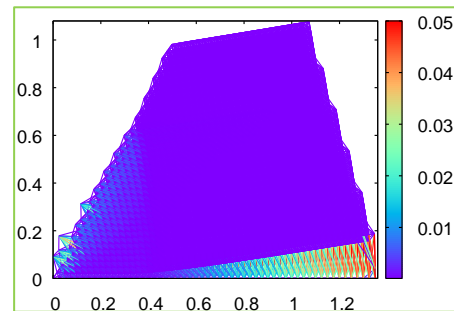


$G_f = 150 \text{ N/m}$ and $L=0.94 \text{ m}$

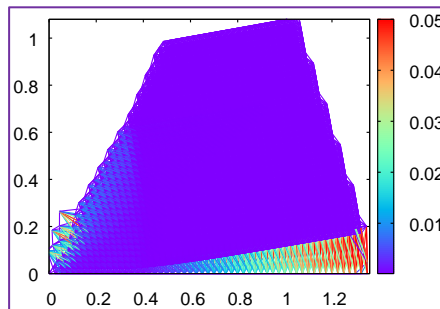
(a) $\delta = 1.5d$



$G_f = 60 \text{ N/m}$ and $L=0.92 \text{ m}$



$G_f = 100 \text{ N/m}$ and $L=0.93 \text{ m}$



$G_f = 150 \text{ N/m}$ and $L=0.95 \text{ m}$

(b) $\delta = 3.01d$

Figure 3.7. Damage Patterns and Crack Lengths at Specific Points for G_f of 60,100,150 N/m for (a) $\delta=1.5d$ and (b) $\delta=3.01d$

In the experiment, the crack length was measured as 1.05 m for both end of MCE loading (i.e., tip displacement is around 1.1 mm) and pushover experiment (i.e., end of curve). However, the cracks at the bottom of the specimens already existed in the experiments. Thus, the crack lengths of G_f of 60,100,150 N/m were observed as 1.056, 1.060 and 1.065 m for $\delta=1.5d$ and 1.049, 1.056 and 1.070 m, respectively. The crack pattern observed from the test seemed to agree well with the base cracking shown in Figure 3.5. There existed some split cracking at the downstream of the dam for $\delta=1.5d$ due to compressive loading. However, this problem was not observed for $\delta=3.01d$. This shows that using a larger δ is also beneficial to model compression in concrete. Crack length at the bottom of the dam was observed in a better agreement with the experiment results for larger δ . In short, it can be stated that the employed SLA overlapping lattice simulation was found to reproduce the test results in a reasonable manner.

3.4 Tension Stiffening Test

In order to test the ability of the overlapping lattice approach in estimating the force transfer between steel reinforcement and concrete, first the basic test of tension stiffening test was simulated. In this test, steel reinforcement with concrete cast around it was subjected to uniaxial tension by applying a force only on the steel bar. In this way, the ability of force transfer from steel to concrete including the axial tensile load-deformation response of concrete and associated crack spacing can be deduced. The test experiment carried out by Gijsbers and Hehemann (1977) was used for the numerical simulations. In their experiment, the concrete bar had 600 mm length and a cross section of 68 mm x 68 mm with a $\phi 8$ mm rebar at the center. Half of the experiment was modeled to get computational efficiency as shown in Figure 3.8. E , f_{cr} , and G_f values were taken as 28.0 GPa, 2.5 MPa, 0.06 kN/m, respectively (Table 1). Modulus of elasticity, E_s and yield stress, f_{yield} , of steel were 192.3 GPa and 400 MPa, respectively. The load was applied from steel and elongation of steel was observed. In order to satisfy the symmetry conditions, roller supports were placed at the top boundary, and a pin support was placed at the left end of the rebar.

OLM was constructed by using a 5 mm grid size and $\delta=3.01d$. The value of EA_t for the truss elements representing the steel rebar were taken as a half of the modulus of

elasticity times cross sectional area of steel ($E_s A_s/2$). Here, A_s was half of the area of 8 mm bar. The softening parameters are given in Table 1 for this simulation. Moreover, load was applied from top right point of the specimen and displacement of this point was taken as the elongation value. The load was multiplied with 2 because of symmetry condition to draw total load elongation response. In addition, there are three types of elements, including concrete, bond and steel represented in purple, red and green respectively in the Figure 3.9.

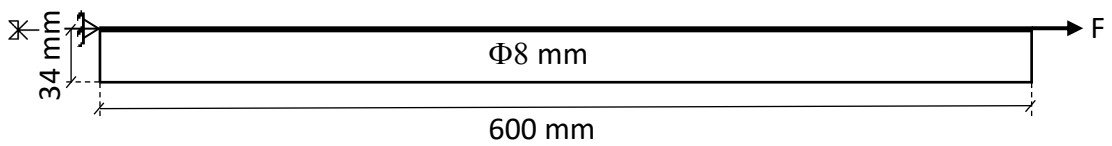


Figure 3.8. Half of the Experiment Geometry

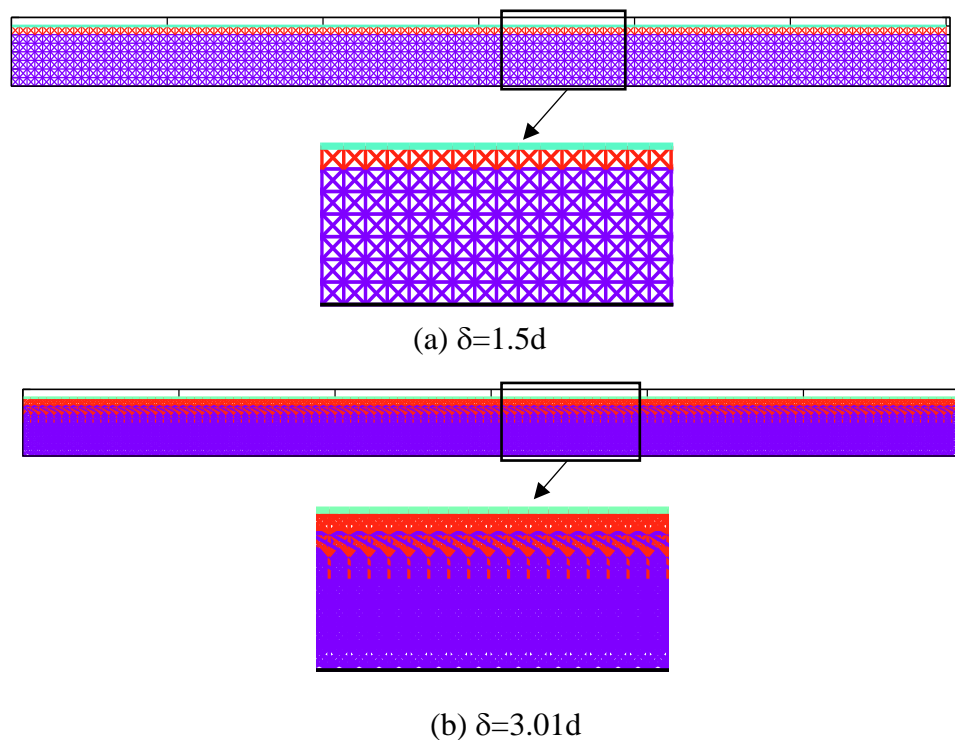


Figure 3.9. Different types of elements for both δ

In the preliminary studies, in order to observe δ and bond strength effect in RC structures, $\delta=1.5d$ with keeping the other properties same was used. The bond strength was taken as 40%, 70%, 100% and 130% of the tensile strength of concrete elements, respectively. Elastic perfectly plastic load-strain response was assigned for bonds (i.e.,

after reaching bond strength with the same stiffness of the concrete members, the stress level was kept constant). The load elongation responses and crack patterns at the end of simulation are shown in Figure 3.10 and Figure 3.11. In comparison with test results, response of $\delta=1.5d$ gave inaccurate result in terms of the ascending part after main cracks initiated. Crack propagation was also observed to be unrealistic because three main cracks was took place in the experiment. If the bond strength was taken too high, cracks initiated just below the level where bond elements end. If the bond strength was chosen too low, some sliding (i.e., pullout) region between concrete and steel was observed. Both of these choices yielded inaccurate simulation results. Thus, it was realized that there must be a range for bond strength. In addition, choosing small horizons ($\delta=1.5d$) did not produce acceptable simulation results. In order to avoid bond failure of the RC structures, the higher δ must be used. In the following simulations, δ was taken as $3.01d$ and the bond strength was taken as 40%, 70%, 100% and 130% of the tensile strength of concrete elements. The responses and crack patterns at the end of simulations are shown in Figure 3.12 and Figure 3.13. Color contours denote the strain values ranging from 0.00012 to 0.005.

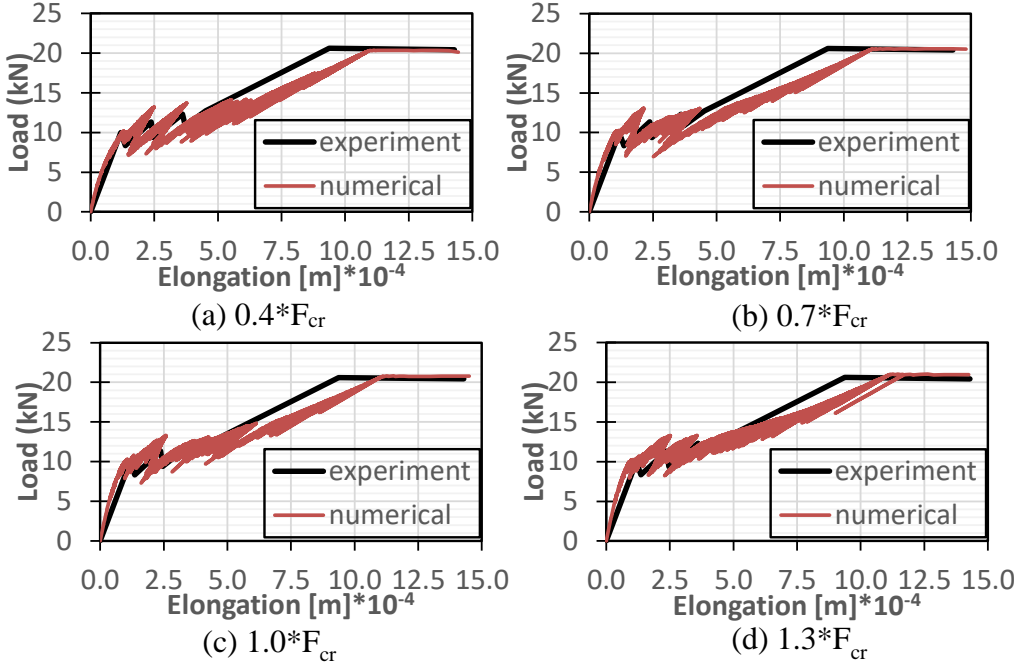


Figure 3.10. Load Elongation Responses for $\delta=1.5d$ with Different Bond Strengths

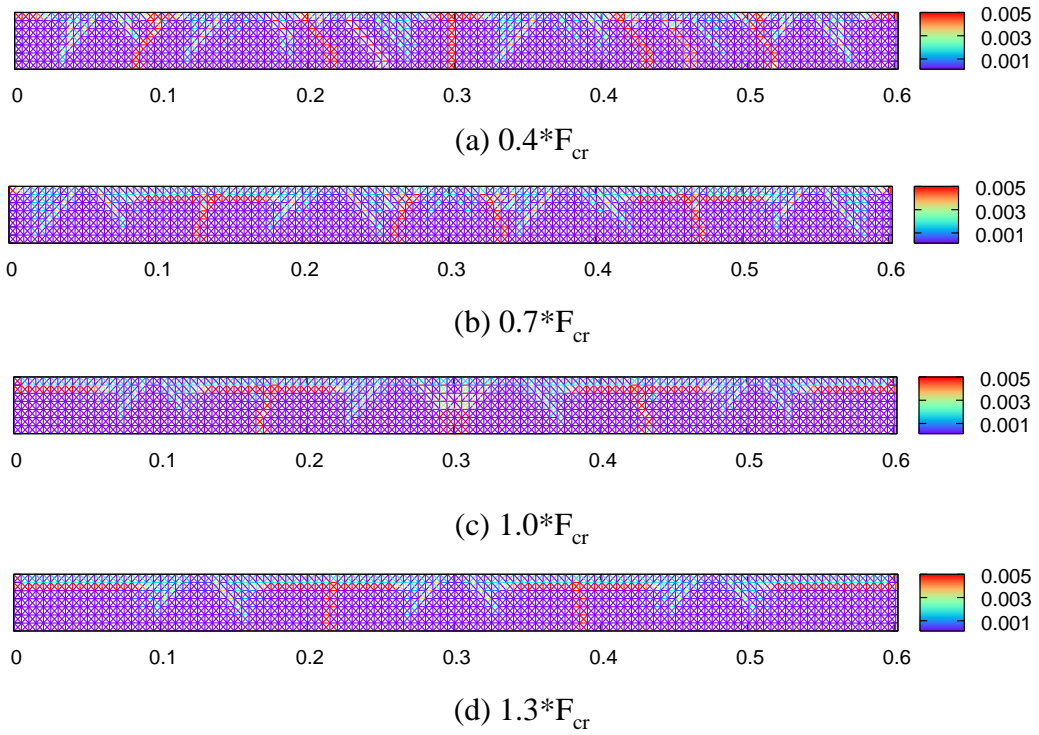


Figure 3.11. Crack Patterns for $\delta=1.5d$ with Different Bond Strengths

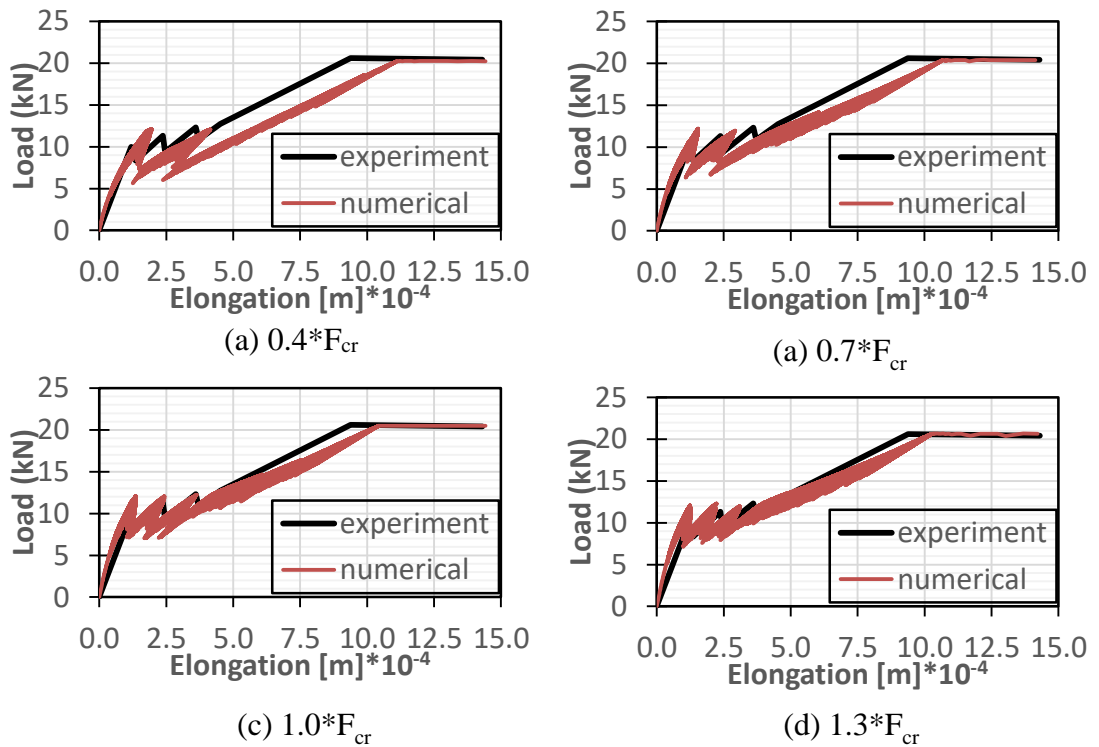


Figure 3.12. Load Elongation Curves for $\delta=3.01d$ with Different Bond Strengths

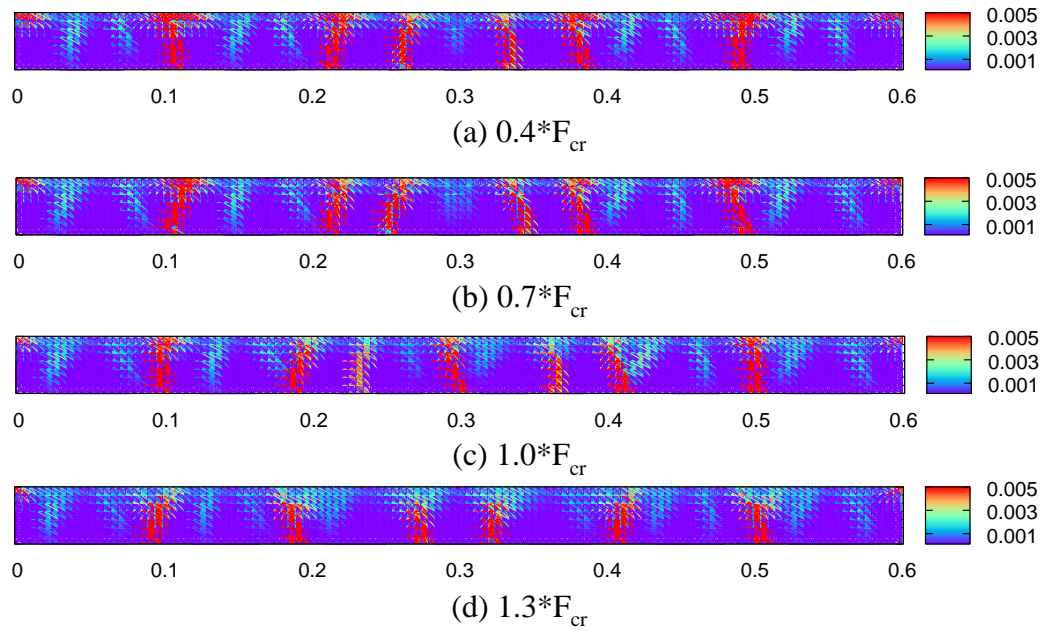


Figure 3.13. Crack Patterns for $\delta=3.01d$ with Different Bond Strengths

The minimum bond strength value was found as 70% of F_{cr} . Using lower than 70% of F_{cr} as bond strength made the system less stiff than desired. Moreover, some sliding regions were observed. Bond strengths higher than 70% was found to adequate for simulations. In summary, a different constitutive law must be applied to overcome bond failure for steel-concrete connections. $\delta=3.01d$ was chosen for OLM rather than $\delta=1.5d$. The minimum value of the bond strength for the RC structures must be taken as 70% of tensile strength of concrete. For those elements, tensile strength of them was taken as 70% of the tensile strength of concrete elements. Load elongation response by using OLM is shown in Figure 3.14.

The four pictures of damage patterns (Figure 3.15) correspond to the consecutively numbered locations on the graph in Figure 3.14. First, tensile cracks initiated at a force level of about 12 kN, afterwards, number of cracks and their widths increased and steel rebar started taking an increasing share of the external load. Finally, steel bar yielded when the external load reached to about 20 kN. Numerical and experimental result perfectly coincide at the yielding point of steel. Computational result was in good agreement with the experimental results. The number of sudden drops in the force-elongation diagram were the indicators of new crack formations agreeing with the experimental results. First, second and third points in the Figure 3.15 represent the formation of first, second and finally third cracks respectively. Fourth point shows the

final damage pattern. For point 4, three main cracks in addition to some minor cracks were observed. The spacing between first and second crack was determined to be around 100 mm, whereas the spacing between the final cracks was around 40 mm in OLM. The crack pattern observed from simulation of Rots et al (2008) is also shown in Figure 3.15(e).

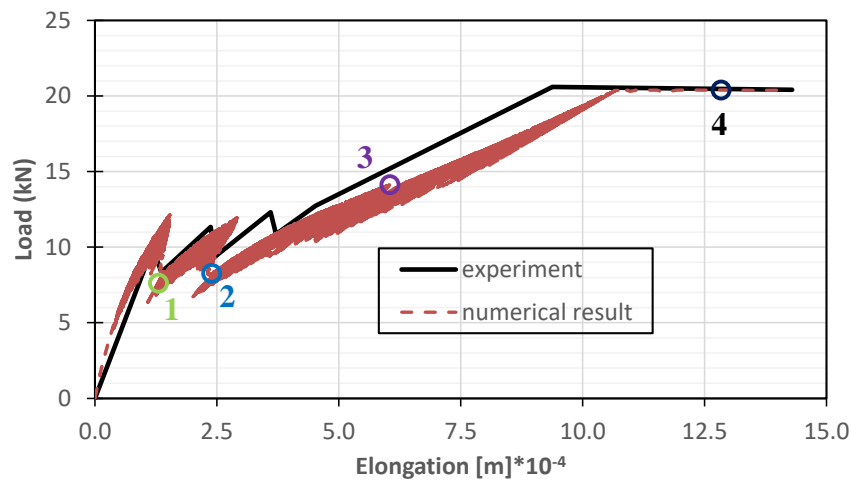


Figure 3.14. Load Elongation [Gijssbers and Hehemann 1977]. (Crack Pattern at Points Identified by Numbers are shown in Figure 3.15)

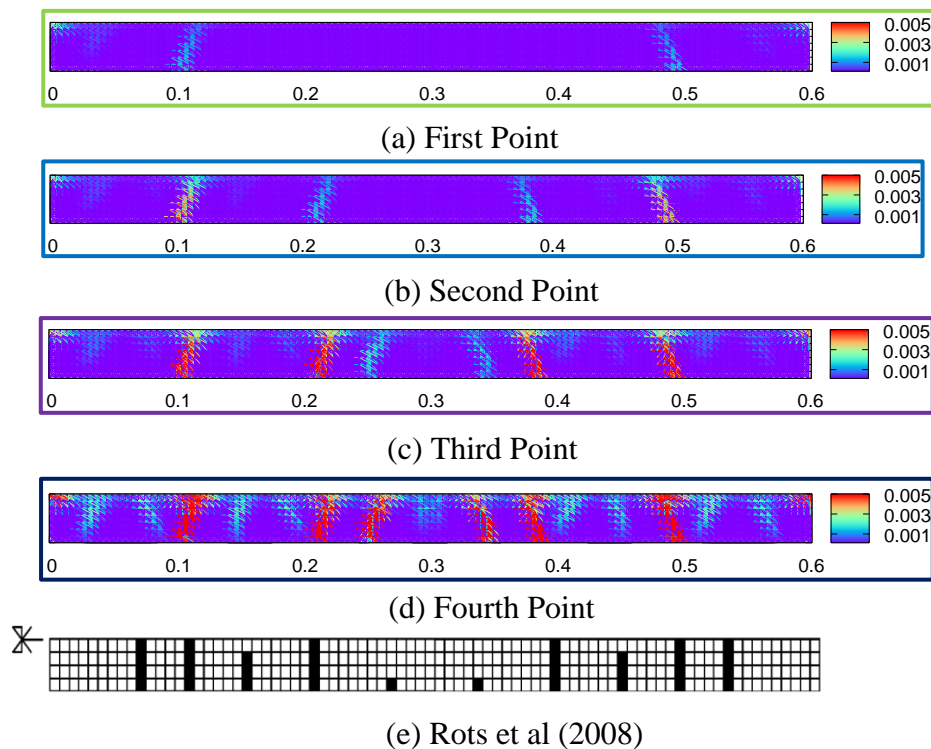


Figure 3.15. Damage Patterns at Specific Points (shown in Figure 3.14) and Crack Pattern by Rots (2008)

These results encourage the use of the overlapping lattice approach to model reinforced concrete structural members under loading, which is investigated with the next validation study.

3.5 Reinforced Concrete Beam Test

As the last validation study, the reinforced beam experiment tested by Walraven (1978) was simulated by OLM. This experiment was a four point bending test for a reinforced concrete beam. Half of the experiment specimen can be shown in Figure 3.16. E , f_{cr} , and G_f values were taken as 25.0 GPa, 2.5 MPa, 0.06 kN/m, respectively from the reported results (Table 1). The beam thickness was 200 mm. The beam had a height of 150 mm and length of 2300 mm with $2\phi 10+1\phi 8$ mm longitudinal rebars whose modulus of elasticity and yield stress were taken as 210.0 GPa and 440 MPa respectively. Force was applied at the point shown in Figure 3.16 and displacement value was measured at the middle point of the test specimen.

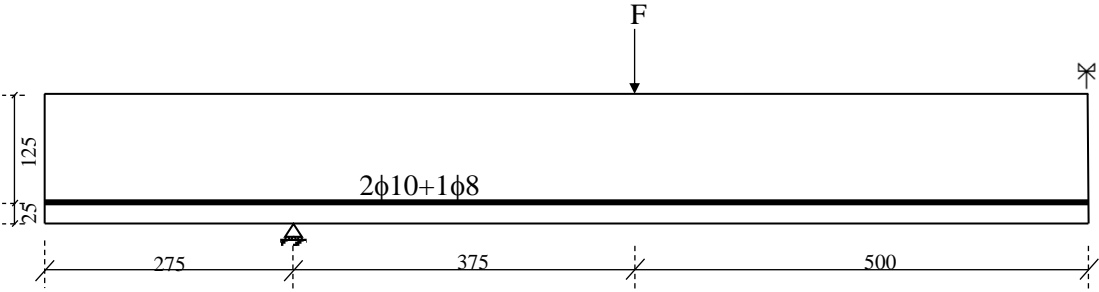


Figure 3.16. Half of the Experiment Geometry (all units are in mm)

In light of the information provided by the tension stiffening simulation, this beam was simulated by using a grid size of 25 mm with a δ of $3.01d$ with OLM. Half of the beam was simulated by placing roller supports at the right of the half beam. The force was applied as a distributed load over 50 mm spanning three elements on the actual loading plate width was not reported. The fracture energy, elastic modulus and tensile strength were reported by Gijsbers and Hehemann (1977) and they were very close to those reported by Walraven (1978). Consequently, same softening parameters employed in

tension stiffening were used in these simulations (Table 1). Displacement was taken from right top corner of the specimen.

In the preliminary studies, $\delta=3.01d$ was chosen to overcome bond failure in RC structures. By using a $\delta=3.01d$, in order to observe effect of bond strength on the results as the tensile strength of lattice elements connected to steel bars taken as 40%, 70%, 100% and 130% of the tensile strength of concrete elements, respectively. Elastic perfectly plastic load-strain response was assigned (i.e., after reaching bond strength, the stress level was kept constant). The responses and crack patterns are shown in Figure 3.17 and Figure 3.18. Color contours denote the strain values ranging from 0.00012 to 0.0008. An amplification factor of 3 was chosen.

If the bond strength was taken lower than 70% the concrete tensile strength, the steel reinforcement pulled out from the concrete as can be seen in Figure 3.17.a and Figure 3.18.a. The structure could not reach the capacity due to the pullout failure upon increasing the strength of bond elements to %70 capacity of tensile strength of concrete with elastic perfectly plastic behavior. If the bond strength was increased above 70% of the concrete tensile strength, it can be observed in Figure 3.17 that both stiffness and strength were overestimated. These results seem to demonstrate optimum bond strength for OLM simulations to be $0.7 \cdot F_{cr}$.

The model was capable of capturing the initial cracking load with a reasonable accuracy (Figure 3.19). The cracked stiffness of the specimen was slightly overestimated up until 5 mm of midspan deflection, afterwards the load deflection curve from numerical simulations followed the result from the test. Ultimate capacity of the test specimen was about 30 kN, which was in perfect agreement with the test result. In short, it can be stated that OLM is quite successful in estimating the load-deformation response of a beam failing in flexural mode.

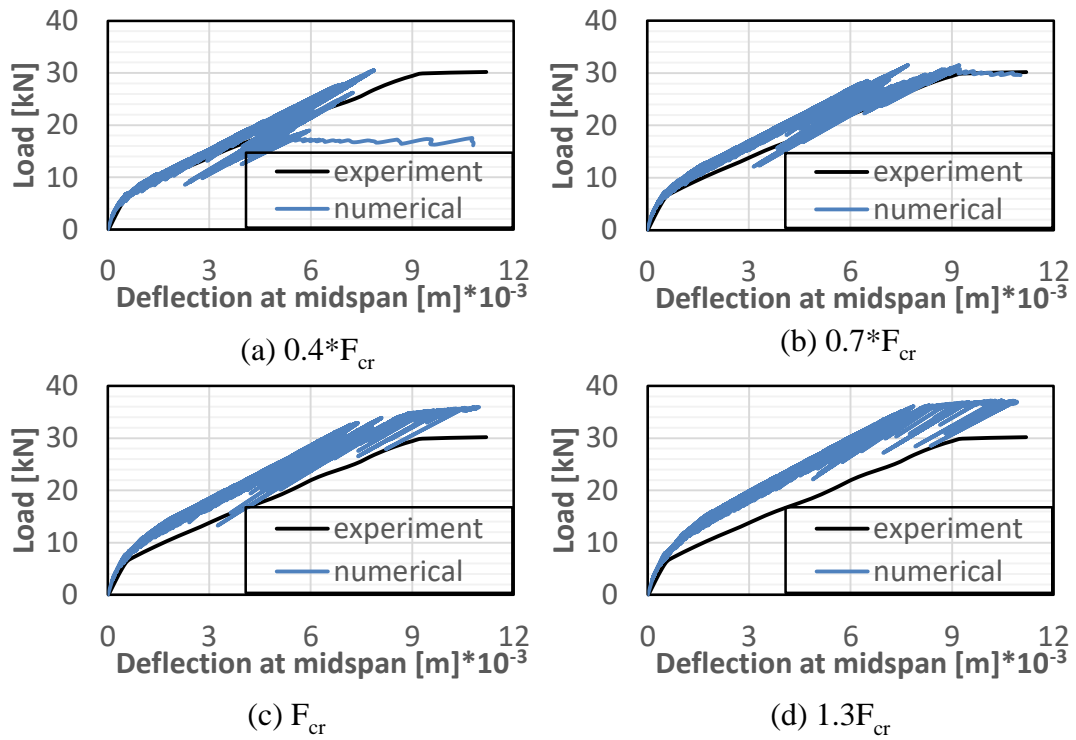


Figure 3.17. Load Deflection Response for Different Bond Strengths

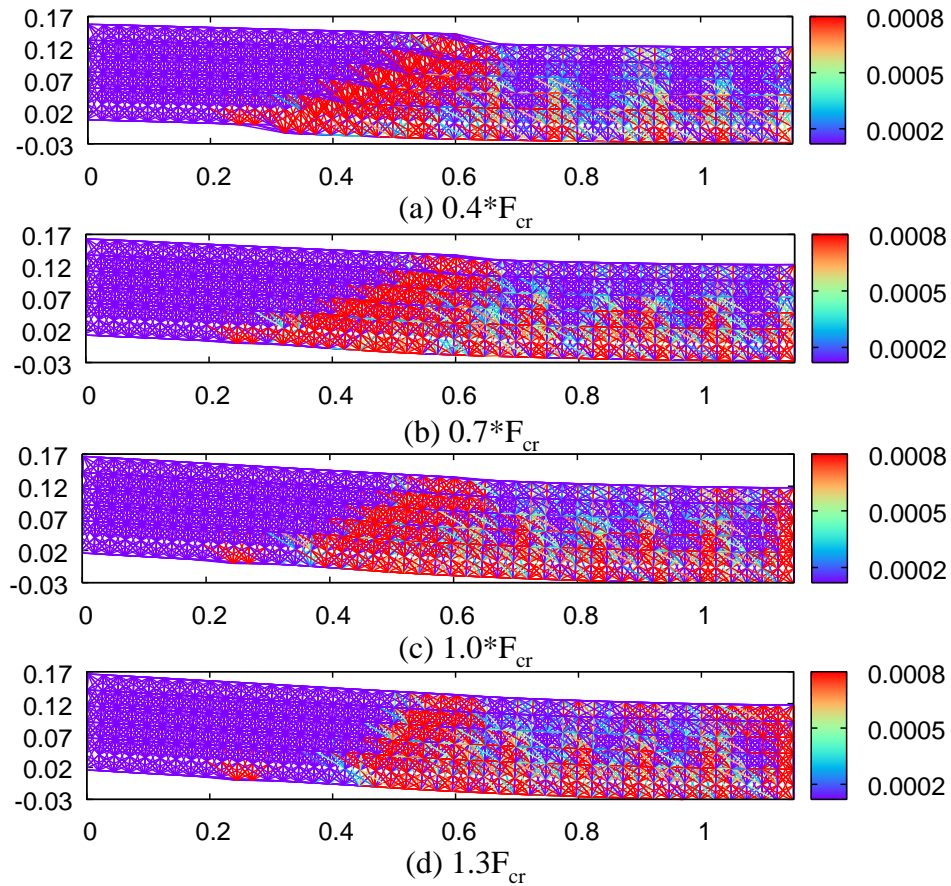


Figure 3.18. Crack Patterns for Different Bond Strengths

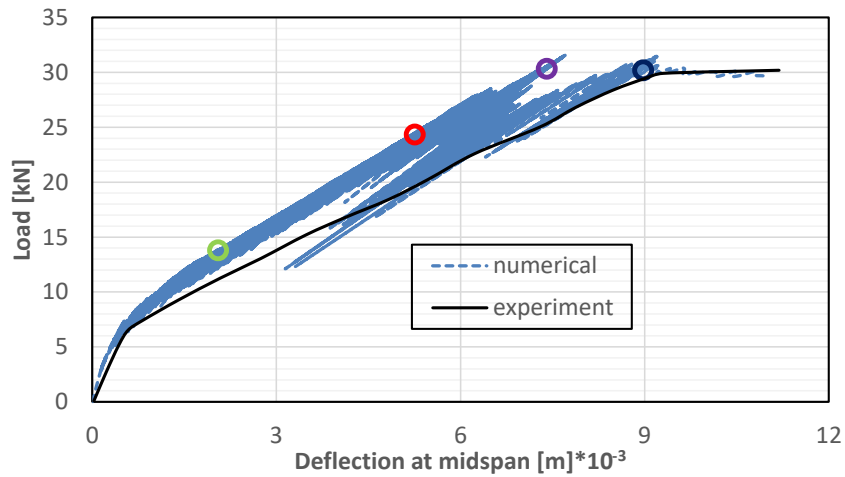


Figure 3.19. Load Deflection at Midspan Curve

Crack patterns in the specimen are shown in Figure 3.20 for 70% of tensile strength of concrete simulation related to given points in the load deflection curve as four different points. In the figure, crack patterns are shown for only half of the beam. Mirror image behavior will occur in the other half of the beam.

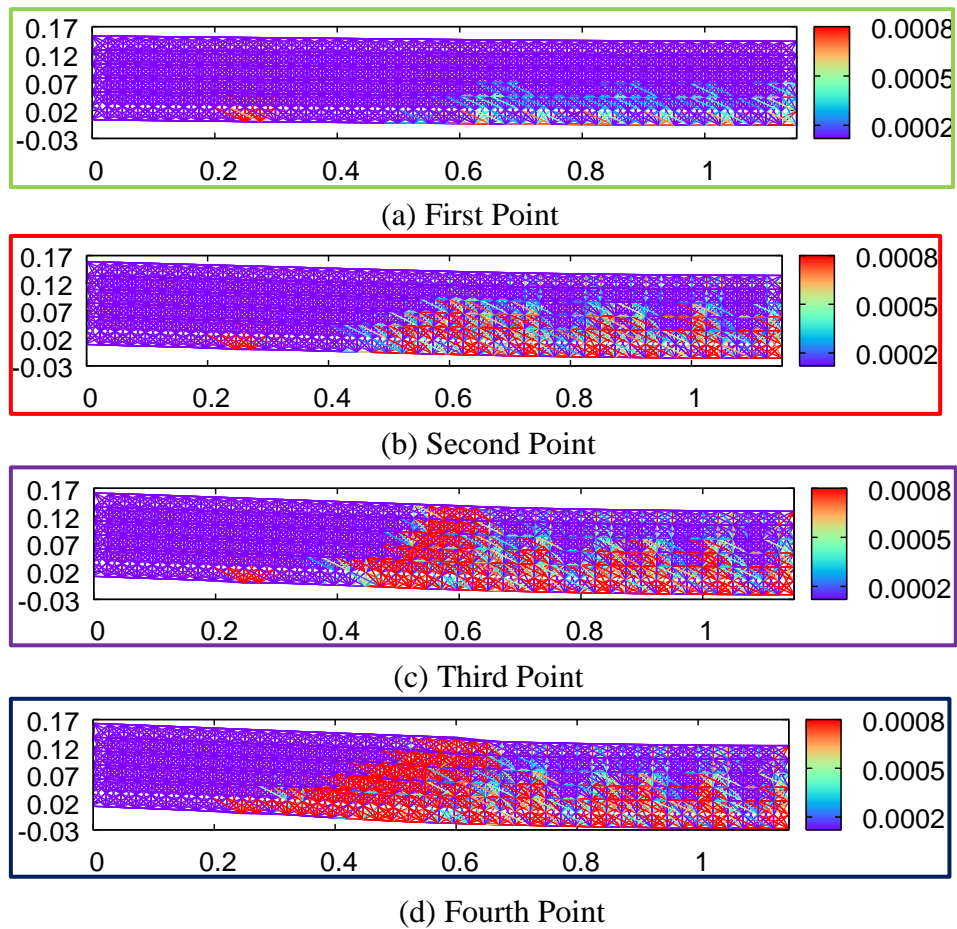


Figure 3.20. Damage Patterns at Specific Points

It can be observed that the flexural cracks were spaced at about 10 cm spacing. The only shortcoming of the simulation result, if to mention one was obtaining slightly diffused crack patterns rather than discretely spaced flexural cracks.

CHAPTER 4

CONCLUSION

4.1 Conclusion

A novel approach was proposed to simulate concrete fracture integrating OLM and sequentially linear analysis. Numerical simulations have shown that the approach has a great potential to estimate the spatial distribution and widths of cracks in both plain and reinforced concrete. The horizon distance, tensile softening function and its regularization for different mesh densities were investigated in detail. Following key conclusions can be drawn based on these results:

- The overlapping lattice modeling is a highly nonlocal approach. This necessitates the calibration of tensile stress-deformation response at the meso-scale in order to successfully match the macro-scale response. In other words, one needs to calibrate three softening function input parameters for its members by using a computational direct tension test. The tensile force-deformation response is found to be sensitive to the softening function input parameters requiring an objective calibration strategy.
- When the tensile force-deformation response of a tension test is calibrated, other crack propagation problems can be tackled with a reasonable level of accuracy and a lower sensitivity to the input parameters.
- Increasing the horizon in the OLM provides smoother force-deformation response with a more realistic crack pattern. However, it requires a finer mesh to account for the geometric irregularities.
- Existence of reinforcing bars requires higher horizon values in order to overcome bond failure of RC structure.
- Analysis of the tension stiffening and RC beam problem suggests that the force/strain curve for steel-concrete interface elements are different than concrete/concrete elements. A close match with tension stiffening and RC beam problems was obtained using elastoplastic steel-concrete interface elements with 70% of tensile strength of concrete-concrete elements.

- SLA provided a robust framework to analyze severely softening problems with no convergence issues favoring the use of it for quasi-brittle problems.

4.2 Future Work

Although, the PD is being widely applied to study crack propagation problem, its application to heterogeneous materials like concrete is quite limited as a consequence of the need for calibration. In this work, a methodology was developed to calibrate for concrete in the context of the OLM. Many research opportunities exist to further advance the OLM. Some of the opportunities are:

- The constitutive model of bond elements could further be studied to describe the bond response more realistically. To this end, the constitutive model could be calibrated with bond failure tests in literature by using OLM simulations.
- Shear and compression experiments could be simulated in order to understand the response of members in OLM other than tensile force (i.e., mode 1 crack).
- Dynamic loading could be incorporated in the OLM procedure so as to observe the response of OLM while modeling the impact/blast type loadings.
- The presented procedure of OLM for RC simulations could be more meaningful if 3D space was considered. In this way, the effect of reinforcements would be simulated accurately.
- The Strut and Tie Model could be combined with the OLM procedure.
- The effect of mesh size and type on the performance of the OLM simulations could be investigated by using different meshes. In addition, a random distribution of nodes and elements could be used to examine the effect of them on the global response.
- The fracture models to describe the compression failure would be implemented in the OLM method.

REFERENCES

- Aldemir, A. (2016), “Seismic Performance Evaluation of Roller Compacted Concrete Gravity Dams By Pseudo Dynamic Testing”, Ph.D. Thesis, Middle East Technical University, Ankara, Turkey.
- Aldemir, A., Binici, B., Arici, Y., Kurc, O. and Canbay, E. (2015), “Pseudo-Dynamic Testing of a Concrete Gravity Dam”, *Earthquake Engineering and Structural Dynamics*, **44**, 1747-1763.
- ASCE (2013). Report card for America’s Infrastructure, <http://www.infrastructurereportcard.org>, last visited 02.01.2017.
- Bazant, Z.P. and Oh, B.H. (1983), “Crack Band Theory for Fracture of Concrete”, *Materials and Structures (RILEM)*, **16**, 155–177.
- Bazant, Z.P., Tabarra, M.R., Kazemi, T. and Pijaudier-Cabot, G. (1990), “Random Particle Model for Fracture of Aggregate or Fiber Composites”, *Journal of Engineering Mechanics*, **116**(8), 1686-1705.
- Beckmann, R., Mella, R. and Wenman, M.R. (2013), “Mesh and Time Step Sensitivity of Fracture from Thermal Strain Using Peridynamics”, *Computer Methods in Applied Mechanics and Engineering*, **263**, 71-80.
- Blaauwendraad, J. (1985), “Realisations and Restrictions - Application of Numerical Models to Concrete Structures”, *Finite element analysis of reinforced concrete structures, Proceeding of US-Japan Seminar, (Meyer C., Okamura H. Eds.)*, ASCE, 557-578.
- Burt, N.J. and Dougill, J.W. (1977), “Progressive Failure in a Model Heterogeneous Medium”, *Journal of the Engineering Mechanics Division, ASCE*, **103**(3), 365-376.
- CEB-FIB (1990), *CEB-FIB Model Code*, Comité Euro-International du Béton.
- Cornelissen, H.A.W., Hordijk, D.A. and Reinhardt, H.W. (1986), “Experimental Determination of Crack Softening Characteristics of Normal Weight and Lightweight Concrete”, *Heron*, **31**(2), 45-56.
- Cusatis, G., Bazant, Z.P. and Cedolin, L. (2003), “Confinement-Shear Lattice Model for Concrete Damage in Tension and Compression: I. Theory”, *ASCE Journal of Engineering Mechanics*, **129**, 1439-1448.

- de Borst, R. and Nauta, P. (1985), "Non-orthogonal Cracks in a Smeared Finite Element Model", *Engineering Computations*, **2**(1), 35-46.
- DeJong, M.J., Hendriks, M.A.N. and Rots, J.G. (2008), "Sequentially Linear Analysis of Fracture under Non-Proportional Loading", *Engineering Fracture Mechanics*, **75**, 5042-5056.
- Der Spiegel Online, <http://www.spiegel.de/international/germany/diw-weak-infrastructure-investment-threatens-german-future-a-907885-2.html>, last visited 02.01.2017.
- Gerstle, W. and Sau, N. (2004), "Peridynamic Modeling of Concrete Structures", In: Li, L., Willam, K., Billington, S. (Eds.), *Proceedings of the Fifth International Conference on Fracture Mechanics of Concrete Structures*, **2**, Ia-FRAMCOS, 949–956.
- Gerstle, W., Sau, N. and Aguilera, E. (2007.a), "Micropolar Modeling of Concrete Structures", *Proceedings of the Sixth International Conference on Fracture Mechanics of Concrete Structures, Ia-FRAMCOS*, Catania, Italy.
- Gerstle, W., Sau, N. and Aguilera, E. (2007.b), "Micropolar Peridynamic Constitutive Model for Concrete", *19th Intl. Conf. on Structural Mechanics in Reactor Technology (SMiRT 19)*, B02/1-2, Toronto, Canada.
- Gerstle, W., Sau, N. and Sakhavand, N. (2009), "On Peridynamic Computational Simulation of Concrete Structures". Technical Report SP265-11, *ACI*, **265**, 245-264.
- Gerstle, W., Sau, N. and Silling, S.A. (2005), "Peridynamic modeling of plain and reinforced concrete structures", *18th International Conference on Structural Mechanics in Reactor Technology (SMiRT 18)*, SMiRT18-B01-2, 1-18, Beijing, China.
- Gerstle, W., Sau, N. and Silling, S.A. (2007), "Peridynamic Modeling of Concrete Structures", *Nuclear Engineering and Design*, **237**(12-13), 1250-1258.
- Gijsbers, F.B.J. and Hehemann, A.A. (1977), "Some Tensile Tests on Reinforced Concrete", Report BI-77-61, TNO Inst. *For Building Mat. and Structures*, Delft.
- Gopalaratnam, V.S. and Shah, S.P. (1985), "Softening Response of Plain Concrete in Direct Tension", *ACI Journal*, **3**, 310-323.

- Griffith, A.A. (1920), “The Phenomenon of Rupture and Flow in Solids”, *A Philosophical Transactions of the Royal Society of London, Series A*, **221**, 163-198.
- Herrmann, H.J. (1988), “Introduction to Modern Ideas on Fracture Patterns”, In *Random Fluctuations and Pattern Growth: Experiments and Models*, ed. H. E. Stanley & N. Ostrowsky. Kluwer Academic, 149-60, Dordrecht.
- Hillerborg, A., Modéer, M. and Petersson, P. E. (1976), “Analysis of Crack Formation and Crack Growth in Concrete by Means of Fracture Mechanics and Finite Elements”, *Cement and Concrete Research*, **6**, 773-782.
- Hrennikoff, A. (1941), “Solution of Problems of Elasticity by the Framework Method”, *Journal of Applied Mechanics*, **8**, 169–175.
- Hsu, T.T.C. (1988), “Softened Truss Model Theory for Shear and Torsion”, *ACI Structural Journal*, **85**(6), 624-635.
- Hsu, T.T.C., Mau, S.T. and Chen, B. (1987), “A Theory of Shear Transfer Strength of Reinforced Concrete”, *ACI Structural Journal*, **84**(2), 149-160.
- Ingraffea, A.R. and Saouma, V. (1985), “Numerical Modelling of Discrete Crack Propagation in Reinforced and Plain Concrete”, *Fracture Mechanics of Concrete*, **4**, 171-225.
- Irwin, G.R. (1958), “Fracture”, *Handbuch der Physik*, **6**, 551-590.
- Jirasek, M. and Bazant, Z.P. (1995), “Particle Model for Quasibrittle Fracture and Application to Sea Ice”, *Journal of the Engineering Mechanics, ASCE*, **121**(9), 1016-1025.
- Katihar, A., Foster, J.T., Ouchi, H. and Sharma, M.M. (2014), “A Peridynamic Formulation of Pressure Driven Convective Fluid Transport in Porous Media”, *Journal of Computational Physics*, **261**, 209-229.
- Kesler, C.E., Naus, D.J. and Lott J.L. (1971), “Fracture Mechanics-Its Applicability to Concrete”, *Proceedings of International Conference on the Mechanical Behavior of Materials*, Kyoto.
- Koutromanos, I. and Shing, P.B. (2012), “A Cohesive Crack Model to Simulate Cyclic Response of Concrete and Masonry Structures”, *ACI Structural Journal*, **109**, 349-358.
- Louis, E. and Guinea, F. (1987), “The Fractal Nature of Fracture”, *Europhysics Letters*, **3**(8), 871-877.

- Macek, W.M. and Silling, S.A. (2007), “Peridynamics via Finite Element Analysis”, *Finite Element Analysis and Design*, **43**, 1169-1178.
- Macek, W.M. and Silling, S.A. (2007), “Peridynamics via finite element analysis”, *Finite Element Analysis and Design*, **43**, 1169-1178.
- Meakin, P., Li, G., Sander, L.M., Louis, E. and Guinea, F. (1989), “A Simple Two-Dimensional Model for Crack Propagation”, *Journal of Physics A: Mathematical and General*, **22**, 1393-1403.
- Mehta, P.K. and Monteiro, P.J.M. (1993), “Concrete: Structures, Properties, and Materials”, Prentice Hall, New Jersey.
- Mehta, P.K. (2002), “Greening of the Concrete Industry for Sustainable Development”, *Concrete International*, **24**(7), 23-28.
- Mitchell, D. and Collins, M.P. (1974), “Diagonal Compression Field Theory—a Rational Model for Structural Concrete in Pure Torsion”, *ACI Structural Journal*, **71**, 396-408.
- Mitchell, J.A. (2011), “A Nonlocal, Ordinary, State-Based Plasticity Model for Peridynamics”, SAND2011-3166. Sandia National Laboratories, Albuquerque.
- Mörsch, E. (1909), “Concrete-Steel Construction”, McGraw-Hill, New York. (English translation by E. P. Goodrich).
- Mörsch, E. (1920), “Der Eisenbetonbau-Seine Theorie und Anwendung (Reinforced Concrete Construction-Theory and Application)”, 5th Edition, Wittwer, Stuttgart, V. 1, Part 1.
- Mörsch, E. (1922), “Der Eisenbetonbau-Seine Theorie und Anwendung (Reinforced Concrete Construction-Theory and Application)”, 5th Edition, Wittwer, Stuttgart, V. 1, Part 2.
- Ngo, D. and Scordelis, A.C. (1967), “Finite Element Analysis of Reinforced Concrete Beams”, *ACI Structural Journal*, **64**, 152-163.
- Nooru-Mohamed, M.B., Schlangen, E. and van Mier, J.G.M. (1993), “Experimental and Numerical Study on the Behavior of Concrete Subjected to Biaxial Tension and Shear”, *Advanced Cement Based Materials*, **1**, 22–37.
- Oliveira, D.V. and Lourenco, P.B. (2004), “Implementation and Validation of a Constitutive Model for the Cyclic Behaviour of Interface Elements”, *Computers and Structures*, **82**(17-19), 1451-1461.

- Palermo, D. and Vecchio, F.J. (2003), “Compression Field Modeling of Reinforced Concrete Subjected to Reversed Loading: Formulation”, *ACI Structural Journal*, **100**(5), 616–625.
- Pang, X.B. and Hsu, T.T.C. (1996), “Fixed-Angle Softened Truss Model for Reinforced Concrete”, *ACI Structural Journal*, **93**(2), 197-207.
- Petersson, P.E. (1981), “II Crack growth and development of fracture zones in plain concrete and similar materials”, II Report TVBM-1006, Division of Building Materials, Lund Institute of Technology, Lund, Sweden.
- Rashid, Y.R. (1968), “Analysis of Prestressed Concrete Pressure Vessels”, *Nuclear Engng. and Design*, **7**(4), 334-344.
- Ritter, W. (1899), “Die Bauweise Hennebique”, *Schweizerische Bauzeitung*, **33**(7), 59-61.
- Rots, J.G. (1988), “Computational Modelling of Concrete Fracture”, Ph.D. Dissertation, Delft University of Technology, Delft.
- Rots, J.G. (2001), “Sequentially Linear Continuum Model for Concrete Fracture”, In: de Borst R, Mazars J, Pijaudier-Cabot G, van Mier JGM, Balkema AA, editors, *Fracture mechanics of concrete structures*, The Netherlands: Lisse, **2**, 831–839.
- Rots, J.G., Belletti, B. and Invernizzi, S. (2008), “Robust Modeling of RC Structures with an “Event-by-Event” Strategy”, *Engineering Fracture Mechanics*, **75**(3-4), 590-614.
- Schlaich, J., Schäfer, K. and Jennewein, M. (1987), “Toward a Consistent Design of Structural Concrete”, *Journal of the Prestressed Concrete Institute*, **32**(3), 74-150.
- Schlangen, E. and Garboczi, E.J. (1996), “New Method for Simulating Fracture Using an Elastically Uniform Random Geometry Lattice”, *International Journal of Engineering Science*, **34**(10), 1131-1144.
- Schlangen, E. and Van Mier, J.G.M. (1992), “Experimental and Numerical Analysis of the Micro-Mechanisms of Fracture of Cement-Based Composites”, *Cement and Concrete Composites*, **14**, 105-118.
- Silling, S.A. (2000), “Reformulation of Elasticity Theory for Discontinuities and Long- Range Forces”, *Journal of the Mechanics and Physics of Solids*, **48**(1), 175-209.

- Silling, S.A. and Askari, E. (2005), “A Meshfree Method Based on the Peridynamic Model of Solid Mechanics”, *Computers and Structures*, **83**, 1526–1535.
- Silling, S.A. and Bobaru, F. (2005), “Peridynamic Modeling of Membranes and Fibers”, *International Journal of Nonlinear Mechanics*, **40**, 395-409.
- Silling, S.A., Epton, M., Weckner, O., Xu, J. and Askari, A. (2007), “Peridynamics states and constitutive modeling”, *Journal of Elasticity*, **88**, 151-184.
- Silling, S.A., Zimmermann, M. and Abeyaratne, R. (2003), “Deformation of a Peridynamic Bar”, *Journal of Elasticity*, **73**, 173-190.
- Van Mier, J.G.M. (2013), “Concrete Fracture a Multiscale Approach”, CRC, Boca Raton.
- van Vliet, M.R.A. and van Mier, J.G.M. (1995), “Softening Behavior of Concrete under Uniaxial Compression”, *Fracture mechanics of concrete structures (FraMCoS-2, Zürich)*, F. H. Wittman, ed., Aedificatio, Freiburg, Germany, 383–396.
- Vecchio, F.J. (1989) “Nonlinear Finite Element Analysis of Reinforced Concrete Membranes”, *ACI Structural Journal*, **86**(1), 26-35.
- Vecchio, F.J. and Collins, M.P. (1986), “The Modified Compression-Field Theory for Reinforced Concrete Elements Subjected to Shear”, *ACI Structural Journal*, **83**(2), 219-231.
- Wagner, H. (1929), “Ebene blechwandträger mit sehr dünnem stegblech (Metal Beams with Very Thin Webs)”, *Zeitschrift für Flugtechnik und Motorluftschiffahrt*, **20**, 8-12.
- Walraven, J.C. (1978), “The Influence of Depth on The Shear Strength of Lightweight Concrete Beams without Shear Reinforcement”, Report 5-78-4, Stevin Laboratory, Delft University of Technology, Delft.
- Weibull, W. (1939), “A Statistical Theory of the Strength of Metals”, *Proceedings of the Royal Swedish Institute for Engineering Research*, **151**.
- Willam, K., Pramono, E. and Sture, S. (1987), “Fundamental Issues of Smeared Crack Models”, *Proceedings of SEM-RILEM International Conference on Fracture of Concrete and Rock*, S.P. Shah and S.E. Swartz (Eds.), 192-207, SEM, Bethel.

APPENDIX A

SEQUENTIALLY LINEAR ANALYSIS CODE

The coordinates of grid nodes and according to δ , the elements were determined by specified the nodes as steel which was inputted with its cross sectional area (A_s) or concrete particles. Modulus of elasticity of concrete, E , and steel if exist, E_s , critical strain values corresponding to their strength of the concrete, ϵ_{cr} , and steel if exist, ϵ_{yield} , and thickness, w , were obtained from experiments. Parameters (a_1, a_2, a_3 and b_1, b_2) were added for the smallest member. Finally, boundary and load points were defined and the points at which displacement value would be liked were determined in simulation.

First, EA_t values from energy balance was computed. Afterward, stiffness matrix was assembled by assigning EA_t of 1 for all elements. The displacements in the nodes were assigned by multiplying 1.001 with x-coordinates of them so the strain value in x direction was taken as 0.001 with fixed strain in y direction as zero (i.e., $\epsilon_x=0.001$, $\epsilon_y=0$). All forces and their corresponding energies were determined by using simple truss solver algorithm. Finally, EA_t value was found by stored energy over this energy (described in Chapter 2). Force strain response of the elements from input file was defined. All initial stiffness and threshold force value, $F_{threshold}$, as F_{cr} of the truss elements were assigned (i.e., $EA_t * \epsilon_{cr}$ for concrete, $E_s * A_s * \epsilon_{yield}$ for steel members). For the reinforced concrete, there are three type of elements which were concrete, steel and bond which connected steel and concrete nodes. Threshold force value was assigned for bond members as %70 of threshold force value of concrete members.

The steps in iteration part were;

- Unit load was applied to the system
- Linear elastic analysis was performed
- Strains corresponding to their displacements were observed
- The forces were found for all members

- Critical element which has the lowest load factor, λ_{\min} (i.e., $\lambda = F_{\text{threshold}}/\text{current force}$) was found
- λ_{\min} is the scale value by which unit load elastic results was multiplied. These results was the point at global response such as load deflection at specified node
- Other elements which have λ value so close to determined λ_{\min} (i.e., $\lambda - \lambda_{\min} < 1.0e-05 * \lambda_{\min}$) were found and assigned as critical elements
- $F_{\text{threshold}}$ (if concrete member) and EA_t of critical elements was reduced according to their constitutive model by using current α

$F_{\text{threshold}}$ was found by using new EA_t of the element and small triangular similarities like Rots (2001) for concrete members. There was no need to evaluate $F_{\text{threshold}}$ for other types of element due to assume elastic perfectly plastic response. Deflection in any point or deflection differences in two points which is the definition of strain gauge used in experiments corresponding to the force could be printed.

APPENDIX B

SEQUENTIALLY LINEAR ANALYSIS CODE WITH INITIAL LOADING

All explained procedures in Appendix A until iteration part was conducted likewise. Then, before starting iteration part, the following steps were implemented for dam OLM simulation;

- 400 kN was distributed to the top grids uniformly (i.e., for 25 mm grid size, 16.67 kN is distributed to the 24 nodes) as a fixed load
 - Linear elastic analysis was performed
 - Strains corresponding to their displacements were calculated
 - The forces (F_v) for all elements were found
 - Iteration part started due to horizontal increment load
 - Unit load was applied to the system
 - Linear elastic analysis was performed
 - Strains corresponding to their displacements were calculated
 - The forces (F_h) were found for all members
 - Critical element which has the lowest load factor, λ_{\min} (i.e., $\lambda = (F_{\text{threshold}} - F_v)/F_h$) was determined
 - λ_{\min} is the scale value by which unit load elastic results was multiplied. These results is the point at global response such as load deflection at specified node.
 - Other elements which have λ value so close to determined λ_{\min} (i.e., $\lambda - \lambda_{\min} < 1.0e-05 * \lambda_{\min}$) were searched
 - $F_{\text{threshold}}$ (if concrete member) and EA_t of critical elements was reduced according to their constitutive model by using current α .
- All other things were same with the code in Appendix A.